Novel Anhydrous Superprotonic Ionic Liquids and Membranes for Application in Mid-temperature Fuel Cells

by

Younes Ansari

A Dissertation Presented in Partial Fulfillment
of the Requirements for the Degree
Doctor of Philosophy

Approved May 2013 by the
Graduate Supervisory Committee:

C. Austen Angell, Chair
Andrew Chizmeshya
Ranko Richert
George Wolf

ARIZONA STATE UNIVERSITY

August 2013

ABSTRACT

This thesis studies three different types of anhydrous proton conducting electrolytes for use in fuel cells.

The proton energy level scheme is used to make the first electrolyte which is a rubbery polymer in which the conductivity reaches values typical of activated Nafion, even though it is completely anhydrous. The protons are introduced into a cross-linked polyphospazene rubber by the superacid HOTf, which is absorbed by partial protonation of the backbone nitrogens. The decoupling of conductivity from segmental relaxation times assessed by comparison with conductivity relaxation times amounts to some 10 orders of magnitude, but it cannot be concluded whether it is purely protonic or due equally to a mobile OTf^- or $H(OTf)_2^-$ component.

The second electrolyte is built on the success of phosphoric acid as a fuel cell electrolyte, by designing a variant of the molecular acid that has increased temperature range without sacrifice of high temperature conductivity or open circuit voltage. The success is achieved by introduction of a hybrid component, based on silicon coordination of phosphate groups, which prevents decomposition or water loss to 250ºC, while enhancing free proton motion. Conductivity studies are reported to 285^{o}C and full H_2/O_2 cell polarization curves to 226^{o}C. The current efficiency reported here (current density per unit of fuel supplied per sec) is the highest on record. A power density of 184 ($mW.cm^{-2}$) is achieved at 226^{o}C with hydrogen flow rate of 4.1 ml/minute.

The third electrolyte is a novel type of ionic liquids which is made by addition of a super strong Brønsted acid to a super weak Brønsted base. Here it is shown that by allowing the proton of transient $HAlCl_4$, to relocate on a very weak base that is also

stable to superacids, we can create an anhydrous ionic liquid, itself a superacid, in which the proton is so loosely bound that at least 50% of the electrical conductivity is due to the motion of free protons. The protic ionic liquids (PILs) described, pentafluoropyridinium tetrachloroaluminate and 5-chloro-2,4,6-trifluoropyrimidinium tetrachloroaluminate, might be the forerunner of a class of materials in which the proton plasma state can be approached.

This thesis is dedicated to my late father, my mother, my sister and my brothers

Reza and Yousef

ACKNOWLEDGMENTS

Firstly, I would like to express my deepest gratitude to my advisor regent Professor C. Austen Angell for having accepted me in his research group and for teaching me all the experimental skills and guiding me through the concepts of my research. I am very thankful for his support.

I would like to thank J.P. Belieres. He laid much of the groundwork for my work.

I also would like to thank my dissertation committee members, Professor Andrew Chizmeshya, Professor George Wolf and Professor Ranko Richert for their support and for giving me their time and expertise to improve my thesis.

My special thanks go to Professor Timothy Steimle. I was honored to be his TA for one semester. I also thank Professor Steimle's postdoc, Dr. Fang Wang, for her help and support.

Many thanks to my friend, Dr. Kazuhide Ueno. I have learned a lot from him.

I would like to thank Dinesh Medpelli for taking the TEM images of our E-TEK electrodes.

I am grateful to Dr. Wei Huang for preliminary NMR studies that will become the subject of a future paper.

I thank John Blanchard and Stephen Davidowsky for the proton NMR spectrum of our molecular solutions made at an early stage of my research (2010).

I must acknowledge Dr. Jennifer Green and my lab mates Iolanda Klein, Dr. Lee, Dr. Zhao, and Greg Tucker for all their help and support and for their productive collaborations. I thank all of you for making the work in the lab an enjoyable experience.

I must also acknowledge Waunita Parrill, our executive assistant, for placing orders, arranging paperwork, and submitting papers.

Here I would like to thank my best friend Behnam Kia for his friendship. He was the one that I could count on.

Last, but not least, I would like to thank my family especially my mother and my brothers, Reza and Yousef for their countless support, without their encouragements this thesis would not have existed.

This thesis was supported by Grants W911NF0710423 and W911NF-11-1-0263 from the Army Research Office (ARO).

Table of Contents

Page

CHAPTER Page

CHAPTER Page

List of Tables

List of Figures

CHAPTER 1

Introduction to Ionic Liquids

1.1. Ionic Liquids

Humphrey Davy was the first person to consciously use an ambient temperature ionic liquid for scientific purposes. His revolutionary work on the electrolytic decomposition of simple molten salts under the influence of an applied dc electric field, to yield the elements that initially had been chemically combined in the salt under study is well-known (Angell *et al.* 2011)[1]. However, the term "ionic liquid" was first used by Barrer R. M. (Barrer *et al.* 1943)[2] to study glasses and polymerized ionic melts. Ionic liquids (ILs) are generally defined as salts which are entirely composed of separate anions and cations and are liquid at ambient temperature. Krossing and his coworkers (Krossing *et al.* 2006)[3] used lattice energies and solvation energies to explain why ionic liquids are liquid at ambient temperature. They successfully showed that size effects and conformational flexibility of ions involved lead to small enthalpies and large entropies which, at ambient temperature, implied that the liquid free energy was lower than the crystal free energy, hence would be the stable state. According to the latest classification (Angell *et al.* 2011)[1], ionic liquids can be classified into "protic" ionic liquids, "aprotic" ionic liquids, "inorganic" ionic liquids and "Solvate (chelate)" ionic liquids. Imidazolium, pyridinium and tetraalkylammonium are the most common cations reacting with various anions such as inorganic anions like tetrachloroaluminate ($AlCl_4^-$) and organic anions like trifluoromethanesulfonate (HOTf).

Ionic liquids possess very interesting properties, comparing to aqueous solutions, such as: high thermal stability (0^oC - 200^oC), high viscosity, very low vapor pressure arising from the large interaction between ion pairs, non-flammability (coming from their low vapor pressure), high ionic conductivity, large electrochemical window, solvability, and the possibility of forming an uncountable number of ionic liquids due to the variety of choices of anions and cations. Such properties are responsible for the fact that over the past 20 years study on ionic liquids has raised noticeably (see figure 1.1).

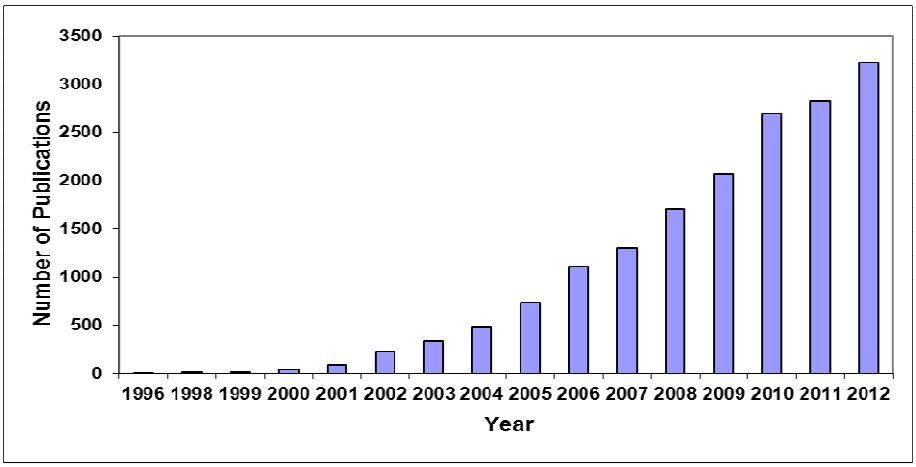

Fig. 1.1. Number of publications per year having the phrase "Ionic Liquid" was derived from "Scifinder"

1.1.1. Inorganic Ionic Liquids (IILs):

Inorganic ionic liquids are a new class of ionic liquids (Angell *et al.* 2011)[1] which are entirely composed of inorganic components and form as consequence of large anions with small cations. An example of inorganic ionic liquids is shown in figure 1.2. In this group of ionic liquids mostly those containing silver and alkali halides show higher viscosity than other inorganic ionic liquids which at ambient temperature exhibit higher

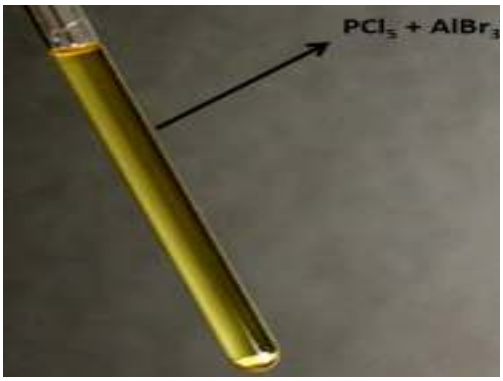

Fig. 1.2. Example of a room temperature inorganic ionic liquid $[PCl_4^+][AlClBr_3^-]$.

ionic conductivity than any aprotic ionic liquids (to be discussed later) due to the highly decoupled state of the silver ions.

Lithium chlorate is another example of inorganic ionic liquids with a melting point around 115ºC, showing a glass forming eutectic when added to lithium perchlorate. Lastly, some unexplored cases (Angell *et al.* 2011)[4] of salts with inorganic molecular cations like PBr_3Cl^+, SCl_3^+, and $ClSO_2NH_3^+$ with appropriate weak base anions.

1.1.2. Solvate (chelate) ionic liquids:

As a largely unstudied type of ionic liquids which includes cases of multivalent cation salts that would not ordinarily be able to satisfy the criterion of $T_m < 100^oC$. $Ca(NO_3)_2.4H_2O$, is considered as the first recognized member of this class of ionic liquids (Angell *et al.* 2011)[1]. They usually are thought of as being solvents however they do not have any solvent function. In such systems, solvent molecules are tightly bonded to high field cations. They have very low vapor pressures at ambient temperatures and they only boil at temperatures close to 200^oC. An example of such ionic liquids is the

LiCTFSI – tetraglyme which was recently studied by Watanabe's group in Japan (Tamura *et al.* 2010)[5].

1.1.3. Aprotic Ionic Liquids (APILs):

Aprotic ionic liquids, thus far, are the most studied type of ionic liquids. This class is responsible for a dramatic increase in the study of ionic liquids since the mid-90's (Angell *et al.* 2011)[4]. An example of such ionic liquids is alkyl pyridinium and dialkylimidazolium cations studied by Hurley and Weir (Hurley *et al.* 1951)[6]. They successfully synthesized an APIL by mixing N-substituted alkyl and aryl pyridinium halides and presented the first phase diagram on an aluminum chloride - organic halides, shown in figure 1.3, system which showed presence of an ionic liquid at a temperature well below the ambient temperature (-40^{o}C).

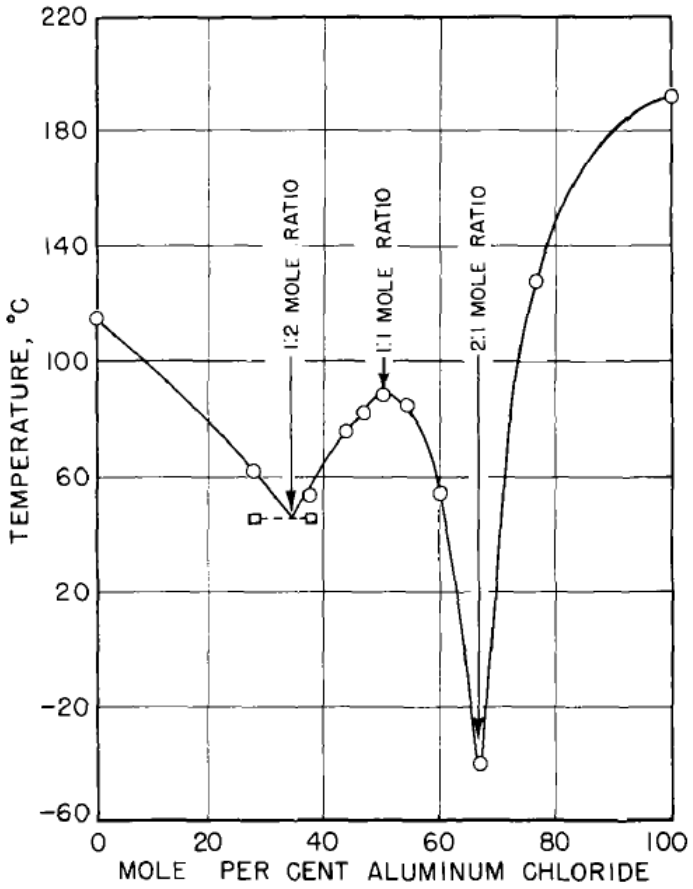

Fig. 1.3. Phase diagram of the system aluminum chloride ethylpyridinium bromide.

Aprotic ionic liquids can be formed by direct combination of halide salts and metal halids (Hussey 1983)[7], Metathesis among halide salts and metal salts (Fuller *et al.* 1994)[8], and quaternization of amines (Bonhote *et al.* 1996)[9]. This group of ionic liquids show low melting point due to irregular packing among organic cations and tiny inorganic anions (Angell *et al.* 2011)[10].

One of the most important applications of aprotic ionic liquids is that they are being used as supporting electrolytes for electrochemical measurements. In addition, they can be used as electrolyte components in protonic membranes (Fericola *et al.* 2008)[11]. It

has been shown that the thermal stability of proteins could be enhanced in the presence of aprotic ionic liquids. (Noritomi *et al.* 2011)[12].

1.1.4. Protic Ionic Liquids (PILs):

They simply form by a reaction between a Brønsted acid (a proton donor) and a Brønsted base (a proton acceptor).

$$HA + B \leftrightarrows HB^+ + A^- \qquad (1.1)$$

The reaction is reversible if the proton transfer energy-gap is not excessively large.

Recently, study on this type of ionic liquids has gained increasing attention due to their interesting applications. One of the applications of protic ionic liquids is in biology. An example of such application is the use of N-butyl-N-methyl pyrolidinium dihydrogen phosphate, and 1-Butyl-3-methylimidazolium (bmim) dihydrogen phosphate as a solvent for proteins.

Fujita (Fujita *et al.* 2005)[13] dissolved significant amount of proteins in these protic ionic liquids. As a consequence, they could increase the thermal stability of their protein.

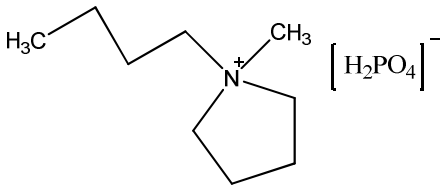

N-butyl-N-methyl pyridinum dihydrogen phosphate

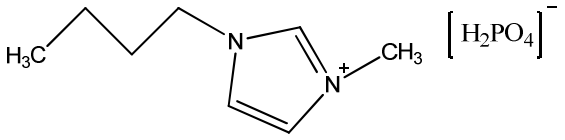

1-butyl-3-methyl imidazolium [bmim] dihydrogen phosphate

Fig. 1.4. The structure of N-butyl-N-methyl pyrrolidinium dihydrogen phosphate and 1-butyl-3-methylimidazolium (bmim) dihydrogen phosphate as solvents for proteins.

Protic ionic liquids are also being used in organic synthesis. Knoevenagel condensation (Hangarge 2002)[14] (see Figure 1.5) is one of the best examples for this application which is a reaction between carbonyl compounds and methylene compounds to form alkenes.

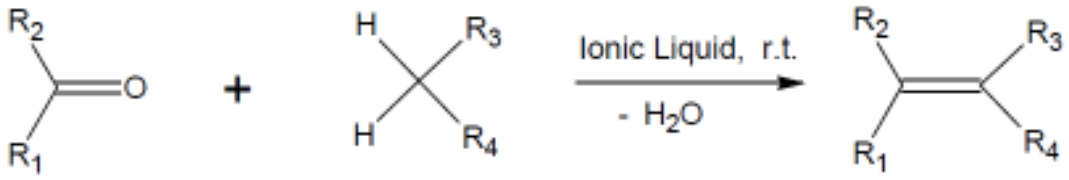

Fig. 1.5. Knoevenagel condensation, a reaction between carbonyl and methylene compounds.

In this reaction, protic ionic liquids play three important roles, they act as the solvent, as the water absorbent, and as the catalyst.

Protic ionic liquids also serve as electrolytes in fuel cells. Fuel cells by definition are devices that can convert chemical energy into electrical energy. Protic ionic liquids are a new class of non-aqueous electrolytes which yield high efficiency fuel cells due to their exceptional characteristics such as low vapor pressure, high thermal stability, high electrochemical stability, and non-flammability. This is one of the most important applications of protic ionic liquids. Details will be discussed in chapter 2.

In ionic liquids, various interactions are involved such as van der Waals, coulombic, and hydrogen-bonding. Ionicity (ionic nature) is one of the key factors affecting the physicochemical properties of ionic liquids. Study of new class of protic ionic liquids with high proton mobility is one of the main objectives of this thesis.

1.2. Protic Ionic Liquids and Ionicity:

Ionic liquids have thought to comprise entirely of separated anions and cations; however, not all of these ions are capable of taking part in conduction processes to a certain degree (degree of ionicity) that is mostly dependent on the nature of anions and cations, hence the ionic liquid, and its structure (Macfarlane *et al.* 2009)[15]. Some ionic liquids exhibit lower molar conductivity, while they show the same or even lower viscosity than the rest. In general, independent ions contribute higher to conductivity than aggregated ones; therefore, understanding factors affecting correlations among ions is of importance. Such correlations influence the electrochemistry and vapor pressure of these materials. A quantitative approach to ionicity was first made in our lab based on the Walden rule. (Xu *et al.* 2003)[16] (Yoshizawa *et al.* 2003)[17] (Angell *et al.* 2007)[18]. According to Walden's viscosity rule (Walden 1906)[19], the product of the molar conductivity (Λ_m) and the viscosity of the solvent (η) is constant for infinitely diluted electrolyte solutions.

$$\Lambda_m \cdot \eta = cte \tag{1-2}$$

$$\log \Lambda_m = \log c + \log \eta^{-1} \tag{1-3}$$

The Walden rule clearly states that in conventional electrolytes, the ionic mobility is inversely proportional to the solution's viscosity or is directly proportional to the fluidity (η^{-1}) of the system. The Walden rule is typically obeyed when solutions hold large and only weakly coordinating ions in solvents with almost no ion-solvent interaction. The Walden rule has been used in our laboratory to classify ionic liquids into "sub", "poor", "good" and "super" ionic liquids. Figure 1.6 shows latest classification of ionic liquids based on the Walden rule well-known as the "Walden plot".

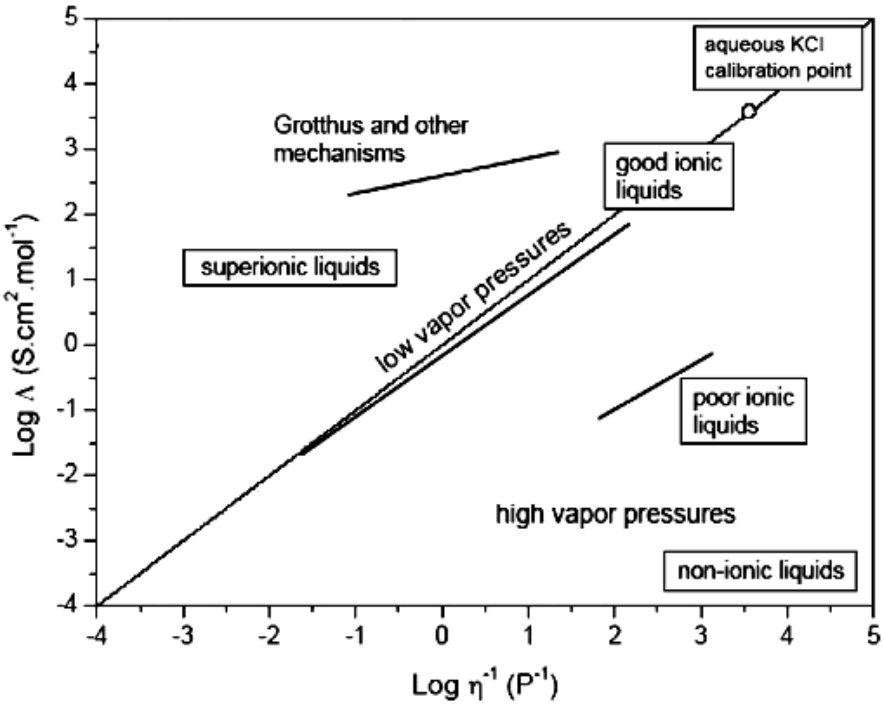

Fig. 1.6. Application of the Walden plot to classify ionic liquids by relating their equivalent conductivity to their fluidity. (Belieres 2005)[28]

Since in this thesis we are dealing with protic ionic liquids, where the mobile ion is the proton, superprotonic ionic liquid expression is used instead of "superionic" ionic liquid. The ideal line in the Walden plot is set by using data for a dilute aqueous solution of KCl (0.01M KCl aq. solution) where ions are fully dissociated showing equal mobilities. It was shown in our laboratory (Angell *et al.* 2003)[17] that a liquid phase, like the crystalline phase, in which ions are symmetrically distributed with regard to ions of the opposite charge, possesses a so called "Madelung energy". The charge distribution in "poor" ionic liquids is not spherically symmetric around each ion throughout the liquid; therefore, they appear below the ideal line in the Walden plot. "Good" ionic liquids have exceptionally

low vapor pressure due to the dipole-dipole interactions among ions in addition to the Madelung energy. Superionic liquids, comparing to "poor" and "good" ionic liquids, show very interesting properties. Indeed, superionic liquids do not follow the Walden rule since their conductivity is decoupled from their viscosity. The decoupling between the conductivity and viscosity in superprotonic liquids is the result of the "Grotthuss mechanism" (Grotthuss 1806)[20] rather than the "Vehicular motion". In protic ionic liquids, proton can be transferred by the entire molecule; this mechanism is called Vehicular motion in which the conductivity of the system is completely dependent on its viscosity. Proton transfer in poor and good ionic liquids is reliant on the diffusion of the system and conductivity and viscosity, in these ionic liquids, completely obey the Walden rule. On the other hand, most superprotonic liquids do not follow the Walden rule and conductivity of the system acts independent of the viscosity. The proton, in such ionic liquids, transfers by Grotthuss mechanism which was first proposed by Grotthuss in the early 19th century (Grotthuss 1806)[20]. Grotthuss proposed that proton, in protonated liquids, can transfer by freely hopping from a protonated species to a nearby molecule. His mechanism consists of two separate steps: (1) free rotation of the protonated species, (2) hopping of the proton to a nearby molecule. The difference between the Grotthuss mechanism and Vehicular motion (Diffusion) are shown in figure 1.7 (Kawaguchi *et al.* 2005)[21].

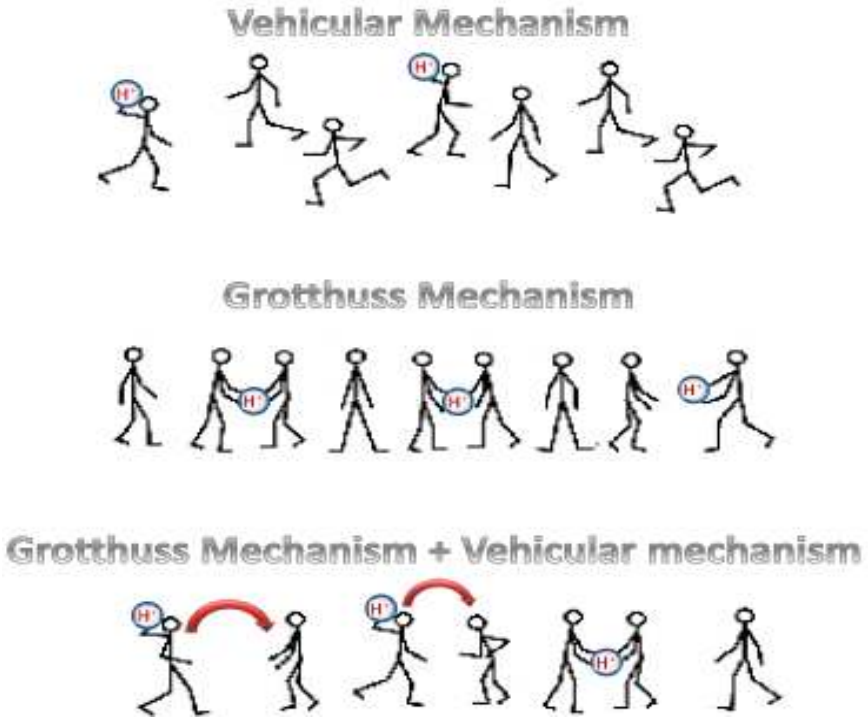

Fig. 1.7. Various Proton Transfer Mechanisms in protic ionic liquids.

As discussed earlier, the required work to vaporize ionic liquids is much higher than molecular liquids due to the Madelung energy. Quantitatively, the probability of the enthalpy fluctuation to permit an ion pair to escape the liquid into the vapor phase is related to the Boltzman factor:

$$p(h) \sim \exp(-h / k_B T) \tag{1-4}$$

where $p(h)$ is the probability, k_B is the Boltzmann constant, T is the temperature in Kelvin, and h is the enthalpy of extraction per ion pair. Some classical equations relate the electrical conductivity to the diffusion by consideration of dilute aqueous solutions where ions are assumed to move completely independent of the others. The Nernst-

Einstein equation is one of the most widely used equations relating the equivalent conductivity to the diffusivity of a system.

$$\lambda_i = \frac{RTz_i D_i}{F^2} \tag{1.5}$$

where the λ_i is the equivalent ionic conductivity, F is the Faraday constant, D_i is the diffusivity of ion (*i*), z_i is the charge of ion (*i*), T is the temperature in Kelvin, and R is the ideal gas constant. The diffusivity D_i can also be related to the viscosity η of the system through the Stokes Einstein equation:

$$D_i = \frac{k_B T}{6\pi\eta r_i} \tag{1.6}$$

where r_i is the ionic radius.

1.3 Ionic conductivity:

Electrolyte solutions play an important role in electrochemical devices which mostly have a crucial drawback as they contain volatile solvents. That is one of the reasons why ionic liquids have recently received much attention as new electrolyte materials. Some ionic liquids possess several striking features such as high concentration of ions and high mobility of the component ions at room temperature; hence, high ionic conductivity, which make them excellent electrolytes. (Ohno *et al.* 2011)[22]

In general, the ionic conductivity can be defined as:

$$\sigma_i = \sum ne\mu \tag{1-7}$$

where n is the carrier ion number, e is the electric charge, and μ is the mobility of carrier ions. The three important electrochemical properties of ionic liquids are their high ionic conductivity, transference number, and potential window and these properties can be influenced by several factors such as moisture absorption, experimental atmosphere, and electrode species. Ionic conductivity can be defined based on the reciprocal of the resistance,

$$\sigma_i = \frac{l}{R_b S}, \quad \text{cell constant} = \frac{l}{S} \tag{1-8}$$

where, l is the distance between the two electrodes and S is the mean area of the electrodes. The ionic conductivity has units of S cm^{-1}, mS cm^{-1}, and $1/\Omega.cm$. The cell constant in practice is determined by using a standard solution like the dilute aqueous KCl (in this thesis 0.01 M).

R_b is not the only resistance usually detected as resistance, the electric charge transfer resistance, and the electrical double layer at the electrode interface can also be detected as resistance. A dc four-probe method or the complex-impedance method is typically used to separate a sample bulk and electrode interface (Monk 2001)[23]. One of the advantages of the impedance spectroscopy is that it can be performed using non-blocking electrodes (the same element for carrier ions and metals) and blocking electrodes (such as platinum or stainless steel) (Ohno *et al.* 2011)[22]. Figure 1.8 shows two different types of ionic conductivity cells.

Absence of perfect contact between sample and electrodes such as bubbles and grain boundary can affect the detected current considerably. For that reason, careful

manipulation of the sample and contact conditions are necessary especially for the case of polymers.

The impedance analyzers use frequency under an alternating current (ac) where the observed impedance depends on the applied frequency. The impedance decreases with increasing frequency.

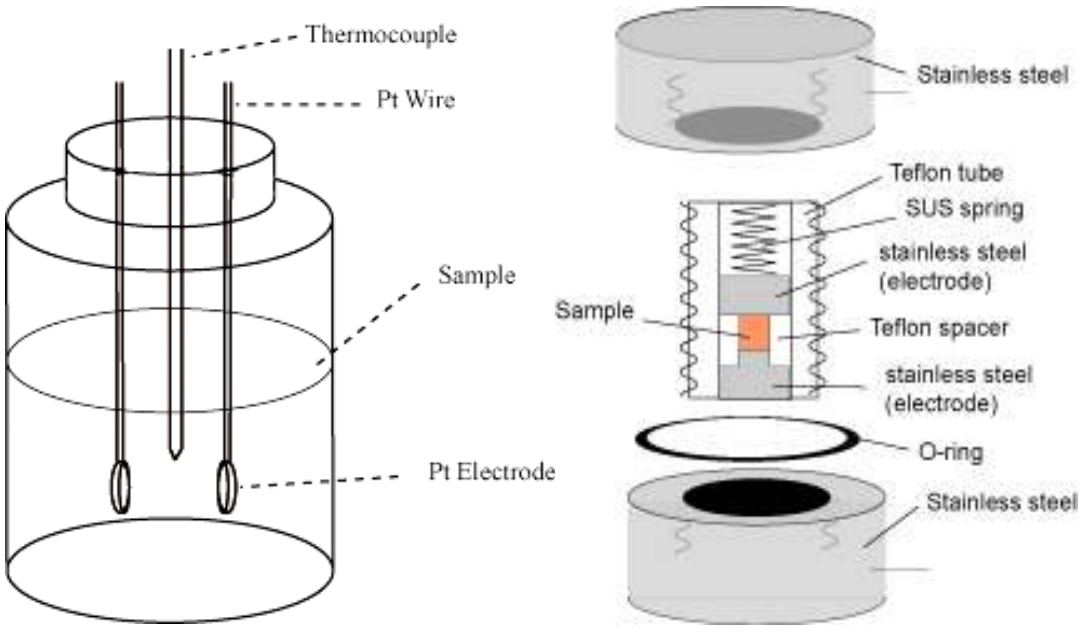

(a) Liquid (b) Solid

Fig. 1.8. Schematic representation of cells used to measure ionic conductivities for (a) liquid and (b) solid samples.

In general the measured frequency is in the range of 1 MHz to 1Hz which is also dependent on the frequency range of the impedance spectrometer. Depending on the sample, a 10 or 100 mV amplitude voltage is desirable. Impedance spectroscopy will be discussed in the experimental section.

1.4 Proton Free Energy Level Diagram:

As was discussed earlier, protic ionic liquids can be formed by the combination of proton donors and proton acceptors. Based on the proton donor and proton acceptor sites, Gurney's framework for aqueous solutions (Gurney 1962)[24] was used in our laboratory to study the proton energy gap required to form a protic ionic liquid and classify them into various electrolytes (Belieres & Angell 2007)[25]. The concept is based on the fact that proton "falls" from an occupied energy level on the donor acid into the free acceptor level on the base to form the protic ionic liquids which is presented in figure 1.9. (Bautista-Martinez 2009)[26]

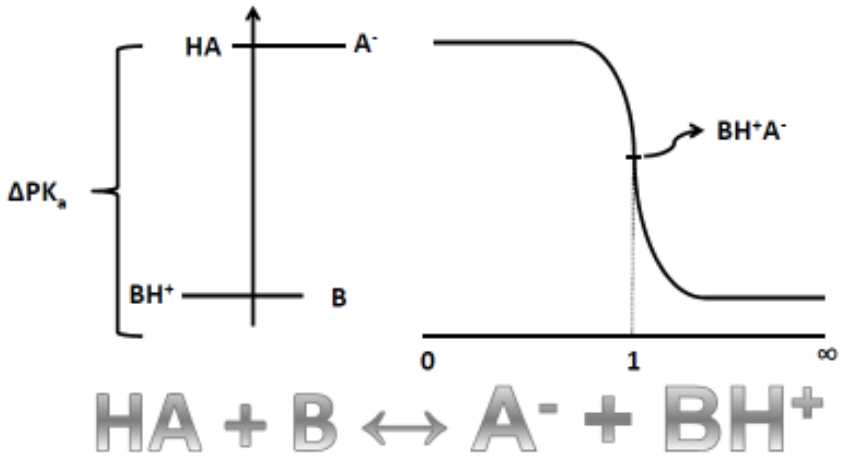

Fig. 1.9. The formation of a protic ionic liquid showing an energy gap across which the proton transfer must occur. The equivalence point of the acid-base (dashed line) titration curve represents the presence of a protic ionic liquid; the abscissa corresponds to the ratio of titrated reactants.

Recognizing aqueous pK_a values as measures of proton affinity, the free energy change of the reaction is related to the difference in pK_a values between the Brønsted acid and the Brønsted base:

$$\Delta pK_a = pK_a^{BH^+/B} - pK_a^{HA/A^-} \qquad (1\text{-}9)$$

The pK_a values were related to the thermodynamic properties of ionic liquids and well supported by examination of the excess boiling point and potentiometric experiments (Yoshizawa *et al.* 2003)[17] (Belieres & Angell 2007)[25] (Bautista-Martinez 2009)[26] (Kanzaki *et al.* 2008)[27]. Precise values of the energetics of transfer of proton can be provided by the actual pK_a values in non-aqueous environment using the Gibbs free energy of proton transfer:

$$\Delta G = -2.303\, RT \Delta pK_a^{PIL} \tag{1-10}$$

The Gurney-type proton free energy level diagram of various acids and bases is based on the pK_a of a 1M aqueous concentration considering water as the acid or the base of the proton transfer couple. An example of the Gurney-type proton free energy level diagram is shown in figure 1.10 published by Belieres and Angell (Belieres & Angell 2007)[25]. A more inclusive Gurney-type proton free energy level diagram for ILs is shown in chapter 6.

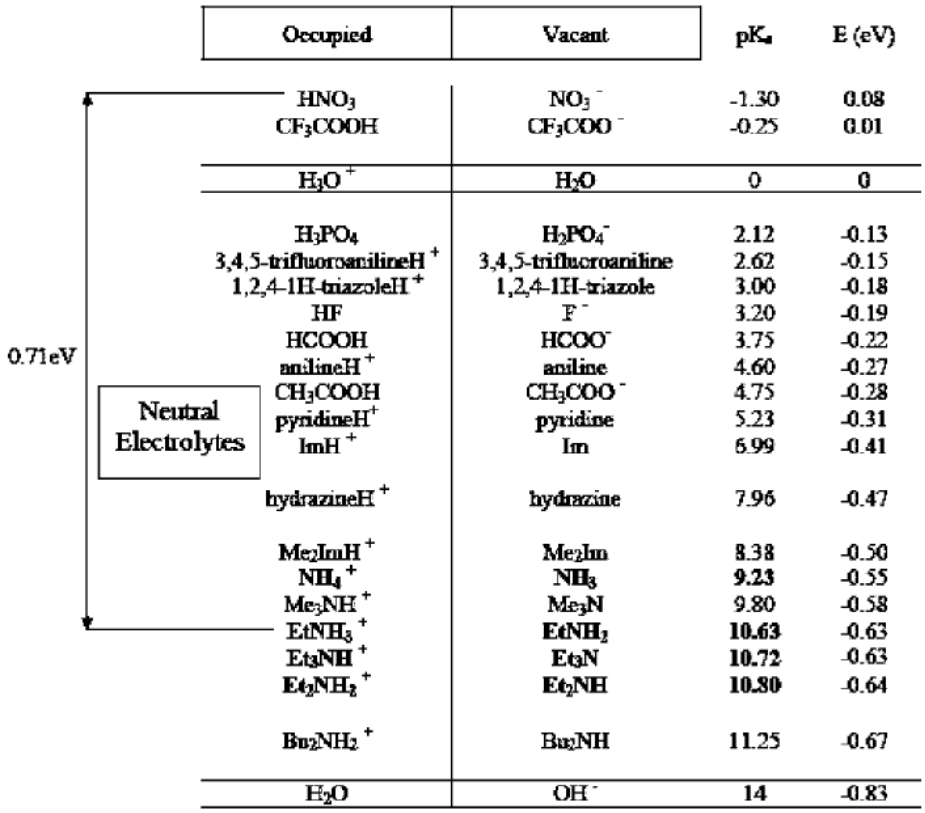

Fig. 1.10. Gurney-type proton free energy level diagram for ILs from Belieres and Angell (Belieres & Angell 2007)[25], showing formation of ionic liquids from moderately strong acids and moderately strong bases to yield neutral ionic liquid products.

Even though the proper acidity or basicity of the ions will almost certainly depart from that in aqueous environments when an ionic liquid forms, the Gurney diagram gives a good estimate of the energy released when combining those acids and bases. Ionic liquids form by the proton "falling" from the upper occupied level into the lower vacant level (Belieres 2005)[28].

CHAPTER 2

Introduction to Fuel Cells

2. Fuel Cells:

By definition fuel cells are devices that can convert chemical energy into electrical energy. Fuel cells were first demonstrated by Sir William Grove in 1839. He introduced the first H_2/O_2 fuel cell with spongy platinum electrodes and sulfuric acid electrolyte. It was a combination of four cells which were connected in series applying a DC voltage to electrolyze water. Becquerel A. C. and Becquerel A. E. (Srinivasan 2006)[29] used a fuel-carbon rod, molten-nitrite electrolyte platinum for direct utilization of carbon as a fuel. After that Mound and Langer were able to enhance the efficiency of Groves's fuel cell by increasing the area of the electrode and using sulfuric acid, as the electrolyte, in a diaphragm. Ostwald introduced some advantage of fuel cells over thermal energies in 1894. After that, coal was used in fuel cell introduced by Jacques (Srinivasan 2006)[29]. In this design, coal was used as a fuel, and the electrolytes were molten potassium or sodium hydroxides.

After Bacon's revolutionary work in the 1950s, fuel cells were effectively developed for the American Space program. Such success, accompanied by a policy to commercialize space technology, led to significant development programs in America and Japan in the 1970s and the 1980s, and more lately in Europe (Larminie & Dicks 2003)[30]. Recently, due to global warming and the need to reduce CO_2 emissions, fuel cell technology has gained increasing attention. Transportation industries are now required to

track technologies which are capable of eliminating emissions and ultimately providing people with zero emission cars.

In general, fuel cells are analogous to batteries with an indispensable difference. In a battery the oxidant and the fuel are typically the electrodes themselves while in a fuel cell, fuel and oxidant are continuously supplied to the electrodes. The energy deriving path in a fuel cell differs from a Carnot engine. In a fuel cell electrical energy is derived by the release of the free chemical energy of reactants to products through oxidation and reduction reactions in the anode and cathode, but in a Carnot engine direct combustion of the oxidant and the fuel provides the required heat for conversion to a mechanical work. It will be discussed in section 2.4 that the maximum efficiency in combustion engines rarely exceeds 30% while in fuel cells the efficiency reaches almost 100%.

2.1 Hydrogen Fuel Cell:

The first demonstration of a fuel cell was by Lawyer and William Grove in 1839. They first electrolyzed water into hydrogen and oxygen by applying an electric current through it. Then they used the produced hydrogen and oxygen, replaced the power supply with ammeter and derived a small current from it. They could combine hydrogen and oxygen to produce electric current. Looking from a fuel cell prospective, the electrolysis is being reversed: the hydrogen and oxygen combine to produce water and generate electric current (Larminie & Dicks 2003)[31]. The amount of current produced by this reaction could be very small if the contact area between the gas, the electrode, and the electrolyte is low or the distance between the electrodes are large, and the resistance of the electrolyte to flow of electric current is high. To enhance the amount of current, the

flat electrodes are being made and thin layers of electrolytes are required. Porous electrodes can also help to let the electrolyte and gas penetrate them to maximize the contact between the electrode, electrolyte, and the gas. However, such details vary for various types of fuel cells. Figure 2.1 shows a schematic representation of the H_2/O_2 cell.

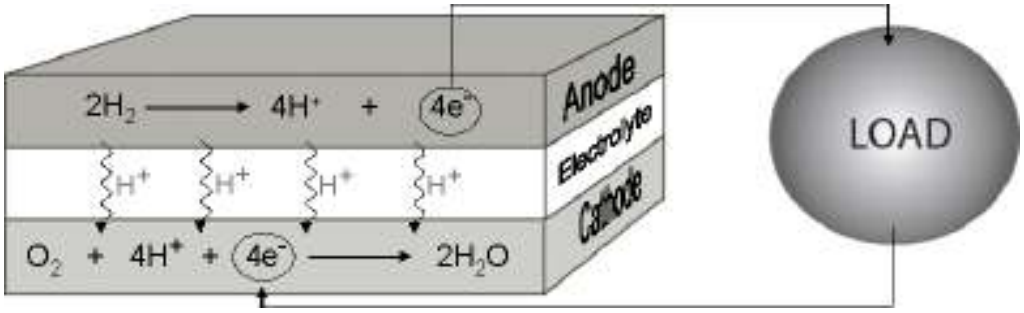

Fig. 2.1. Schematic representation of a "Hydrogen – Oxygen" fuel cell.

As it is shown in figure 2.1, at the anode side of the fuel cell (acid electrolyte) two hydrogen molecules are ionized releasing four protons and four electrons which releases energy.

$$2H_2 \longrightarrow 4H^+ + 4e^- \qquad (2\text{-}1)$$

At the cathode side, on the other hand, oxygen reacts with electrons (passing through the electrical circuit) and protons (passing through the acid electrolyte) to form water.

$$O_2 + 4e^- + 4H^+ \longrightarrow 2H_2O \qquad (2\text{-}2)$$

The acid can be a liquid containing free H^+ ions to allow the protons to pass through the electrolyte or a polymer containing mobile protons.

In this case the relationship between the theoretical maximum energy from combustion and the electrochemical reactions is:

$$\Delta G^o = -RT \ln K_{eq} = -nFE^o \tag{2-3}$$

where the ΔG^o is the standard Gibbs free energy of the combustion reaction, R is the ideal gas constant, T is the absolute temperature in Kelvin, K_{eq} is the equilibrium constant, n is the number of electrons, F is the Faraday constant, and E^o is the reversible equilibrium potential.

Nernst equation is another equation which is derived from Eq. (2-4). The Nernst equation for the anodic half-cell is:

$$E_{rev,anode} = E^o_{H_2/H^+} + \frac{RT}{nF} \ln\left[\frac{a^2_{H^+}}{a_{H_2}}\right], \tag{2-4}$$

and the cathodic side:

$$E_{rev,cathode} = E^o_{O_2/H_2O} + \frac{RT}{nF} \ln\left[\frac{a^2_{H^+} \cdot a^{1/2}_{O_2}}{a_{H_2O}}\right] \tag{2-5}$$

where the a_{H^+}, a_{H_2}, a_{O_2}, and a_{H_2O} are the activity of H^+, H_2, O_2, and H_2O species respectively, R is the ideal gas constant, T is the absolute temperature in Kelvin, n is the number of electrons, F is the Faraday constant, and E_{rev} is the theoretical potential of the cell under non-equilibrium conditions.

Then the reversible potential can be defined as:

$$E_{rev} = E_{rev,cathode} - E_{rev,anode} \tag{2-6}$$

$$E_{rev} = E^o_{O_2/H_2O} - E^o_{H_2/H^+} + \frac{RT}{2F} \ln\left[\frac{a^2_{H_2} \cdot a^{1/2}_{O_2}}{a_{H_2O}}\right] \tag{2-7}$$

In Alkaline fuel cells, the overall structure is the same as hydrogen/oxygen fuel cells; however the reactions taking place at each electrode are different. The mobile ion on alkali fuels cells are OH^-. The following reaction occurs at the anode side:

$$2H_2 + 4\,OH^- \longrightarrow 4H_2O + 4e^- \qquad (2\text{-}8)$$

As it is shown again energy and electrons, and water (unlike hydrogen/oxygen fuel cell) produce at the anode. At the cathode side, Oxygen, electrons and water react to form hydroxide anions.

$$O_2 + 2H_2O + 4\,e^- \longrightarrow 4OH^- \qquad (2\text{-}9)$$

The reaction proceeds continuously, allowing hydroxide ions to be able to pass though the electrolyte and electrons to pass through an electrical circuit. A general scheme of this type of fuel cell is shown in figure 2.2.

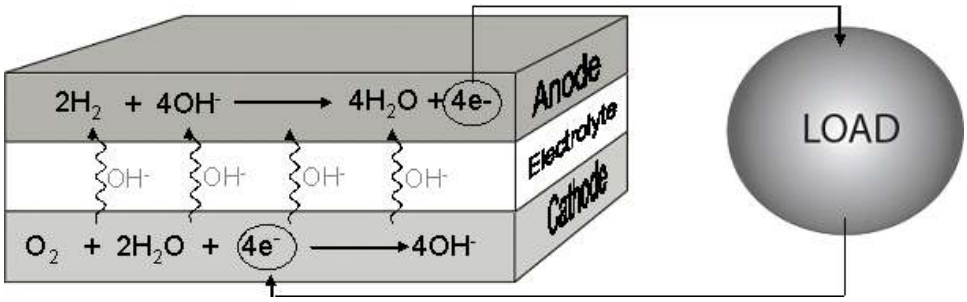

Fig. 2.2. Schematic representation of an alkaline fuel cell.

This type of fuel cell has the advantage of using a reasonably priced electrolyte, potassium hydroxide (KOH). However, they are subject to poisoning in the presence of even a small amount of carbon dioxide (CO_2), resulting a cell malfunction as is shown in Eq. 2-10.

$$2KOH + CO_2 \rightarrow K_2CO_3 + H_2O \qquad (2\text{-}10)$$

2.2 What limits the current in fuel cells?

The amount of energy releasing at the anode side does not mean that the oxidation reaction can proceed without activation energy. The classical energy of this reaction is shown in figure 2-3.

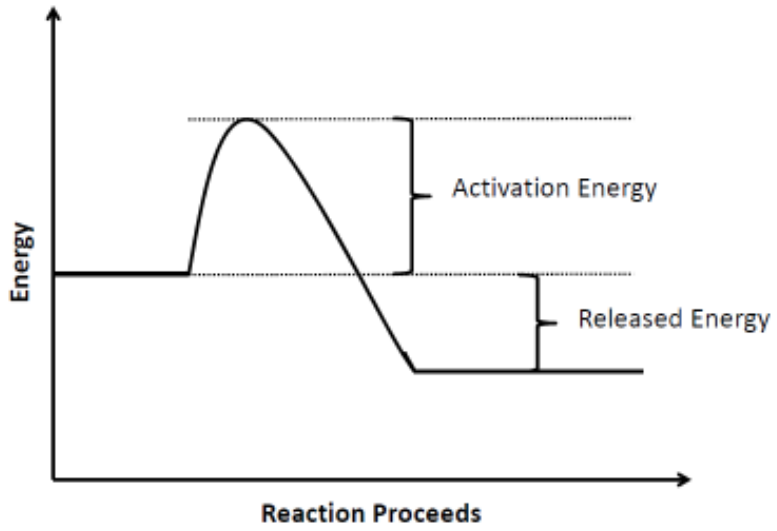

Fig. 2.3. The diagram shows the classical energy for a simple exothermic chemical reaction.

In this reaction activation energy is required to get beyond the "energy hill", though the reaction is exothermic. At low temperatures, the probability of molecules having enough energy to pass the barrier is low, resulting a slow process; however at high temperatures, like in higher temperature fuel cells, the reaction proceeds very fast since probability of molecules having enough energy is higher. In addition, in a fuel cell several factors influence the reaction rate,

- Increase in temperature

- Presence of a catalyst
- Increase in the electrode area.

Presence of a catalyst and increase in the temperature are the two options that can be applied to any chemical reaction, however increase in the electrode area is an important item which is special to fuel cells. On the surface of electrodes hydrogen gas and protons come together to let the reaction proceed; hence, the rate of reaction in a fuel cell is directly proportional to the electrode area. One way to enhance the electrode area is through porosity. In modern fuel cells, electrodes have a microstructure giving them a surface area much greater than their straightforward "length × width". Figure 2.4(a) and 2.4(b) show the nano-structural design of the electrodes used for fuel cell tests in this thesis.

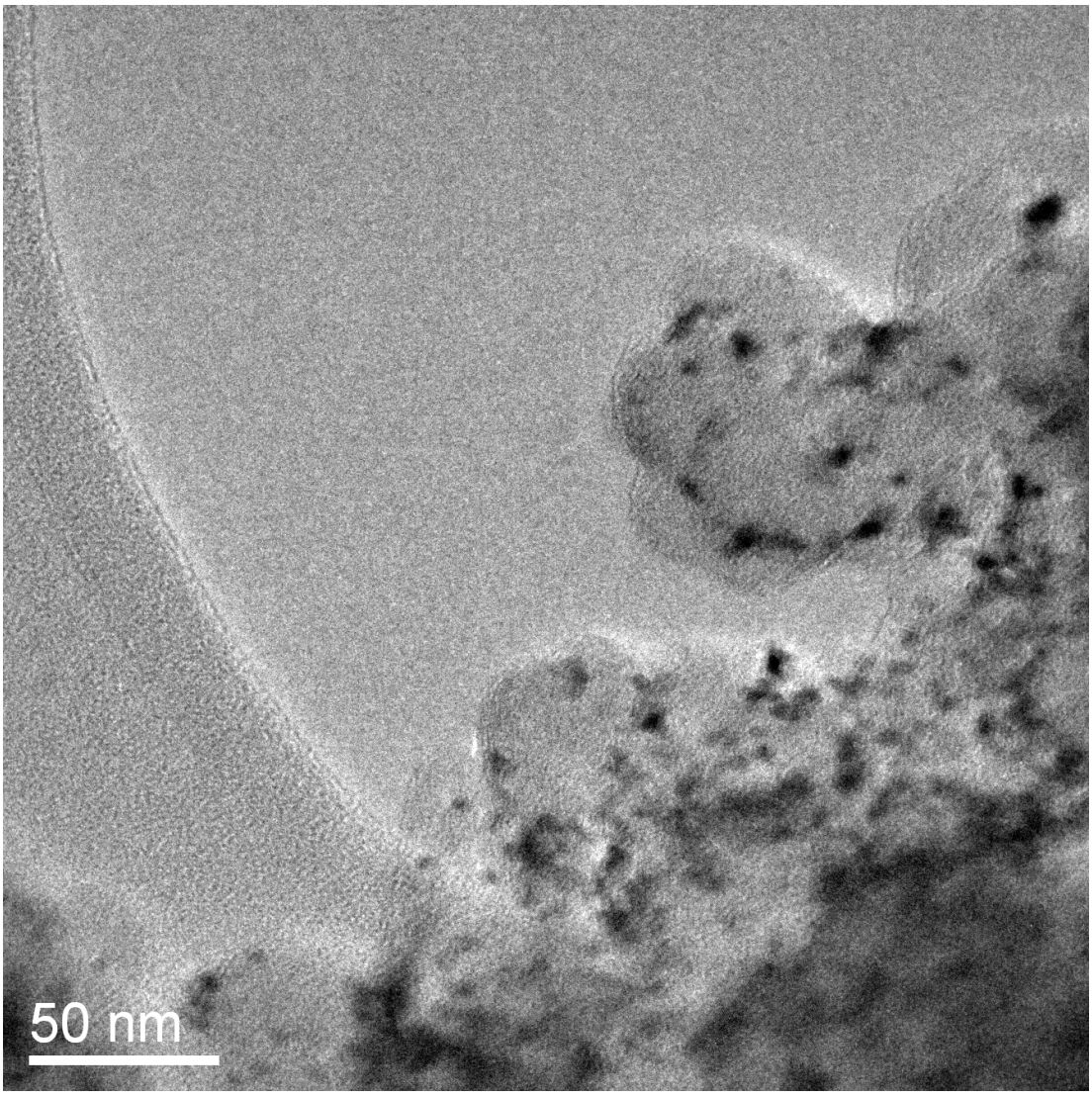

Fig. 2.4(a). The Transmission Electron Microscope (TEM) (scale bar 50 nm) of the E-Tek electrode used to test the fuel cell performance of all electrolytes studied in this thesis. The black specks are the platinum catalyst particles finely divided over a carbon support showing a large surface area.

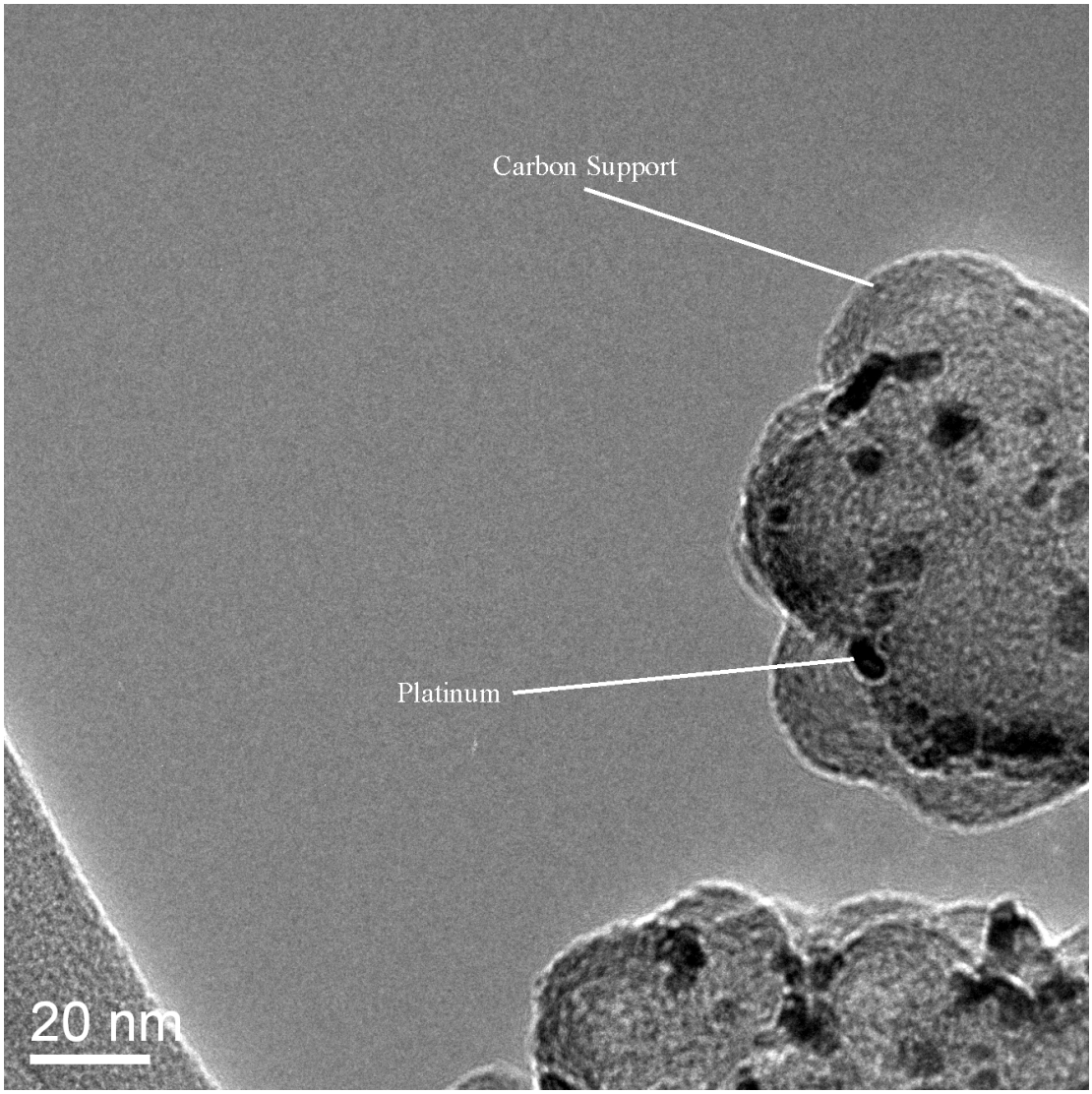

Fig. 2.4(b). The Transmission Electron Microscope (TEM) (scale bar 20 nm) of the E-Tek electrode used to test the fuel cell performance of all electrolytes studied in this thesis. The black specks are the platinum catalyst particles finely divided over a carbon support showing a large surface area.

2.3 Different types of Fuel Cells:

The electrolytes, in fuel cells, are being used to classify them into several types. Several factors can be considered in determining using this classification such as the chemical reaction which takes place in the cell, the type of electrolyte used, the range of temperature at which the fuel cell can operate, the required fuel, and finally the type of catalyst required. Various types of fuel cells are briefly discussed below.

2.3.1 Polymer Electrolyte Membrane Fuel Cell or Proton Exchange Membrane Fuel Cell (PEMFC):

In this type of fuel cell, the electrolyte is made of a polymer that has the characteristic of high-quality proton conduction in the presence or absence of water. The mobile ion in this type of fuel cell is proton, usually hydrated or the hydroxide ion. PEMFCs were first used in the 1960's for the NASA programs. They have the advantages of low volume and weight comparing to other types of fuel cells. In this type of fuel cell, leaking of electrolyte is not an option. They usually operate at low temperatures; therefore, no warm-"up" time is required. The catalyst in this type of fuel cell is mostly platinum that makes it expensive. However, some efforts have been done to replace noble-metals with inexpensive materials such as carbon nanotubes as reported by Wang and his coworkers (Wang *et al.*, 2003)[32]. Proton exchange membrane fuel cells are mainly used for stationary and transportation applications. Currently, Nafion or the hydrated perfluorosulfonic acid polymer membrane (chemical structure is shown in figure 2.5) is considered a standard in polymer electrolyte membrane fuel cells which are quite costly, approximately $\$1200/m^2$, according to *Ion-power Inc.* (Brett *et al.* 2008)[33].

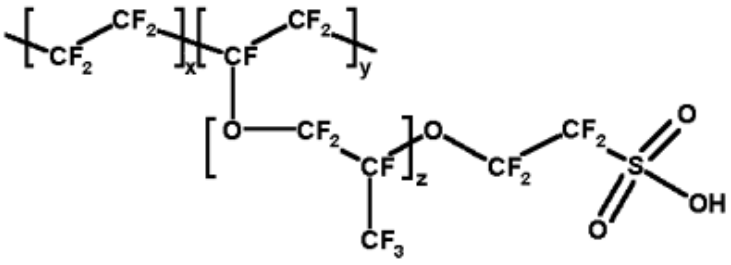

Fig. 2.5. The chemical structure of Nafion (perfluorosulfonic acid polymer membrane).

Figure 2.6 shows a typical assembly in PEMFCs.

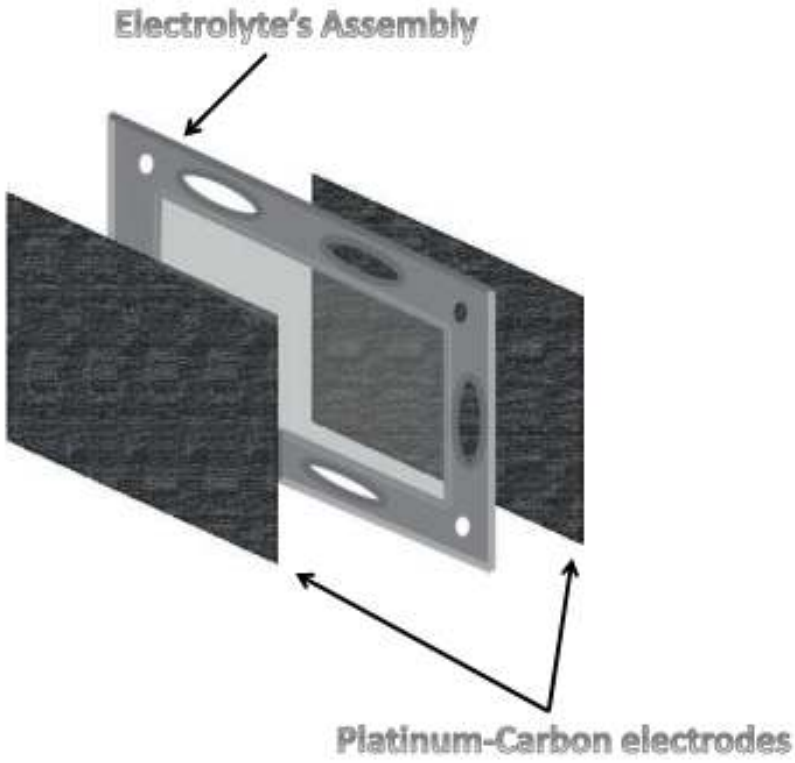

Fig. 2.6. The electrolyte assembly in a proton exchange membrane electrode. The assembly contains the electrolyte, itself, along with the appropriate catalyst. The platinum-carbon electrodes (E-TEK) are also responsible for the diffusion of the fuel.

Some advantages and disadvantages of polymer electrolyte membrane fuel cells are listed in table 2.1.

Advantages	Disadvantages
Solid Electrolyte	Low operating temperature (Below 120^{o}C)
High power density	Water management (If hydrated)
Rapid start-up	Quite costly, mostly because of the electrolyte
Minor possibility of leaking	Poisoning in the presence of CO

Table. 2.1. Advantages and disadvantages of proton exchange membrane fuel cells.

2.3.2 Direct Methanol Fuel Cells (DMFCs):

Direct methanol fuel cells are powered by purified methanol, which is usually diluted with steam and directed to the fuel cell anode. In this type of fuel cell the electrolyte is a polymer as in proton exchange membrane fuel cells. The charge carrier in this type of fuel cell is also proton. The oxidation reaction at the anode side is:

$$CH_3OH + H_2O \rightarrow CO_2 + 6H^+ + 6e^-, \qquad (2\text{-}11)$$

and at the cathode side, electrons and protons react with oxygen to form water.

$$O_2 + 4H^+ + 4e^- \rightarrow H_2O. \qquad (2\text{-}12)$$

The operating temperature in this type of fuel cell is between 50^{o}C to 120^{o}C. Technology of the direct methanol fuel cell is new and its development is approximately a couple of years behind that of other types of fuel cells. The advantages and disadvantages of this type of fuel cell are listed in table 2-2.

Advantages	Disadvantages
No fuel reformer	Low efficiency & fuel crossover
Low cost	Low operating temperature (Below 120^{o}C)
Room to develop	Low power density

Table. 2.2. Advantages and disadvantages of direct methanol fuel cells.

2.3.3 Alkaline Fuel Cells (AFCs):

Alkaline fuel cells, were discussed earlier in this chapter, are old in fuel cell technology. They were first studied by Reid (Reid 1902)[34]. They were used to produce water and energy in the U.S. space programs. The electrolyte in this type of fuel cell is an aqueous solution of potassium hydroxide (KOH). The working temperature range in this type of fuel cell is between 60^{o}C and 260^{o}C (Gülzow 1996)[35]. There exist various types of alkaline fuel cells:

- cells with a free liquid electrolyte between two porous electrodes,
- ELOFLUX cell with liquid KOH in the pore-systems,
- matrix cell where the electrolyte is fixed in the electrode matrix,
- and the falling film cell.

All types of alkaline fuels cells contain porous electrodes. Some advantages and disadvantages of this type of fuel cell are listed in table 2-3.

Advantages	Disadvantages
Low cost	Preparation method of the electrodes
Variety of electrodes	Sensitive to poisoning by CO_2
Rapid start-up	Low life time of the electrode

Table. 2.3. Advantages and disadvantages of alkaline fuel cells.

2.3.4 Phosphoric acid fuel cells (PAFCs):

It was the first fuel cell to be commercialized. (Larminie & Dicks 2003)[30] Phosphoric acid fuel cell is based on an immobilized phosphoric acid electrolyte. The operating temperature is between 150-220^{o}C (under applied pressure), since the ionic conductivity of phosphoric acid is much lower at low temperatures.

In this type of fuel cell usually air is used as the oxygen source and hydrogen as the fuel. One of the advantages of phosphoric acid fuel cells comparing to alkaline fuel cells is that they tolerate approximately 2% of the carbon monoxide (Kordesch & Simader 1995)[36].

Phosphoric acid fuel cell utilizes platinum electrodes (the catalyst) incorporated into porous carbon electrodes. The charge carrier in this type of fuel cell is the proton. Some advantages and disadvantages of phosphoric acid fuel cells are given in table 2.4.

Advantages	Disadvantages
High stability	Low operating temperature at ambient Pressure (<150^{o}C)
High performance	Expensive platinum as catalyst
Low cost	Large size
Low contamination with CO	Large weight
Simple construction	Low power
Low electrolyte volatibility	Low current

Table. 2.4. Advantages and disadvantages of phosphoric acid fuel cells.

2.3.5 Molten Carbonate fuel cells (MCFCs):

They are usually preferred, more than phosphoric acid fuel cells, when it comes to operation of the fuel cell on coal derived fuels. They operate at high temperatures[37] 650^{o}C, their efficiency is higher than phosphoric acid fuel cells; as a result, the polarization of the oxygen cathode reduced significantly. At the anode and cathode side the following reactions take place,

$$H_2 + CO_3^{-2} \rightarrow H_2O + CO_2 + 2e^- \quad (2\text{-}13)$$

$$\frac{1}{2}O_2 + CO_2 + 2e^- \rightarrow CO_3^{-2} \quad (2\text{-}14)$$

Since they operate at very high temperatures, they can be used in a combined cycle configuration to produce more electricity from their high-grade waste heat. According to Kordesch & Simader (Kordesch & Simader 1995)[36], molten carbonate fuel cells can be used both in gas turbines and steam turbines, in a combined cycle configuration, in order

to enhance the overall electrical efficiency. The electrolyte in this type of fuel cell is typically nickel-based or more recently a mixture of lithium carbonate and sodium carbonate (Li_2CO_3-Na_2CO_3) or lithium carbonate and potassium carbonate (Li_2CO_3-K_2CO_3). Some advantages and disadvantages for this type of fuel cell are listed in table 2.5.

Advantages	Disadvantages
High efficiency	Slow start-up
Low polarization	Reduction of high temperature corrosion
Low-cost electrolyte	Short lifetime
Absence of an external fuel processor	The need to scale up components

Table. 2.5. Advantages and disadvantages of molten carbonate fuel cells.

2.3.6 Solid oxide fuel cells (SOFCs):

This type of fuel cell has a significant thermodynamic advantage since it can be used as the topping device of a triple cycle in grouping with gas and steam turbines. Such combination can considerably enhance the efficiency of this fuel cell. This type of fuel cell does not suffer from poisoning at all. In addition there is no chance of leakage or high vapor pressure problems which are typical in other type of fuel cells. As a room temperature insulator, Zirconia freely conducts oxygen ions at temperatures above 900^{o}C (Kordesch & Simader 1995)[36]. The reactions that take place in each electrode are,

$$H_2 + O^{2-} \rightarrow H_2O \qquad (2\text{-}15)$$

$$\frac{1}{2}O_2 + 2e^- \rightarrow O^{2-}. \qquad (2\text{-}16)$$

In general solid oxide fuel cells operate over a wide range of temperature starting from 600^{o}C to 1000^{o}C. Alternative electrolytes are also available. Ceramic materials such as Y_2O_3-ZrO_2 are good conductors to oxygen ions as well. Since they operate at very high temperatures, they have been considered as the best type of fuel cell for high-power applications such as industry and extensive power stations as discussed by Minh (Minh 2004)[38]. Advantages and disadvantages for this type of fuel cell are listed in table 2-6.

Advantages	Disadvantages
Wide operating temperature	Very slow start-up
Absence of gas cross-over	Expensive material for construction
High efficiency	Sealing problems
No Poisoning or leakage	The need to scale up components

Table. 2.6. Advantages and disadvantages of solid oxide fuel cells.

2.3.7 Biological fuel cells (BFCs):

This type of fuel cell uses an organic fuel, such as ethanol or methanol. However, enzymes are involved rather than conventional chemical catalysts like platinum electrodes. In this type of fuel cell, the energy is being derived from organic fuels. There is no commercial application for this type of fuel cell.

2.3.8 Regenerative fuel cells (RFCs):

This type of fuel cell, typically known as "redox flow" cell was studied by Vincent & Scrosati (Vincent & Scrosati 1997)[39] where during charging the reactants are removed from the electrodes then stored. Therefore its capacity can be huge. By resupplying the reactants to the electrodes, the discharging occurs.

They are called fuel cells because of the supply of chemicals to the electrodes. They are usually being used to make large capacity rechargeable batteries. They possess different types of cells, For instance:

- cells based on vanadium have been introduced (Shibata & Sato 1999)[40]
- zinc-bromine system (Lex & Jonshagen 1999)[41]

This type of fuel cell can be best exemplified as "Regenesys" fuel cell as was first introduced by Zito (Zito 1997)[42] and then followed by Price and his coworkers (Price *et al.*, 1999)[43].

The operation of Regenesys is based on a two fluid system as shown in figure 2.7. A sodium sulfide (Na_2S_2) aqueous solution feeds to the negative electrode when the system is fully charged.

$$2Na_2S_2 \rightarrow Na_2S_4 + 2Na^+ + 2e^- \qquad (2\text{-}17)$$

The sodium ions then pass through the electrolyte and an ion selective membrane to allow the following reaction to occur:

$$NaBr_3 + 2Na^+ + 2e^- \rightarrow 3NaBr \qquad (2\text{-}18)$$

The principle of operation of a redox flow cell is shown in figure 2.7.

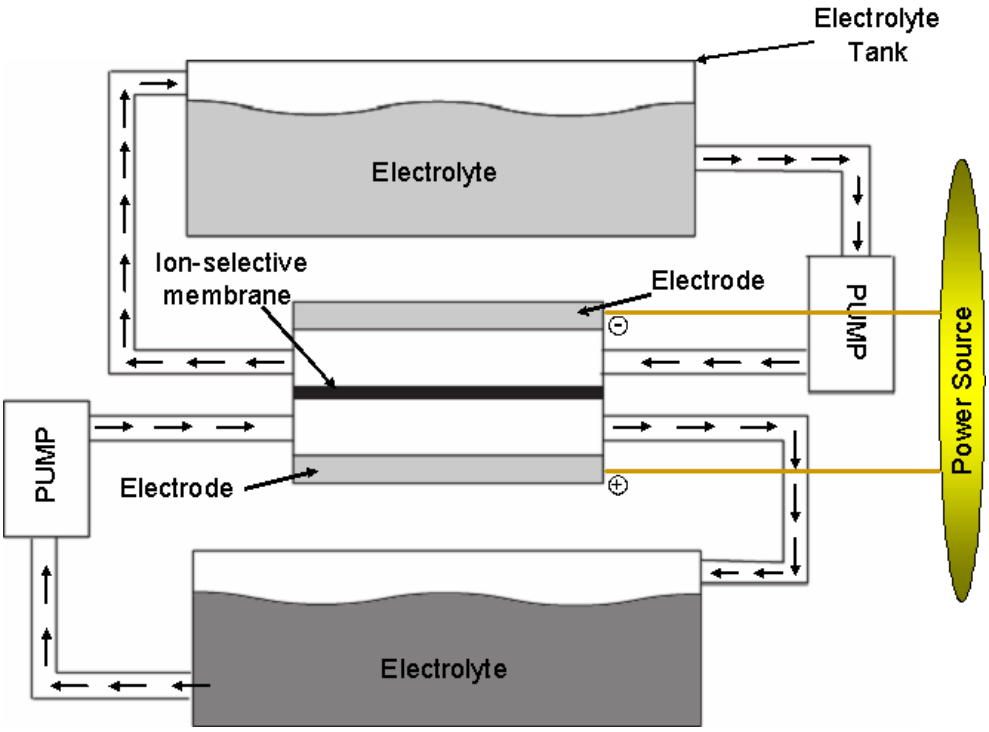

Fig. 2.7. The schematic representation of a redox flow cell or regenerative fuel cell explained above.

Some applications and main advantages of various types of fuel cells are summarized in figure 2.8.

Efficiency of fuel cells will be discussed in a different section in detail.

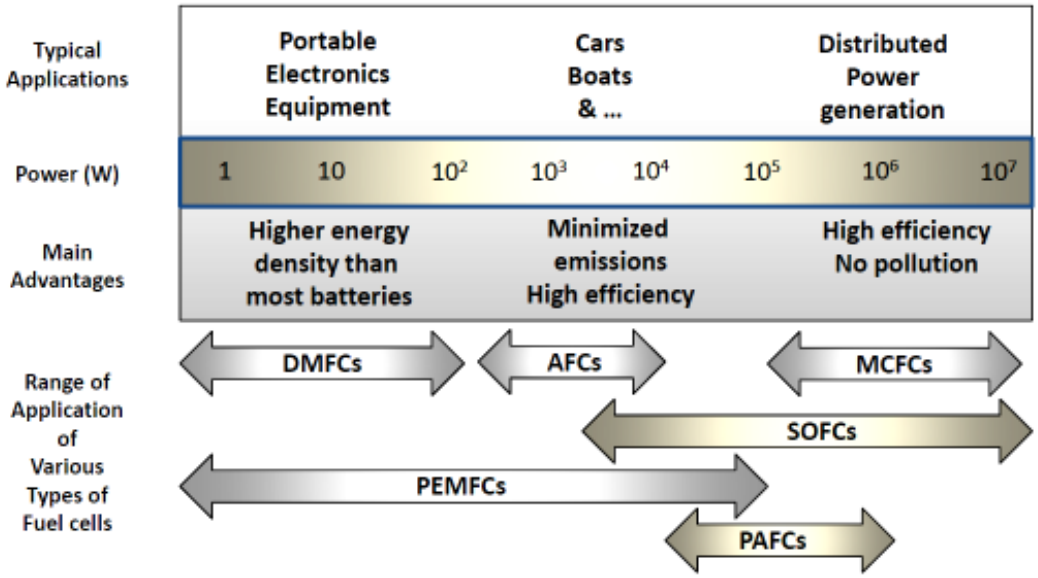

Fig. 2.8. Some typical applications and main advantages for different types of fuel cells adapted from Mench, (Mench 2008)[47] with permission.

2.4 Efficiency (ε) in Fuel Cells:

According to thermodynamics (Carnot Cycle), under ideal conditions no heat engine can convert all the heat energy into mechanical energy. The maximum efficiency in the Carnot engine can be defined as:

$$\varepsilon_{\max} = \frac{T_h - T_l}{T_h} \quad , \tag{2-19}$$

where T_h is the heat generated at high temperature, T_l is the temperature of the system after some work is done by the mechanical energy. As it can be inferred from Eq. 2-19, the maximum efficiency can be achieved when the difference between T_h, and T_l is greatest. The maximum efficiency in combustion engines rarely exceeds 30%. However, the story is quite different for fuel cells. It is well known that fuel cells are not subject to the Carnot efficiency limit. It is generally supposed that if the system has minimum

irreversibilities then the efficiency in principle reaches approximately 100%. In fuel cells, the electrical energy is directly generated from chemical energy at constant temperatures. So the efficiency of such devices can be defined as:

$$\varepsilon_{electrochemical\ device} = \frac{Electrical\ Energy\ \ Generated}{Changes\ In\ \ The\ Gibbs\ Free\ Energy} \tag{2-20}$$

Since fuel cells use materials that are usually burnt, it would make sense to compare the heat that would be produced by burning the fuel to the electrical energy produced in a reaction. This is well known as calorific value and to be more precise "reaction's enthalpy of formation (ΔH)". Since the energy is released the enthalpy of formation is negative. Therefore, the thermodynamic efficiency of a fuel cell can also be defined as the ratio of the chemical energy produced over the changes in the enthalpy of the reaction.

$$\varepsilon_{fuel\ cell} = \frac{-\Delta G_{reaction}}{-\Delta H_{reaction}} \tag{2-21}$$

Figure 2-9 compares the maximum efficiency of hydrogen fuel cells at standard pressure to the Carnot limit.

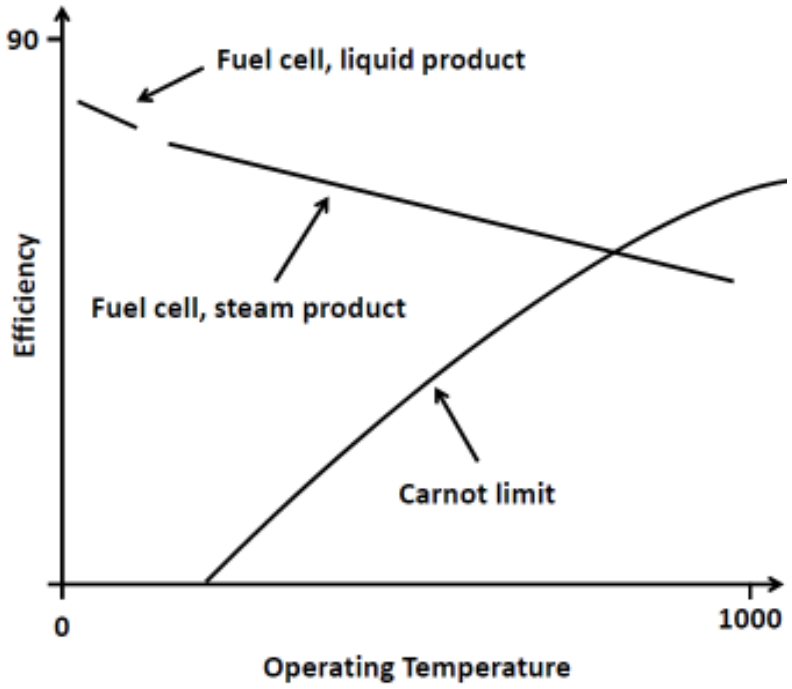

Fig. 2.9. Maximum efficiency of hydrogen fuel cells at standard pressure compared with the Carnot limit with a 50°C exhaust temperature.

The overall fuel cell's efficiency can be obtained from equation 2-22.

$$\varepsilon_{Total} = \varepsilon_t \, \varepsilon_v \, \varepsilon_u \tag{2-22}$$

where, ε_t : is the thermodynamic efficiency

$$\varepsilon_t = \frac{-\Delta G}{-\Delta H} \tag{2-23}$$

ε_v : is the voltage efficiency reflecting irreversible polarization losses of the system which includes ohmic polarization, concentration polarization, and activation polarization. The voltage efficiency is typically defined as:

$$\varepsilon_v = \frac{V}{E_{rev}} = \frac{E_o - \Delta V_{ohmic} - \Delta V_{concentration} - \Delta V_{activation}}{E_{rev}} \tag{2-24}$$

where V is the actual operational voltage of the fuel cell, E_{rev} is the reversible thermodynamic voltage, E_o is the open circuit potential, ΔV_{ohmic} is the voltage drop due to ohmic polarization, $\Delta V_{concentration}$ is the voltage drop due to concentration polarization, and $\Delta V_{activation}$ is another voltage drop which occurs due to activation polarization. All types of voltage drops will be discussed in detail later in this thesis.

ε_u : is the fuel utilization efficiency which can be expressed as the ratio of the amount of fuel used by the fuel cell to the amount of fuel introduced as the input. If the amount of current generated by the fuel cell is, i, and the fuel is supplied with a rate equal to r_{input} in (mol/sec) then the utilization efficiency can be defined as:

$$\varepsilon_u = \frac{i}{n F r_{input}}, \tag{2-25}$$

where n is the number of electrons generated by the fuel cell, and F is the Faraday constant. Reasons to such loss in voltage are (a) the application of reactant for auxiliary purposes. For instance a typical method to take away the produced water from the cathode side in a fuel cell is to exert excess flow of oxygen to push the water aside from the membrane especially for water sensitive membranes. (b) the diffusion of reactants (gases) through the membrane well known as crossover of gasses. (c) the partial oxidation of the fuel introduced to the fuel cell.

It is generally accepted that there exist a connection between the maximum electromotive force (or the reversible open circuit voltage) (E) of the cell and operating voltage of the fuel cell to the maximum efficiency of the fuel cell.

$$E = \frac{-\Delta H}{2F} \tag{2-26}$$

Then the cell efficiency can be defined as:

$$\varepsilon_{cell} = \frac{V_c}{E} \tag{2-27}$$

The maximum efficiency of a fuel cell can be up to three times higher than that of a Carnot cycle combustion engine resulting a more efficient way of generating energy.

The operating efficiency for various types of fuel cells is shown in table 2-7.

Type of Fuel cell	Fuel	Mobile ion	Temperature‡ ^{o}C	Operating efficiency† (%)
AFC: Alkaline fuel cell	H_2	OH^-	100-250	40-55
SOFC: Sold oxide fuel cell	Hydrocarbons, CO	O^{2-}	700-1000	Above 50
MCFC: Molten carbonate fuel cell	Hydrocarbons, CO	CO_3^{2-}	500-700	Above 50
PEMFC: proton exchange membrane fuel cell	H_2	H^+	30-110	35-45
PAFC: Phosphoric acid fuel cells	H_2	H^+	150-250	40
DMFC: Direct methanol fuel cell	Methanol fuel	H^+	20-90	30-35

†: (Hoogers, 2003)[44]
‡: (Haile, 2003)[45]

Table 2.7. This table compares the operating temperature ranges and efficiencies in various fuel cells.

2.5. Polarization curves in fuel cells:

The typical illustration of a polarization curve for a fuel cell is shown in figure 2.10.

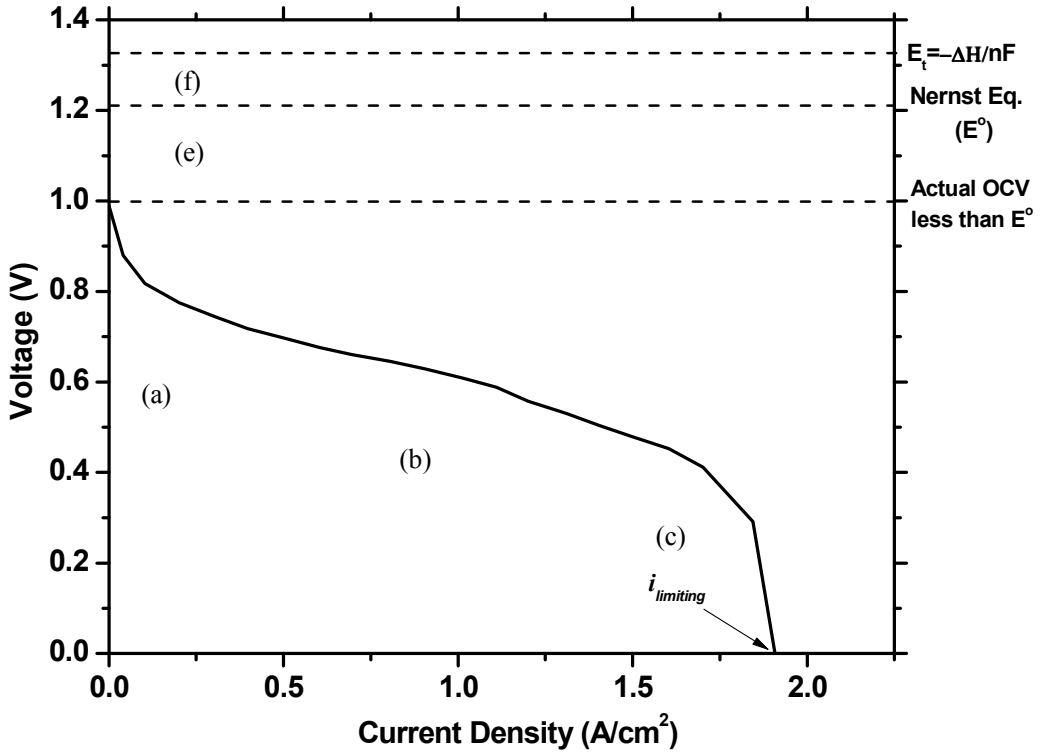

Fig. 2.10. A typical polarization curve for a fuel cell with negative entropy of reaction (i.e. hydrogen-oxygen fuel cell) showing: kinetic, ohmic, concentration and crossover potential losses.

This type of polarization curve which represents a cell voltage-current density relationship a typical method of evaluation of fuel cells performance. The current density, scaled by geometric electrode area allows results to be scalable among various size cells. The five regions (Mench 2008)[46] on the polarization curve show:

(a) The loss due to the activation (kinetics) overpotential at the electrodes.

(b) Losses due to the ohmic polarization of the fuel cell including all electrical and ionic conduction losses through the electrolyte, layers, catalyst, contacts, and cell interconnects.

(c) Losses in this region are due to the concentration polarization of the fuel cell caused by mass transport limitations of the reactants to the electrodes.

(d) In this region losses occur due to the departure from the Nernst thermodynamic equilibrium potential which could be major loss due to undesired species crossover through the electrolyte, internal currents from electron leakage through the electrolyte or any impurities.

(e) The losses in region (f) represent the departure from the maximum thermal voltage. This can cause because of the entropy change which cannot be engineered. In condition that the changes in entropy are positive (which is not the case here) the Nernst voltage is actually greater than the thermal voltage and heat generation by entropy change will be negative.

The ohmic losses occur when there is a current; however it only dominates losses in region (b). The activation overpotential also dominates in the low-current region (a) but if still contributes to the cell losses at higher current densities where the ohmic or concentration polarizations dominate.

2.5.1 Activation polarization:

This type of polarization dominates losses at low current density. Activation polarization is the required voltage overpotential to overcome the activation energy of a reaction (on the catalytic surface) electrochemical in nature. (Mench 2008)[47]

$$E_{cell} = E^{o}(T,P) - \left[\varepsilon_{a,a} + \left|\varepsilon_{a,c}\right|\right]^{\#} - \varepsilon_{r} - \varepsilon_{m,a} - \left|\varepsilon_{m,c}\right| - \varepsilon_{x} \qquad (2\text{-}28)$$

The activation polarization at the anode and cathode shown in the bracket $[\ldots]^{\#}$ in the above equation are the anodic (*a,a*) and cathodic (*a,c*) polarizations representing the required voltage loss to initiate the reaction.

Electrical Double Layer, is an additional expression for the activation polarization at an electrode which is a microscopic process occurring at the electrodes during charge transfer. A schematic representation of the electrical double layer is shown in figure 2.11. The electrical double layer is a complex structure. At the surface of electrode and the adjacent electrolyte a build-up of charge occurs. Depending on the electrolyte the charge could be positive or negative. At the anode side, the potential is lower than the surrounding electrolyte so a buildup of negative charge along the surface of the catalyst (mostly Pt) and positive charge in the surrounding electrolyte forms a double layer structure. The double layer structure consists of an "inner Helmholtz plane" exists along the electrical centers of specifically adsorbed reactant ions. An "outer Helmholtz" plane forms along the locus of the centers of nearest layers of solvated ions in the

electrolyte. Beyond the outer layer (dashed line), other solvated ions in the electrolyte can interact with catalyst surface through the long-range electrostatic interaction in the diffuse layer. The three layers of the electrical double layer usually width less than 10 nm.

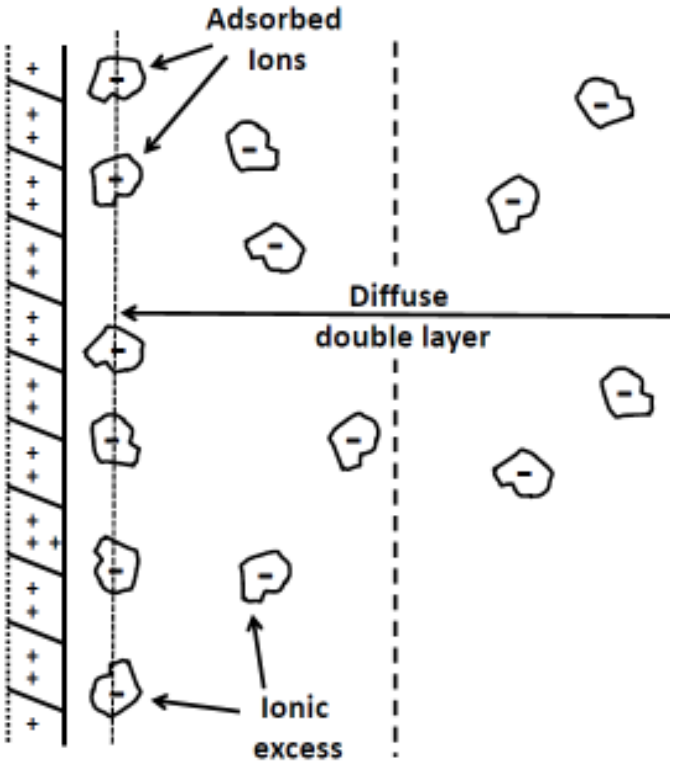

Fig. 2.11. Schematic representation of the electrical double layer.

The activation polarizations are non-linear and appears as a sharp initial drop in cell voltage from open-circuit conditions followed by showing an excess loss as the current is increased through ohmic and concentration polarization regions. Different activation losses occur in each one of the electrodes and reactions occurring at each electrode are related to the conservation of charge. The activation polarization losses can be influenced by:

(1) ***Reaction Mechanism*:**

Typically, a more complex reaction will cause a greater overpotential which is required to break the chemical bonds and generate current. Also, there exist other factors involved.

(2) ***Type of catalyst:***

It is generally accepted that poor choices of catalyst causes greater loss, hence requires a greater polarization to enable the electrochemical reaction to occur. Depending on the type of electrolyte, and the electrochemical reaction, different catalyst must be chosen and it does not exist as a single ideal catalyst. At low-temperatures, noble metal catalysts such as platinum work the best and at higher temperatures less expensive metals such as nickel or cheap alloys could be used.

(3) ***Catalyst layer morphology:***

One of the factors strongly affecting the effectiveness of a catalyst is the microstructures of a catalyst. The potential reaction locations on a three dimensional catalyst are restricted to locations with immediate access to ionic and electronic conductors, catalyst, and the fuel (gas).

(4) ***Operating Parameters:***

Like chemical reactions, the catalytic reaction in fuel cells increases by temperature due to an increase in the kinetic energy of the reaction, thus; higher probability of collisions. Other thermodynamic parameters such as pressure are also effective.

(5) ***Poisoning and Impurities:***

In general, presence of any catalyst poisons or impurities in the reaction flow can lessen the performance to a great extent. Impurities, as low as parts per million, such as carbon monoxide and sulfur dioxide can radically reduce the performance of a fuel cell.

(6) ***Concentration of species:***

Throughout a highly non-equilibrium electrochemical reaction process, there exist a concentration effect on the activation polarization of the system. More sparse species can cause the double layer polarization more time to draw enough reactant. When the concentration is minimized no reaction can take place across the double layer.

(7) ***Service history:***

Other factors, such as environmental condition, load cycling and voltage history, generally known as the service history; can affect the performance of a fuel cell as well.

(8) ***Age:***

Finally, the operating life time of a fuel cell can change its performance to a great extent. This can be due to physical morphological or chemical changes in the catalyst.

2.5.2 Ohmic polarization:

The ohmic polarization appears as a primarily linear region in the polarization curve. Any reduction in voltage in this region is dominated by the internal ohmic losses (ε_r) through the fuel cell. The activation polarization and concentration polarization are still present in this region. The ohmic polarization can be represented as:

$$\varepsilon_r = i\,A\left(\sum_{k=1}^{n} r_k\right), \tag{2-29}$$

where r_k is the area-specific resistance of any individual cell which includes:

- ionic resistance of the electrolyte
- electric resistance of bipolar plates interconnects
- contact resistance between mating parts

Electronic and ionic resistance:

According to the ohm's law:

$$V = I\,R = i\,A\,R \tag{2-30}$$

where R is the resistance in units of ohms ($\Omega = Js/C^2$), A is the electrode surface area. The resistivity ρ is a property of a material which is related to resistance through the distance between the electrodes (l) and the cross-section area of electrodes (A). The resistance and resistivity are typically used to describe the ohmic drop in a specific material that shows resistance. By definition:

$$\sigma = \text{conductivity} = \frac{1}{\rho} = {}^{1}\!/_{\Omega\,m} = {}^{S}\!/_{m} \tag{2-31}$$

and conductance:

$$G = \text{conductance} = \frac{1}{R} = \Omega^{-1} = S \tag{2-32}$$

Then ohm's law can be written as:

$$V = i\,A\frac{l}{\sigma\,A} = \frac{i\,l}{\sigma} = i\,\rho\,l \tag{2-33}$$

Some factors affecting the ohmic losses are:

- Material conductivity
- Material thickness
- Contact resistance
- Cell Assembly

Typical conductivity and resisitivity in various fuel cell materials are shown in table 2.8.

Component	Typical Bulk Through-Plane Conductivity σ	Typical Electrolyte's Thickness	Functional Dependencies
PEFC electrolyte	10 S/m (hydrated)	50-200 μm	Temperature, water content
SOFC electrolyte	1-10 S/m (>800°C)	10-300 μm	Temperature, dopants (conductivity through oxygen Vacancies)
AFC electrolyte	on the order of 1-100 S/m at operating temperature	05-2.0 mm	Ion concentration, temprature charge number on ion, dielectric constant of solution, mobility, viscosity, degree of ion dissociation. Other liquids
MCFC electrolyte	on the order of 1-100 S/m at operating temperature	05-2.0 mm	See AFC electrolyte
PAFC electrolyte	on the order of 1-100 S/m at operating temperature	05-2.0 mm	See AFC electrolyte
PEFC bipolar plate (graphite)	5000-20,000 S/m	2-4 mm each	Oxide film (corrosion), materials, coating
PEFC gas diffusion layer (GDL)	10,000 S/m	100-300 μm	Approximately constant
PEFC catalyst layer	≈1-5 S/m	5-30 μm	Morphology, Nafion and carbon loading, age
Contact resistance for cell	Very low if built well; resistance ≈ 30 $m\Omega\ cm^2$	Not available	Compression, pressure, temperature, age (corrosion), number of cycles, and others. current collector total landing area
Total cell resistance (based on active cell area)	Total resistance < 100 $m\Omega\ cm^2$ --------	Not available	See above

Table 2.8. Typical conductivity and resisitivity in different types of fuel cells. Adapted from Mench (Mench 2008)[47] with permission.

2.5.3 Concentration polarization:

A reduction in reactant in the reactant surface concentration can cause concentration polarization which reduces the thermodynamic voltage from the Nernst equation and the current density. Some factors affecting the concentration polarization are:

(1) Gas-phase diffusion limitation

(2) Liquid-phase Accumulation and pore blockage limitation

(3) Build-up of Inert Gases

(4) Impurities

2.5.4 Other types of polarization losses:

The departure from the theoretical OCV is another loss appears in the polarization curve which can cause due to:

(1) Electrical short circuit in the fuel cell:

This can happen if the cell is poorly designed or assembled or more usually the electrolyte is not an absolute isolator for electrons. The electrical short circuit is commonly occurred in high-temperature fuel cells.

(2) Crossover of reactants:

It causes mixed-potential reaction at the opposite electrode. The species is crossover also more likely to occur in “high-temperature fuel cells” and in thin membranes in proton exchange membrane fuel cells as shown in figure 2.12.

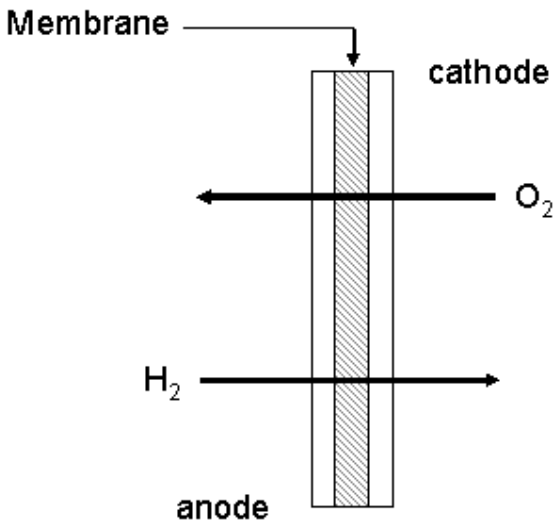

Fig. 2.12. Gas Crossover in proton exchange membrane fuel cells.

2.6. Cost and production in fuel cells:

As it was mentioned earlier in this chapter, some important features of fuel cells such as their efficiency, startup time, weight, size, and type of electrode, type of electrolyte, lifetime, and reliability can affect their popularity. Chemical reactors are regularly fabricated with a few or even single devices; however fuel cells and energy generation reactors for future distributed power generation are heading for mass production, hence; fabrication in fuel cells is considered the most critical issue. For more information regarding cost production of fuel cells please see reference 48 (Kolb 2008)[48]

2.6.1 Factors affecting fuel cell's cost:

Studies by Arthur D. (Teagan *et al.* 1998)[49] along with reports set by the US Partnership of New Generation Vehicles (PNGV) (Kolb 2008)[48] have shown that the cost

for a drive train fuel processor had been limited to 30-50 US$ kW^{-1} which seems to be very ambitious. The target cost for fuel cell systems were around 1500 US$, however recent investment costs are approximately 15000 to 20000 US$. (Garche & Jörissen 2003)[50]. There exist four major factors affecting the cost of fuel cells:

- Type of fuel cell
- Fabrication technique
- Production quantity
- Cost of catalyst

The type of fuel employed is considered one of the most important factors affecting the cost of fuel cells. The fabrication techniques which are suitable for mass production need to be used. The cost of catalyst used in fuel cells might play an important role in the overall cost and can reach values as high as 38%. Lastly, the quantity of fuel cells produced has a strong impact on fuel cell's cost.

CHAPTER 3

Experimental

A brief description to various methods used to research the materials in this thesis are given in this section. The method of preparation of each material, used in to study, will be given in its corresponding chapter.

3.1 Electrochemical reaction:

Electrochemistry has always been a bridge between the electrical and chemical effects. A considerable part of electrochemistry deals with the understanding of chemical changes caused by passing of electric current and production of the energy (electrical) by a chemical reaction. This is an interesting field covering a wide variety of phenomena such as corrosion and devices like sensors, batteries, and fuel cells. In this section, the terms and concepts which are being used to describe the electrode reactions are introduced. Among the electrode/electrolyte interface, the charges are transported through the circuit by the movement of electrons. In the electrolyte phase, on the other hand, the charge carriers are ions. In an electrochemical cell, the difference in the electric potential between electrodes can be measured which is usually done by an impedance voltmeter. The cell potential is the difference in potential (voltage) between two electrodes. Figure 3.1 shows two typical types of electrochemical cells. (Bard & Faulkner 2001)[51]

Cell (a) can be written compactly as:

$$Zn / Zn^{2+}, Cl^{-} / AgCl / Ag , \qquad (3\text{-}1)$$

where the slash represents a phase boundary, and a comma simply distinguishes the two components.

Cell (b) also can be written as:

$$Pt / H_2 / H^+, Cl^- / AgCl / Ag\,, \tag{3-2}$$

Since, in here, the gaseous phase is involved should be written next to its corresponding conducting element.

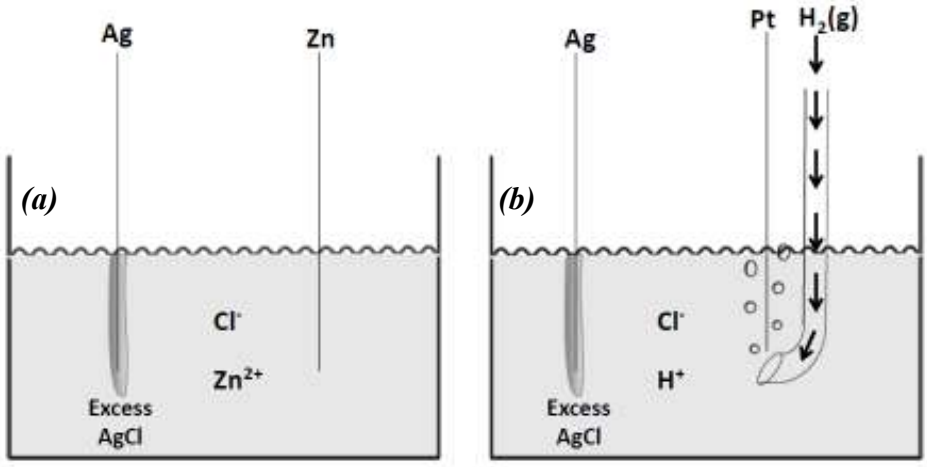

Fig. 3.1. Two typical electrochemical cells. (a) Zn and Ag (covered with AgCl) in $ZnCl_2$ solution and (b) Pt/H_2 along with AgCl in HCl solution.

Each half reaction is related to the interfacial potential difference at the corresponding electrode. Usually one of the half reactions is of interest which occurs at the *working* electrode. The other side of the cell can be standardized by using the *reference* electrode.

The primary reference which is accepted internationally is the *standard hydrogen electrode* (SHE) or *the normal hydrogen electrode* (NHE) which can be presented as:

$$Pt / H_2 (a = 1) / H^+ (a = 1, aqueous) \tag{3-3}$$

The potentials are reported with respect to the reference electrodes. Another reference electrode is the *saturated calomel electrode* (SCE) which is:

$$Hg / Hg_2Cl_2 / KCl\ (saturated\ in\ water) \quad (3\text{-}4)$$

Its potential is 0.242V versus NHE. Another typical type of reference is the *silver-silver chloride electrode* which can be shown as:

$$Ag / AgCl / KCl\,(saturated\ in\ water) \quad (3\text{-}5)$$

where the potential in this type of reference is 0.197V versus NHE.

The reference electrode has always the same constant makeup and therefore its potential is constant, hence the changes in the cell are ascribed to the working electrode. As was mentioned earlier, the redox reaction occurs in an electrochemical cell. At some specific point, the electrons in the electrolyte (on solutes) find it (free) energetically advantageous to transfer to/from the electrode, depending on the direction of current flow. This flow of electrons from the electrolyte to the electrode is an oxidation current which possesses a critical potential which is related to the standard potential E^o, but of course depending on actual concentrations (Nernst equation).

3.2 Impedance spectroscopy:

The concept of electrical impedance was first introduced by Oliver Heaviside in the 1880s. The common approach of impedance spectroscopy is to apply an electrical voltage or current to the electrodes and observe the resulting current or voltage. The current is dependent on the ohmic resistance of the electrodes, the electrolyte and on the rate at which the reaction takes place at the interface of the electrode and the electrolyte. It is usually considered that the electrode/electrolyte's interface is absolutely smooth, by means of an uncomplicated crystallographic orientation, however; in reality they are uneven, containing structural defects.

Various types of electrical measurement techniques: (Barsoukov & Macdonald 2005)[52]

(1) One technique is to apply a *signal composed of random noise* to the interface and measure the resulting current. This technique has the advantage of fast data collection due to the fact that only one signal is applied to the interface for a short time.

(2) Another approach which is **the most common and the standard approach** is to measure the impedance by *applying a single frequency voltage or current to the interface* and measuring the phase shift and amplitude or the real and imaginary parts of the resulting current at that specific frequency using an analog circuit of the response. Commercial instruments are available which measure the impedance as a function of frequency automatically in the frequency ranges of about 1mHz to 1MHz and are easily interfaced to laboratory microcomputers. The advantages of this approach are the availability of these instruments and the ease of their use, as well as the fact that the experimentalist can achieve a better signal-to-noise ratio in the frequency range of most interest.

Impedance is a more general concept than resistance since the phase differences are taken into account, and it leads to a fundamental and essential concept in electrical engineering. Typically, the impedance can be measured from the ratio of the cell voltage

to the cell current. As it was mentioned earlier, the working electrode acts as an electron counter. Since the electronic state of this electrode (the working electrode) is varied a layer on the surface of this electrode forms which balances the electronic charges between the electrode (electrons) and electrolyte (ions). Applying a small excitation signal makes the cell to response in a linear or pseudo-linear fashion. In such linear system, a sinusoidal potential exerts a sinusoidal current at the same frequency. However, it shows a shift in the current. This is shown in figure 3.2.

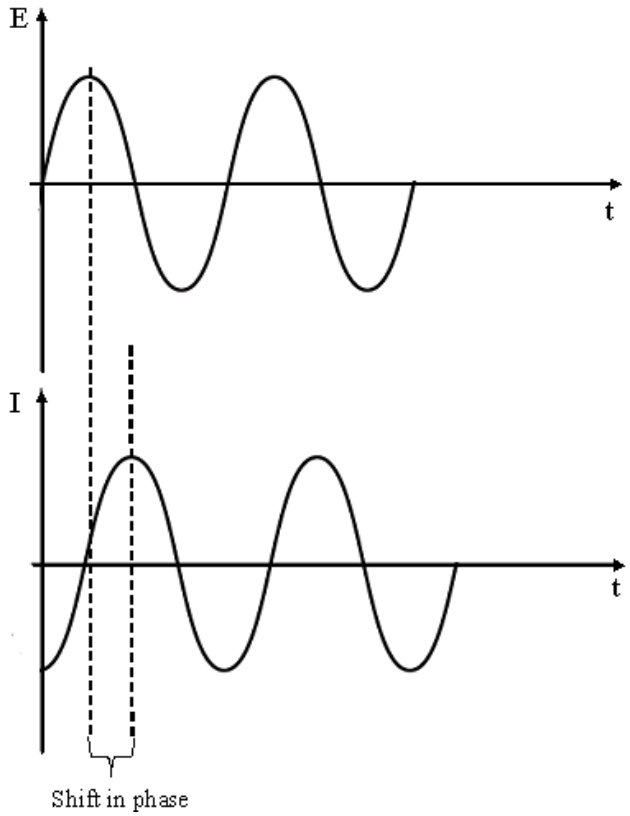

Fig. 3.2. The current response in a linear system.

The amplitude of this current and its phase angle φ can be expressed as:

$$I(\omega) = I_0 e^{i(\omega t+\varphi)} \tag{3-6}$$

where the ω is the frequency in (rad/s), φ is the phase angel in radians. Then the impedance (Z) is:

$$Z = \frac{E}{I} e^{-i\varphi} \tag{3-7}$$

and the real and imaginary part of the impedance are:

$$Z' = \frac{E}{I}\cos(\varphi) \tag{3-8}$$

$$Z'' = -\frac{E}{I}\sin(\varphi) \tag{3-9}$$

The impedance it typically in plotted in a *Nyquist plot* where the real part is shown in the X-axis and the imaginary part is shown in Y-axis of the impedance with a negative phase angle.

An example of the Nyquist plot is shown in figure 3.3.(Gamry Instruments 2010)[53]

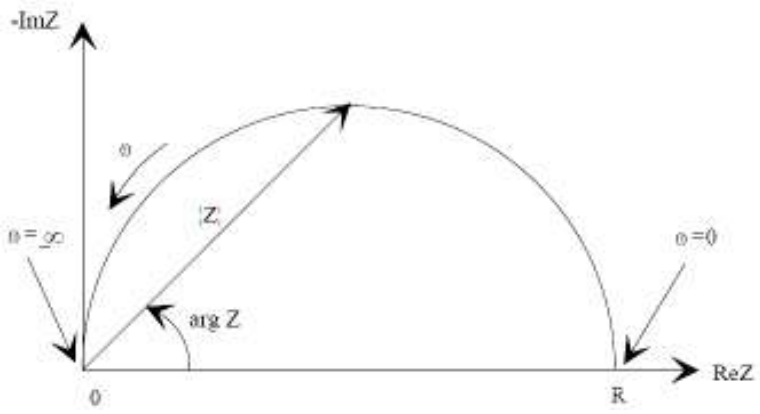

Fig. 3.3. The impedance in the Nyquist plot represented as vectors (arrows) with length $|Z|$ with phase angle of φ shown as arg Z. (Gamry Instruments 2010)

The electrochemical cells can be modeled by equivalent electric circuit with capacitor, resistor, and other components. The Nyquist plot in Figure 3.4 is resulted from the electrical circuit shown in figure 3.4.

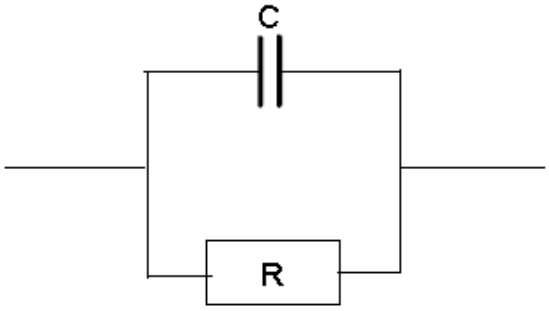

Fig. 3.4. The equivalent electric circuit for a resistor (R) and capacitor (**C**) connected in parallel.

The electrolyte resistance can be determined from the real axis value at the high frequency intercept shown as (R) in the figure 3.4. In our lab in order to conduct the impedance of our samples a PARStat 2273 Potentiostat with PowerSine software was used.

3.3 Viscosity measurements:

Viscosity, as the migration of linear momentum down a velocity gradient, is one of the fundamental characteristics of liquids known. Typically, the measure of the resistance of liquids to flow or shear is called viscosity. It is a function of pressure and temperature. Viscosity exists in two different forms, (a) Dynamic viscosity (b) Kinematic viscosity.

(a) Dynamic Viscosity is the ratio of the shear stress to the velocity gradient. Or the force per unit area which is required to slide on different layers which are shown in figure 3.5 (Viswanath *et al.* 2007)[54].

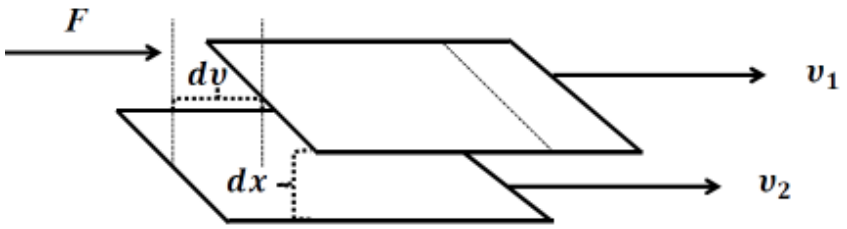

Fig 3.5. A simple form of a shear of a liquid film with two layers on top of each other.

In this figure F is the force causes the two layers to slide at two different velocities υ_1 and υ_2. Viscosity is a measure of resisitivity of a fluid to flow, in mathematical form can be shown as:

$$\text{Shear stress} = \eta \text{ (shear rate)} \tag{3-10}$$

where η is the dynamic viscosity. The shear stress (s) is related to the viscosity by:

$$\eta = s\frac{x}{\upsilon} \tag{3-11}$$

in this equation x is the length, and υ is the velocity or $\frac{dx}{dt}$.

(b) The Kinematic viscosity is dependent on the density ρ of the liquid as well at each individual pressure and temperature. The relation between the Dynamic and Kinematic viscosity is:

$$\kappa = \frac{\eta}{\rho} \tag{3-12}$$

The common unites for viscosity is poise (P), and stokes (St). However the most convenient unit to report the absolute viscosity is *Centipoise* which is one percent of poise. The SI units of Dynamic viscosity are $\frac{N.s}{m^2}$, $\frac{kg}{m.s}$ or $Pa.s$.

All dynamic viscosities reported in this thesis are measured from Kinematic viscosities using two CANNON Kinematic viscometers appropriate for ranges between (a) 500 – 2500 cSt , and (b) 7 – 100 cSt. A specific aluminum block was built for the two viscometers in order to avoid temperature fluctuations larger than ±0.2°C. Figure 3.6 shows the cross-sections of this aluminum block.

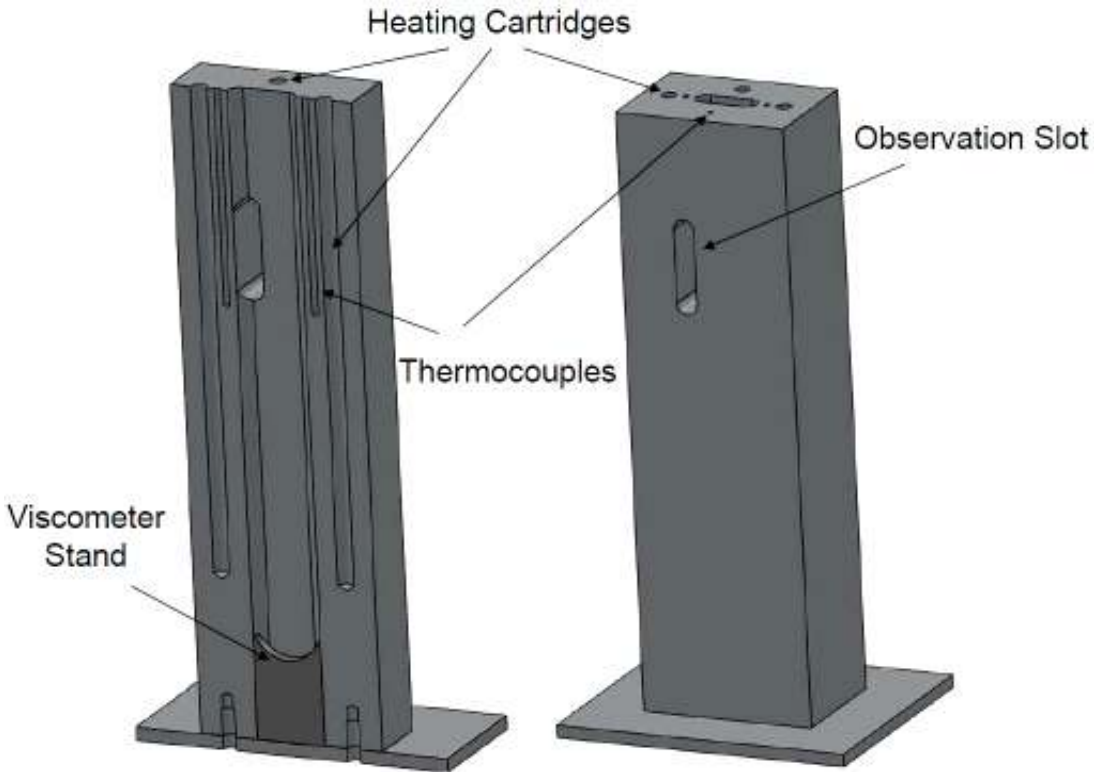

Fig 3.6. Design of the aluminum block used to hold our kinematic viscometers (right) and its cross-section (left).

The precise densities were measured with a graduated 5mm NMR tube and a 1ml graduated test tube in order to convert the Kinematic viscosities into the absolute viscosities.

3.4 Fuel cell polarization:

Fuel cell polarization curve is one of the most accepting methods to test proton conducting electrolytes and membranes. In order to measure this, the proton conducting electrolyte or membrane is typically placed in a Teflon cell and sandwiched between to platinum-carbon electrode, typically the standard E-TEK electrodes which are attached to a platinum-mesh and a wire in order to allow connections to the Pstat. Hydrogen and oxygen (or air) may supply to the cell as fuels. By applying a linear load ramp to the cell, the desired I/V curve can be obtained. For this purpose a PARSTAT 2273 (potentiostat/galvanostat) with high compliance voltage up to ±100 V up to 2A with 1.2 fA of current resolution was used. In order to measure liquid electrolytes, a Teflon cell similar to the one shown in figure 3.7 was used. The electrode surface area for this type of fuel cell is 0.5 cm^2

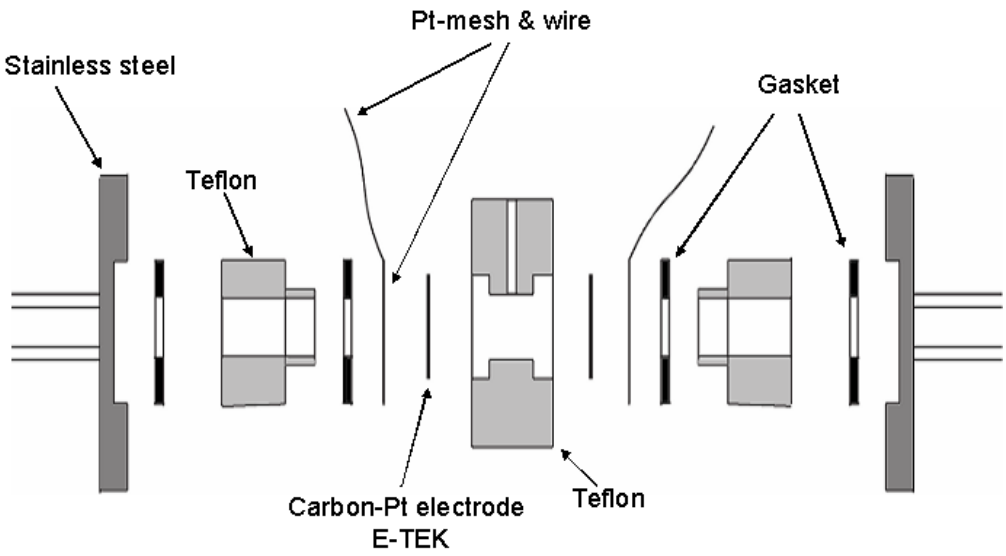

Fig 3.7. The Schematic representation of the Teflon Cell used to measure the polarization curve for our liquid electrolytes.

Figure 3.8 shows the schematic of our polymer membrane fuel cells. In order to solve the contact problem between the membrane and electrode and performance of the cell, a thin layer of ionic liquid (just wetting the surface of electrode), such as demaTf (diethylmethylammonium triflate) which has high thermal stability, and high proton conductivity can be used.

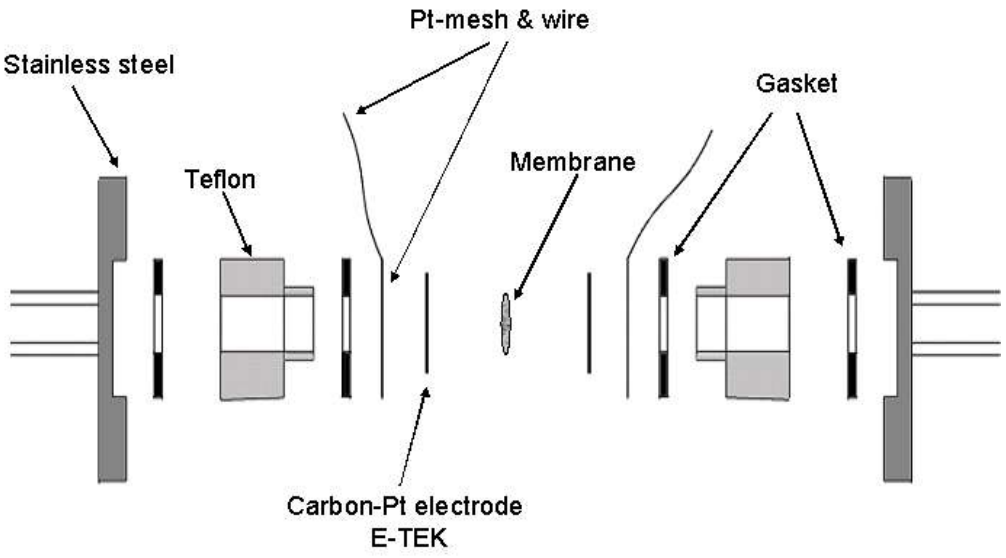

Fig 3.8. The schematic representation of the Teflon Cell used to measure the polarization curve for our solid electrolytes.

3.5 Infrared (IR) Spectroscopy:

Infrared Spectroscopy is a method to either gather information about the structure of a compound and to assess the purity of a compound. It is a part of electromagnetic spectrum in between the visible and microwave regions. The IR region has been divided into the near, mid, and far IR regions. Figure 3.9 shows the wavelengths of various electromagnetic spectrums. Molecules can absorb the Infrared radiation generated by the IR source and based on the vibrational frequency of the bond. In organic molecules most absorption occurs in the mid IR range, therefore the mid IR range is of great use to organic chemists. The IR spectrums are typically reported in micrometer (μm) or in units of wavenumber ($\bar{\nu}$).

All IR spectrums were taken by an FT-IR Matteson Instrument 2020 Galaxy Series using various types of windows (KBr, CaF) based on the nature of the sample.

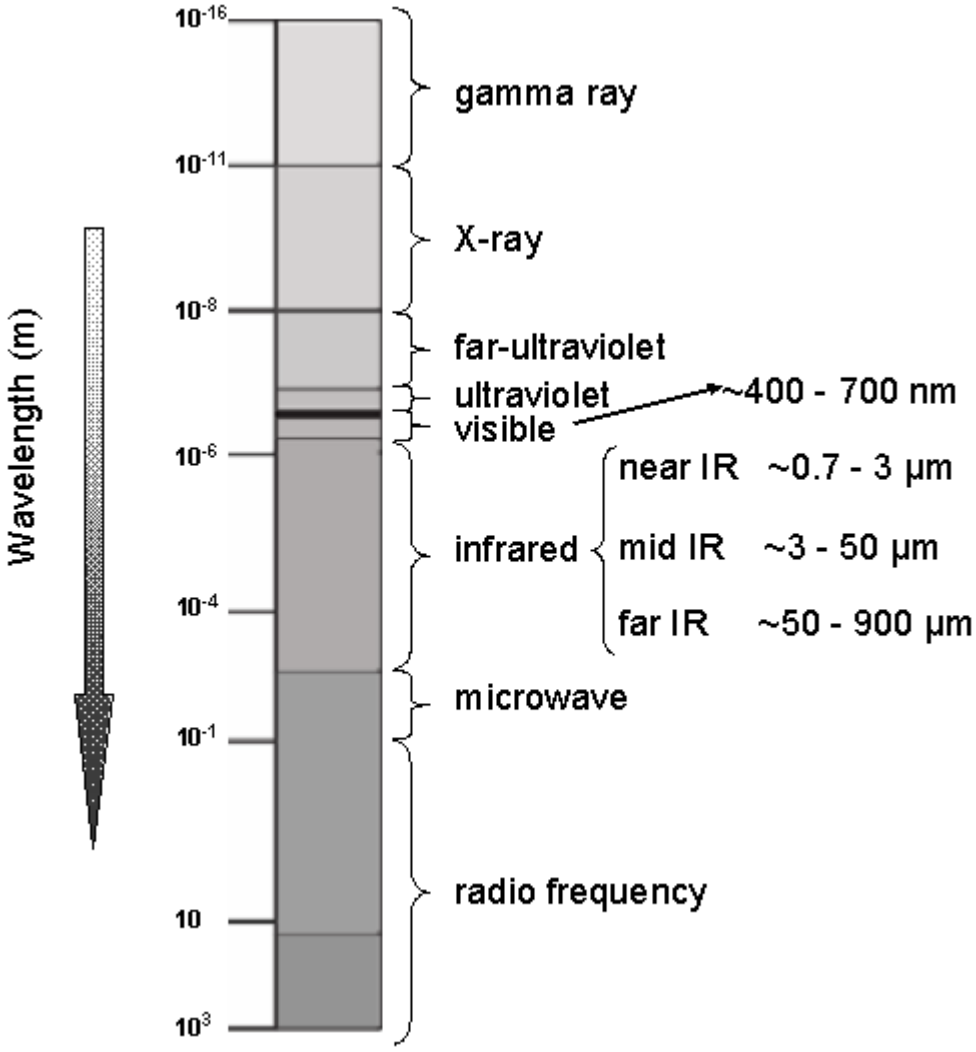

Fig 3.9. Infrared region is compared to other regions of electromagnetic spectrum.

3.6 Nuclear Magnetic Resonance (NMR):

Nuclear Magnetic Resonance (NMR) is a phenomenon in which the nuclei of certain atoms are immersed in an applied magnetic field. Any atom with a nucleus containing odd atomic number, mass or both contains a spin angular momentum, characterized by the nuclear spin quantum number (I) and magnetic moment.

$$I = \frac{1}{2}n \quad n = 0,1,2,\ldots . \tag{3-13}$$

The nuclear spin number can determine the allowed spin states which is "$2I + 1$". Atoms with a spin angular momentum of zero do not show this phenomenon. Atoms with isotopes which are active nuclei in NMR (such as ^{1}H, ^{13}C, ^{15}N, ^{19}F, …) when placed in a magnetic field can absorb a photon with a specific frequency. When the atom is placed in a magnetic field of strength "B", its electron circulates about the direction of the applied field which causes a tiny magnetic field at the nucleus. This tiny magnetic field opposes the external magnetic field. A half spin nucleus has two allowed orientation or two spin states. One about the direction of the field (low energy), which contains higher population, and one against it (high energy). The applied magnetic field with an appropriate frequency increases the number of spins with higher energy level. Such difference is frequency can be used to distinguish various active nucleuses using NMR spectroscopy. In order to obtain the NMR spectrum of our samples a Varian 400MHz NMR spectrometer with various deuterated solvents were used.

3.7 Differential Thermal Analysis (DTA):

Differential thermal analysis is a method in which the substance under investigation and a reference substance i.e. Alumina (Al_2O_3) with high thermal stability

are placed in one furnace or aluminum block. Then the temperature is raised up or cooled down at a constant rate and the difference between the temperature of the sample and reference is being tracked. If the sample undergoes any exothermic or endothermic process a peak appears in the plot of difference between temperatures of the sample and reference (Y-axis) versus temperature (X-axis) or time. (See Figure 3.10)

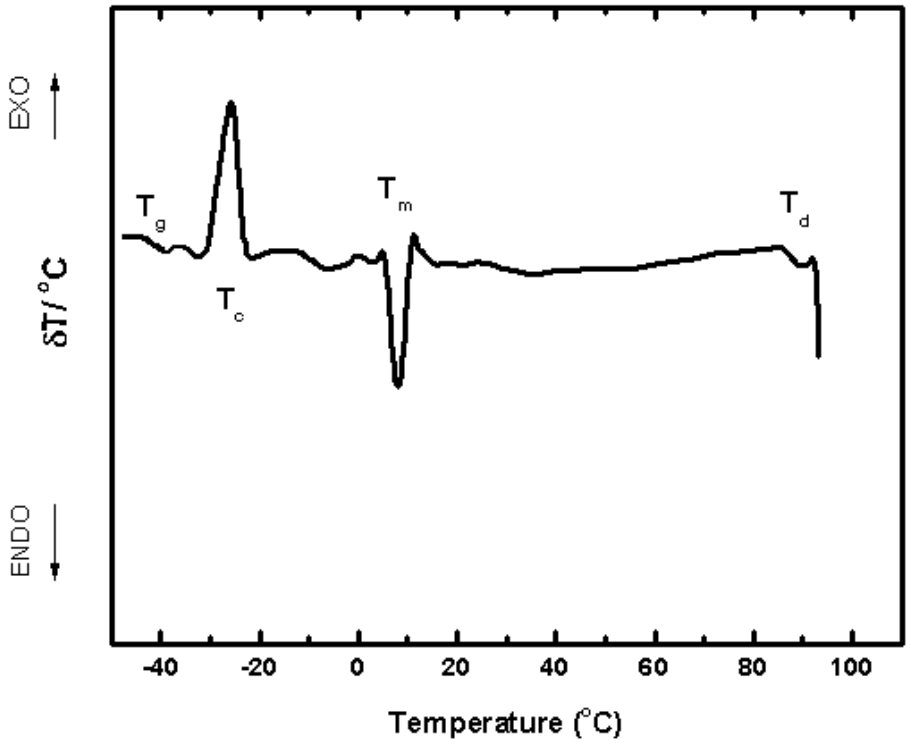

Fig 3.10. The Differential Thermal Analysis thermogram of the protonated tetrahydrofuran (THF), using triflic acid (HOTf) as the protonating agent, showing the glass transition (T_g), crystallization (T_c), melting (T_m), and decomposition (T_d) or boiling temperatures.

All DTAs were measured using twin digital voltmeters with a sensitivity of microvolt using two K-type thermocouples. 0.2 ml of the samples and reference were transferred into two small (~1 ml) Pyrex tubes and placed into an aluminum block which was

designed for this purpose. Using Daniels' method (Daniels 1973)[55], anhydrous Alumina was used as a reference for all samples. Tiny Pyrex capillaries were used to avoid direct contact of samples and thermocouples. The tube and capillaries were sealed by Teflon tapes. Heating rates of 10-20 K/min were applied. An initial test was done for Benzimidazole with a melting point of 171^{o}C to assure the calibration of the instrument. DTA is very sensitive to the type of thermocouple used to track the temperature. A 200 Watts cylindrical shaped heating cartridge was used and the heating rate was controlled by a Barnant Company heating controller.

3.8 Differential Scanning Calorimetry (DSC):

Differential scanning Calorimetry is an analytical method which tracks changes in heat flow, associated with any changes in sample's phase or even a reaction, versus temperature. Like DTA, DSC also studied the difference between the sample and reference (an empty aluminum pan) as a function of temperature. DSC operates at constant pressure therefore the heat flow can be measured from:

$$\left(\frac{dq}{dt}\right)_p = \frac{dH}{dt} \tag{3-14}$$

where the dH is the enthalpy changes at constant pressure, and the heat flow $\frac{dH}{dt}$ is measured per seconds. The difference between the heat flow of the sample and reference is

$$Difference\ in\ heat\ Flow = \left(\frac{dH}{dt}\right)_{sample} - \left(\frac{dH}{dt}\right)_{reference} \tag{3-15}$$

In endothermic processes the heat flow to the sample is higher than the reference and in exothermic processes the heat flow of the sample is lower than the reference. An interesting property of DSC is that heat capacities can be measured on either side of the glass transition so that the heat capacity changes at the glass transition (a kinetically controlled version of a second order transition) can be obtained.

$$C_p = \frac{dH}{T} \tag{3-15}$$

A sample of a differential scanning calorimeter thermogram is shown in figure 3.11. In this figure, T_g represents the glass transition temperature (endothermic), T_c is the crystallization temperature (exothermic), and T_m represents the melting temperature (endothermic).

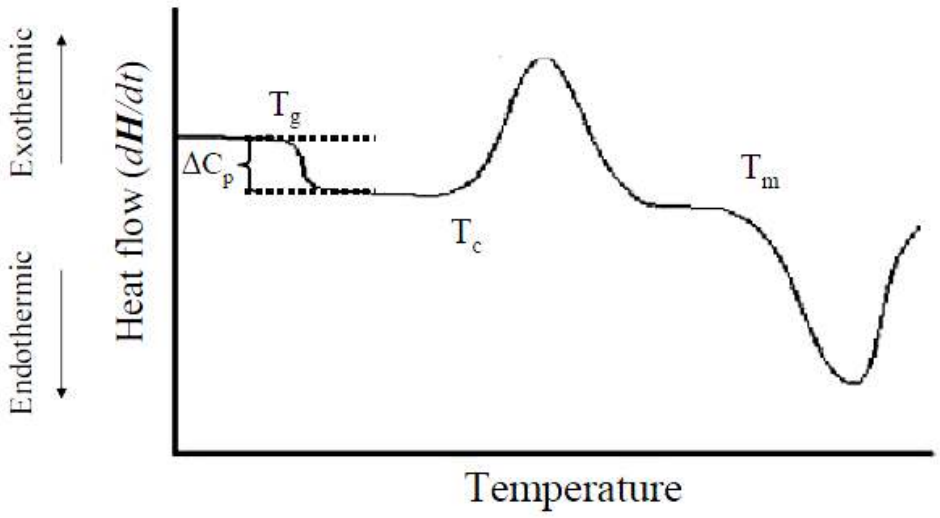

Fig 3.11. A Typical Differential Scanning Calorimetry thermogram showing the glass transition (T_g), crystallization (T_c), melting (T_m).

3.9 Inductively Coupled Plasma (ICP):

ICP is widely used method for elemental analysis and in some cases isotopic analysis. Currently, ICP is the most commonly used technique for the determination of trace concentrations of elements. The coupled plasma can be generated by directing the energy in the range of radio frequency into a suitable gas, usually ICP argon. Other plasma gases that can be used are Helium and Nitrogen. The plasma gas must be pure since contaminants in the gas might quench the torch.

CHAPTER 4

Anhydrous Superprotonic Polymer by Superacid Protonation of Cross-linked $(PNCl_2)_n$

Polymer membranes for fuel cells typically contain water to enhance the conductivity. The best known case, Nafion, functions properly only when the polymer is swollen with water to the extent of some 10-20 H_2O molecules per sulfonate group. (Kreuer 2001)[56] (Yang *et al.* 2004)[57] The associated restriction of operating conditions to temperatures below 80°C prevents the use of intermediate temperatures, 150−200°C, which could avoid the major problems associated with catalyst poisoning.

A related problem attends the use of phosphoric acid as the electrolyte. Although the operating temperature is extended to 150°C, loss of the modest water content (corresponding to 0.1−1.0 H_2O per phosphate group) again results in major decreases in conductivity. (Kreuer 2001)[56] (Hasiotis *et al.* 2001)[58] More success has recently been achieved with the use of anhydrous phosphoric acid absorbed into polybenzimidazole, (Li & Scott 2010)[59] by interaction between the most acidic proton and the imide nitrogen. Although this is not a strong enough proton transfer to classify the material as a "polycationic" protic ionic liquid, it is a step in that direction. Similar attempts have been made by absorbing H_3PO_4 into polyvinyl or polyvinylidene chloride types of polymer, with some success, (Narayan *et al.* 2006)[60] but the conductivity is found to become higher as the proton transfer becomes less energetic and to be highly dependent on some water being present.

An alternative route to medium-temperature fuel cell electrolytes has been found using protic ionic liquids of both inorganic (Belieres *et al.* 2006)[61] (mixed ammonium salts) and organic cation types [of which the best examples are 2-fluoropyridinium triflate (Thomson *et al.* 2008)[62] and diethylmethylammonium (DEMA) triflate (Nakamoto *et al.* 2007)[63]]. Indeed, DEMA triflate absorbed into an imide sulfonate membrane gives very promising performance. (Thomson *et al.* 2008)[63]

In this work, we have been seeking to create completely anhydrous superprotonic electrolytes of the protic (Angell *et al.* 2012)[1] (Ansari *et al.* 2013)[64] ionic liquid class, by taking advantage of the proton energy level scheme of Belieres and Angell (Belieres & Angell 2007)[25] to obtain liquids that are both superacidic and highly ionic, and have been characterizing their superprotonicity. Along the way, we have encountered a case of the same type in which the proton acceptor is also a crosslinked polymer, indeed, a rubbery solid. In this case, the product of protonation is a truly superprotonic material with respect to the global viscosity, but whether it is superprotonic with respect to the segmental relaxation time is not immediately clear, and this question will form part of the discussion.

Polyphosphazene-based polymers (Allcock 2003)[65] have been used as a basis for fuel cell membranes by a number of workers but only as a backbone to which side groups active in the proton-transfer process, are attached.(Tura *et al.* 2009) [66] (Wycisk & Pintauro 2008) [67] Much effort and expense has been devoted to obtaining linear polyphosphazenes for this purpose. (Allcock 2003)[65] In the present work, we have adopted a different approach more akin to that used by those who react phosphoric acid with basic entities on the chain (polybenzimidazole) (Hasiotis *et al.* 2001)[58] or pendant to

the chain (polyvinyl propylamine) (Narayan *et al.* 2006)[60] and is motivated by the expectation that interaction with a sufficiently strong acid could result in a polycationic, polymeric, superprotonicall conducting medium. In short, we have protonated the backbone of polydichlorophosphazene (commonly referred to as PDCP). In this way, we have obtained a new protonconducting polymer that exhibits very high conductivity, 2 orders of magnitude higher than its corresponding room temperature liquid superacid and comparable to that of optimally hydrated Nafion.

The nitrogen in $(PNCl_2)_3$ and its polymeric forms is expected to be a very weak Brønsted base, and only a few superacids, namely, $HClO_4$, CF_3SO_3H (trifluoromethylsulfonic acid, abbreviated HOTf), and $HAlBr_4$, have been reported to be capable of "forming adducts" with it, (Heston *et al.* 2004)[68] that is, protonating it. Our own initial efforts using transient $HAlCl_4$ (Ansari *et al.* 2013)[64] ended in failure. The ^1H NMR spectrum, at 100°C, of the liquid solution of $(PNCl_2)_3$ protonated by HOTf [one mole HOTf per mole of $(PNCl_2)_3$] showed partial protonation with a new line at 12.18 ppm [referenced to tetramethylsilane (TMS)] that is 1.92 ppm downfield from that of pure triflic acid (see the Experimental Section) and 5.4 ppm downfield from the dominant solution ^1H resonance at 7.15 ppm (which is presumed to be for HOTf largely separated from other HOTf molecules). The 12.18 ppm line is assigned to the symmetric $H[OTf]_2^-$ species that results from the NH^+ protonation (more details later).

The conductivities of protonated PDCPs [or even of $(PNCl_2)_3$ + HOTf solutions] have not previously been investigated. Here, we carry out a study of the conductivity and glass transition (determined by segmental relaxation time) of cross-linked PDCP, protonated wholly or partly by pure triflic acid.

4.1 Experimental Section:

4.1.1 Materials:

Hexachlorophosphazene [$(PNCl_2)_3$] and toluene (99.99%) were purchased from Sigma-Aldrich and used without any further purification. Trifluoromethanesulfonic acid (triflic acid, HOTf) (>99%) was purchased from Sigma-Aldrich and was freshly distilled under a nitrogen atmosphere before use. It yielded a single proton NMR resonance at 10.26 ppm, which is less downfield than the most anhydrous case reported by Xu et al. (Xu *et al.* 1999)[69], 10.51 ppm, in their careful study of water contents of HOTf and their consequences.

4.1.2 Synthesis and Separation of PDCPs:

PDCP was synthesized through ring-opening polymerization of the molecular $(PNCl_2)_3$ liquid. (Allcock 2003)[65] Seven grams of $(PNCl_2)_3$ was placed in a 50 mL ground glass capped tube in a low-dew-point glovebox. The tube was sealed; removed from the glovebox; and heated at 260°C for 12 h, during which time a rubbery solid polymerized mass was formed. Typically, the PDCP polymer consists of a combination of linear and cross-linked PDCP. As reported by Allcock, (Allcock 2003)[65] shorter reaction times and lower temperatures can reduce the extent of cross-linking. Excess (unreacted) molecular $(PNCl_2)_3$ was removed by heating the mixture well above the sublimation temperature of approximately 120°C and collecting the gas under a flow of nitrogen gas.

Linear PDCP is flexible within the rubber and could be dissolved in a variety of solvents such as toluene, tetrahydrofuran, cyclohexane, and benzene, in which the cross-

linked PDCP is quite insoluble. To separate into linear and crosslinked polymer fractions, 40 mL of toluene was added to the PDCP polymer. After 24−48 h, depending on the shape of container, a large increase in the volume of the polymer was observed. When the linear fraction had completely dissolved in the solvent, the rubbery polymer component was detached from the glass tube by a sharp blade, and the liquid and rubbery fractions were separated by filtration under nitrogen gas. The cross-linked polymer was washed repeatedly with 50 mL of additional solvent and then dried and stored in a drybox.

The solvent containing the linear polymer was treated separately (by vacuum evaporation) to recover the linear $PNCl_2$ for separate study. Of the original $(PNCl_2)_3$, 8% was recovered as linear polymer (a very viscous liquid), and 79% was obtained in the rubbery cross-linked form. The remaining 13% unreacted $(PNCl_2)_3$ was recovered as a sublimate during the polymerization process.

4.1.3 Protonation of PDCP:

Samples of protonated PDCP were prepared individually, under a nitrogen atmosphere in a low dew-point glovebox, by direct addition of measured quantities of triflic acid to rubbery polymer samples of approximately constant mass, sliced from the rubbery polymer mass and punched out with a metal press. Samples were trimmed with a razor blade to weigh 0.50 g (containing 4.31 mmol of nitrogen) and then were reacted with the following millimolar quantities of (anhydrous) triflic acid (formula weight = 150.078 g/mol): 0.48, 1.44, 2.53, 4.31, 7.34, 12.94, 24.45, and 38.83. Each amount of pure triflic acid was gradually added from a micropipette to separate 0.50 g samples of the cross-linked PDCP to form rubbery solutions with shapes suitable for subsequent

study in a stainless steel piston-type conductance cell designed for use with polymer samples. The HOTf mole fractions, x(HOTf), corresponding to the listed quantities are 0.10, 0.25, 0.37, 0.50, 0.63, 0.75, 0.85, and 0.90 molar fractions of triflic acid, respectively. Here, x = 0.5 corresponds to one proton per nitrogen.

In all cases, about one day was required to achieve a uniform protonated network structure. A change in the color of the polymer from colorless to light brown was observed. The most pronounced change in color was observed for the case in which every nitrogen was protonated. To visual observation, it seemed that the polymer was able to take up to a remarkable 98 mol% HOTf before a separate liquid acid phase was observed. However, physical measurements were temperature-reversible only up to 75% acid.

We noted a large increase in the volume of PDCP resulting from addition of the acid, which was particularly marked for samples with x(HOTf) > 0.5.

4.1.4 Measurements:

Thermogravimetric Studies:

Thermogravimetric analysis can provide information on the binding of liquids into media with which they react by physical or chemical means. Here, we are interested in the binding of triflic acid by the proton-transfer interaction. Unfortunately, triflic acid is too corrosive to permit study in a commercial apparatus, so attempts were made to carry out thermogravimetric analysis manually, using samples with different mole fractions of triflic acid in small glass vials that were weighed and then heated in an aluminum block for various times and temperatures up to 200 °C.

Unfortunately, the samples gained water more rapidly than they lost HOTf, so these measurements were abandoned.

Ionic Conductivity Measurements:

Ionic conductivities of the easily reshaped rubbery samples were determined by electrochemical impedance spectroscopy (EIS) using a Princeton Applied Research (PARSTAT 2273) potentiostat/galvanostat, with a modulation amplitude of 100 mV over frequencies ranging from 1.0 Hz to 200 kHz, using the cylindrical conductivity cell shown in Figure 4.1. For each sample, conductivities were obtained using two different Teflon spacers that yielded cell constants of 0.25 and 0.5 cm^{-1}. Conductivities were found to be independent of the cell constant, as expected.

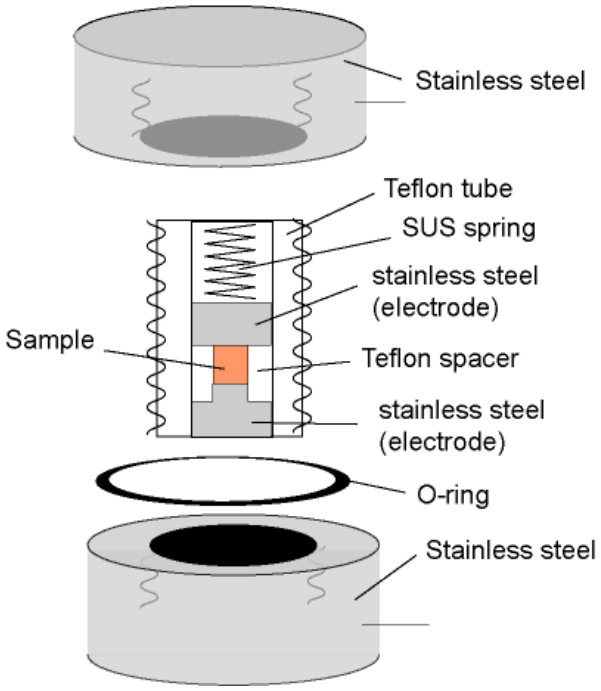

Fig 4.1. Design of the stainless steel (SUS) conductivity cell.

A single composition of the protonated linear polymer, corresponding to x(HOTf) = 0.5, was made. This sample was not a rubber but rather an extremely viscous liquid. It was possible to study its conductivity in the same piston cell. Provided that the samples were scrupulously anhydrous, the SUS grade (Japan) stainless steel cell electrodes were not corroded. The normal expectation would be for the linear polymer system to have a higher conductivity, but this proved not to be the case, as discussed later in this chapter.

For measurements of the lower conductivity of pure triflic acid, a simple dip-type cell with platinum wire electrodes was used. The cell constant was determined by calibration with 0.01 M KCl solution, before and after measurement. That our conductivity values were not significantly higher than the lowest values on record testifies to the dryness of our materials (implied by the NMR resonance frequency reported in the **Materials** section (4.1.1)).

Glass Transitions:

The glass transition temperature (T_g) of PDCP was determined using a differential scanning calorimeter (model DSC-7, Perkin-Elmer). The instrument was calibrated by the two-point method with cyclohexane (solid-solid transition, TS1→S2 = −86.6 °C) and indium (Tm = 156.6°C) as the two standards for the high-temperature and low temperature regions, respectively. The cross-linked PDCP:HOTf solutions were isolated in stainless steel pans under nitrogen flow and scanned at a rate of 20 K min^{-1} under helium atmosphere.

4.2 Results:

Ionic Conductivities:

The strong interaction of the HOTf with the cross-linked $PNCl_2$ is demonstrated by the major (1.5 orders of magnitude) increase in conductivity, from the relatively small value of pure HOTf, $10^{-3.5}$ S cm^{-1} at 25°C, to the value observed at HOTf saturation, $10^{-2.0}$ (S cm^{-1}), as seen in Figure 4.2. The latter value, discussed below, is comparable to that of wet Nafion (under ambient conditions). Our conductivity value for pure HOTf is lower than most of the values reported for pure HOTf, but is not the lowest, which is $<10^{-5}$ S cm^{-1} (in the presence of P_2O_5) (Russell & Senior 1980)[70].

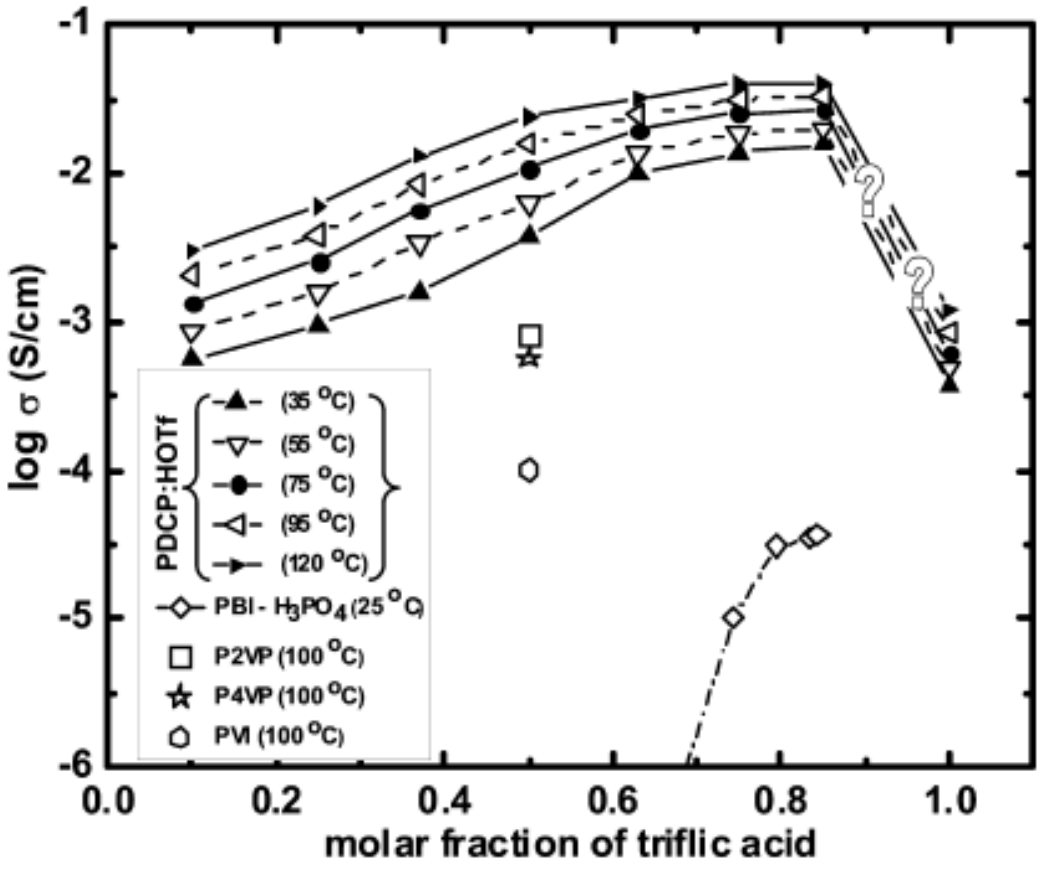

Fig 4.2. Conductivity isotherms for various compositions of the protonated crosslinked $PNCl_2$ (PDCP). No data were taken between x(HOTf) = 0.85 and 1.0. Comparisons are made at 25 and 100°C, with conductivities of some polymeric materials swollen by weak acid-base interaction with H_3PO_4, as follows: [poly(2,5-benzimidazole)] (PBI), (Russell & Senior 1980)[70] poly-2-vinylpyridine phosphates (P2VP), poly-4-vinylpyridine phosphates (P4VP) (Narayan *et al.* 2006)[60], polyvinylimid-azoline phosphates (PVI) (Narayan *et al.* 2006)[60]. The intrinsic conductivity of the acid in those cases is much higher than that of HOTf.

It is reasonable to interpret this conductivity increase in terms of protonation of the polymer, together with a conductivity-enhancing mechanism associated with cross-linking, which is of special interest. Note that partial protonation of the unpolymerized molecular liquid $(PNCl_2)_3$, which is evident in ^1H NMR spectra mentioned earlier, does not produce any significant increase in conductivity over that of HOTf itself (see Figure 4.3). The ^1H NMR spectrum for the liquid solution shows an -$[NH^+]$ triplet (at 5.63, 5.56, and 5.42 ppm) and an acid $[TfO{-}H{-}OTf]^-$ resonance at 12.18 ppm, in addition to the (dominant) molecular HOTf peak at 7.15 ppm (versus TMS). Figure 4.3 shows that, even when the linear (viscous liquid) polymer is protonated, the conductivity does not increase by more than a few percent.

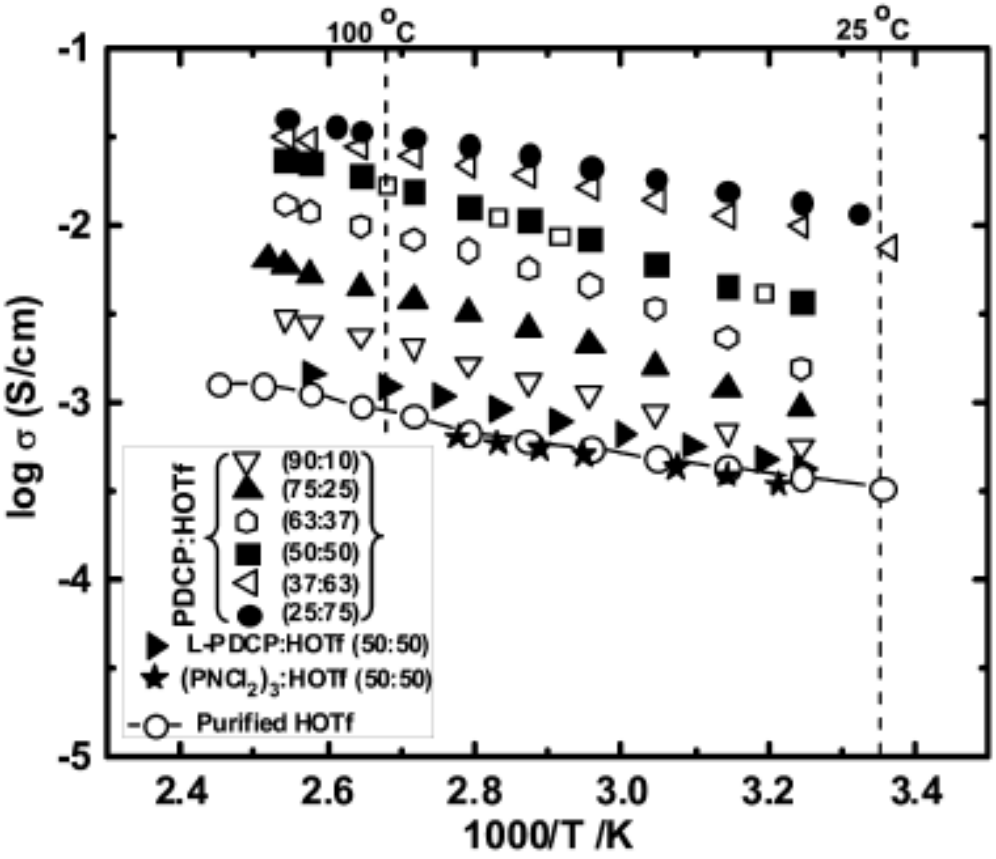

Fig 4.3. Arrhenius representations of the conductivity of the protonated crosslinked $PNCl_2$ (PDCP) of different HOTf contents. For the 50:50 composition both heating and cooling data are shown. Comparison is made with the cases of (i) HOTf + molecular $(PNCl_2)_3$ at mole ratio 1:1 (one proton per 3N) (ii) linear $PNCl_2$ (L-PDCP) at x(HOTf) = 0.5, (one proton per N), and (iii) pure triflic acid (HOTf).

The large increase in conductivity, according to Figure 4.3, comes when the cross-linked (rubbery) polymer absorbs HOTf [compare the plot for linear PDCP with that for cross-linked PDCP at x(HOTf) = 0.5 or the plot for 50:50 $(PNCl_2)_3$ with that for PDCP:HOTf = 75:25]. Such an increase in conductivity occurring in the face of the loss of fluidity is a provocative observation. It implies that the spatial organization of the proton sites (nitrogens) in the cross-linked polymer acts as an aid to proton hopping, just

as the Grotthus mechanism works well in phosphoric acid because of the hydrogen-bonded network that is established. We note that the HOTf distribution in the protonated $PNCl_2$ rubber samples was homogeneous. This could be established by measuring the conductivity of different parts of a single sample (prepared as described above) and showing that the results were independent of the section tested. This test was made for each composition up to 75% HOTf.

Conductivity isotherms for some protonated polymer samples of different compositions are also shown in Figure 4.2. Comparisons with some other polymeric materials obtained by absorbing acid (phosphoric acid) in polymers are made. For instance, it can be seen that the conductivity at 35°C (and 25°C; see Figure 4.3) in the present rubber is far above any ambient-temperature value obtainable with phosphoric acid in the polybenzimidazole membranes of Asensio *et al.*, (Asensio *et al.* 2002)[71] although phosphoric acid itself is more highly conducting at ambient temperature (10-1.5 S/cm). The polybenzimidazole membranes are also partly hydrated to improve conductivity, whereas the present system is anhydrous by design.

Unfortunately, the present systems were unstable above 125°C, where irreversible changes in conductivity, associated with some chemical decomposition, occurred. This high-temperature limit appears to be independent of the composition.

Glass Transitions:

Differential scanning calorimetry (DSC) thermograms are shown in Figure 4.4,

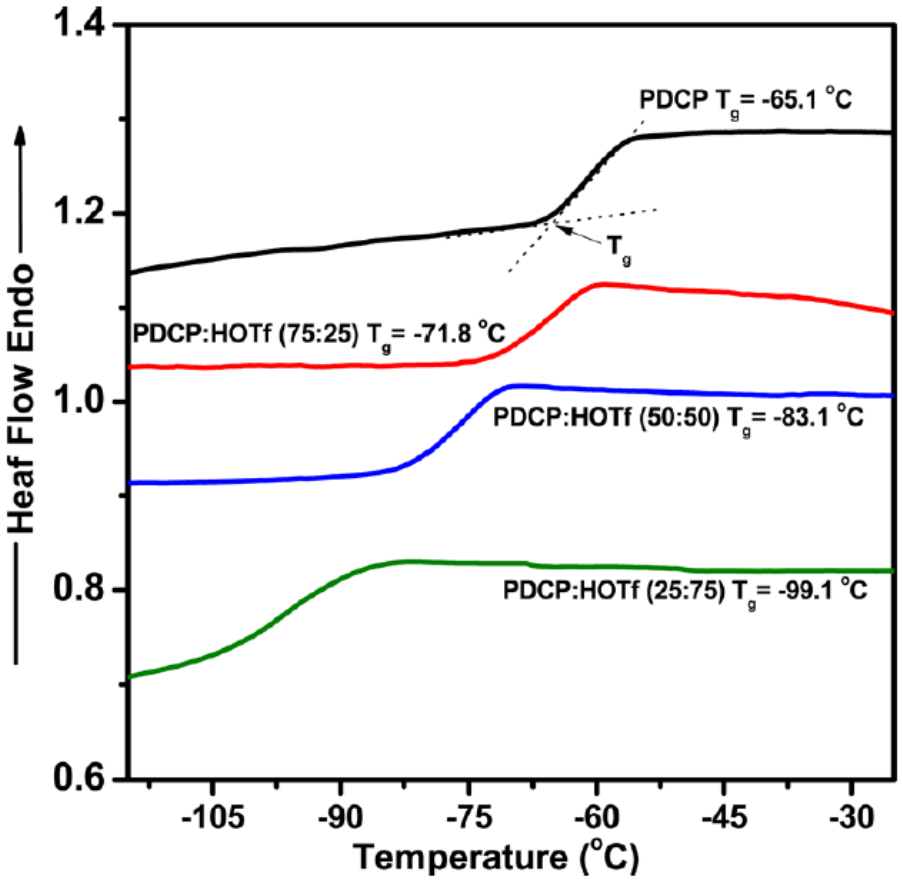

Fig 4.4. DSC thermograms for selected compositions in the system $PNCl_2$ (crosslinked polymer) + HOTf, measured using stainless steel pans and scan rate of 20 K min^{-1}. The glass transition is defined from the onset of the heat flow jump. For compositions beyond stoichiometric protonation, the endotherm is smeared out, implying the presence of severe composition fluctuations.

from which glass temperatures were obtained by the standard "onset" T_g construction shown in the upper endotherm. The variation of T_g, thus defined, with composition is shown in Figure 4.5.

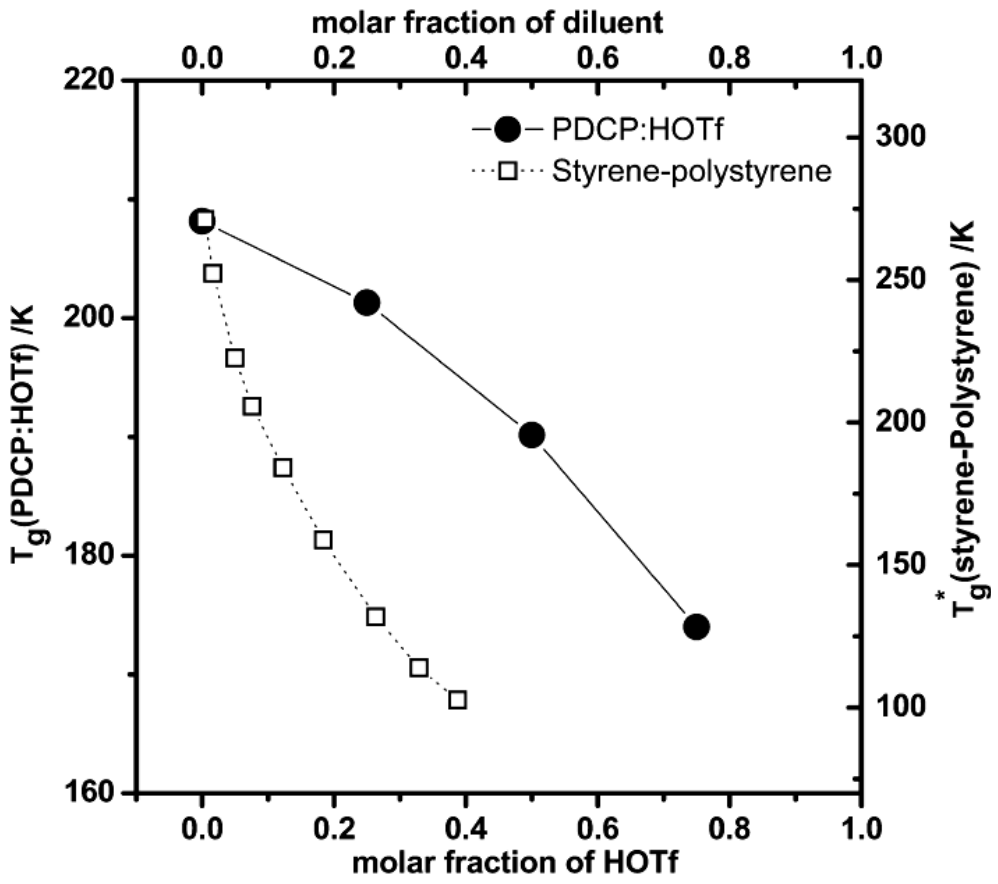

Fig 4.5. Variation of T_g (K) with mole fraction of HOTf. Comparison is made with the variation of T_g with mole fraction of diluent in a typical ideal polymer diluent system. Here the data are for the classical polymer-diluent system, polystyrene + styrene (dashed line). Values for the latter are scaled by the ratio of the pure polymer T_gs. (The starting point is made to coincide with that of the p-$PNCL_2$-HOTf system by the scaling Tg* = Tg(PS-S) × (Tg(PS)/Tg(PDCP)).

4.3 Discussion:

It is obvious from Figure 4.2 that either the dissociation of HOTf (which is much less in the pure state than for sulfuric acid or orthophosphoric acid), or the proton mobility, is strongly promoted by the interaction with the nitrogens of the crosslinked $PNCl_2$. Promotion of the proton mobility is suggested by Figure 4.5, which shows that the

cohesive energy of the polymer, as monitored by its glass temperature, is not increased by the HOTf content. Rather than increasing as seen in previous proton-transfer interaction studies, it decreases systematically as the HOTf content is increased. On the other hand, relative to the behavior of the classical polymer + diluent system, polystyrene + styrene, included in Figure 4.5, it can be seen that the T_g decrease in the present system has a pronounced upward bulge, with maximum displacement in the vicinity of the equimolar composition. This is a clear indication of non-ideal mixing, attributable to the protonation effects.

If the polymer effect on T_g is subtracted out, using the polystyrene−styrene data as a baseline, then a T_g maximum similar to that observed when triflic acid is added stoichiometrically to 2-methylpyridine (α-picoline) (Yoshizawa *et al.* 2003)[17]) would be seen near the stoichiometric composition.

Thus, we conclude that the proton-transfer interaction produces a major dissociation of the HOTf molecular state, to produce a state of rather high ionicity permitting the observation of conductivities in a rubbery polymer that are comparable to those of the hydrated Nafion system, even though the present system is quite anhydrous. This is a significant result.

A question of importance then arises. Is the conductivity mechanism purely protonic in character, that is due to free protons hopping through the network structure, or is the proton firmly bound to the nitrogen as the relatively huge anion, or even dianion, diffuses in response to the applied field? Undissociated HOTf molecules might be present and mobile, but their movement cannot produce ionic current. Motion of ionic species in

polymers is rarely free of correlation to the segmental relaxation time, so the question has much intrinsic interest content.

A significant observation here is that the conductivity at x(HOTf) = 0.5 is much higher in the cross-linked polymer than it is in the linear polymer despite the more mobile state of the latter system (T_g of the pure linear polymer is -63°C) (Coleman *et al.* 1982)[72]. This is almost never the case for ionic mobilities and strongly hints at a purely protonic conduction mechanism.

To judge whether the motion of conducting species is free of restrictions by the matrix, it helps if the system responses to different stresses (e.g., electrical field compared with mechanical shear or thermal gradient) can be compared using the same units. For simple liquids, the mechanical properties can be represented in units of time, namely, the shear relaxation time (dating from Maxwell in 1850). The shear relaxation time is obtained as the ratio of the liquid-like property, the shear viscosity η, to the solid-like property, the infinite-frequency shear modulus G_∞ (where "infinite" means at frequencies far above the inverse relaxation time). Thus, we have

$$\tau_s = \frac{\eta}{G_\infty} \tag{4.1}$$

Following Macedo, Moynihan, and Bose (Macedo *et al* 1972)[73], the electrical conductivity process can then be represented, also in units of time, by using the electrical equivalent of equation 4.1 in which the viscosity is replaced by the resistance and the shear modulus is replaced by the electrical modulus. The electrical modulus, M_∞ ,is just the inverse of the high-frequency dielectric constant, converted using the permittivity of free space, e_0. Thus, we have

$$\tau_\sigma = \frac{\rho e_0}{M_\infty} \tag{4.2}$$

If we then replace the analogue quantities of equation 4.1, ρ and M_∞, by the familiar quantities $\sigma = \frac{1}{\rho}$ (S/cm) and $\varepsilon_\infty = \frac{1}{M_\infty}$, the approximate electrical relaxation time becomes

$$\tau_\sigma = \frac{\varepsilon_\infty e_0}{\sigma} \tag{4.3}$$

It is found that ε_∞, measured not too far above T_g, typically has values of 7-20 for ionic and protonic glasses.(Hodge & Angell 1977)[74] (Ambrus *et al.* 1971)[75] (Angell 1990)[76] Therefore, from the generally accepted finding that the relaxation time for enthalpy relaxation at T_g (measured by DSC at a scan rate of 20 K/min) is ~100 s, we can obtain an approximate idea of the relaxation time ratio $R_\tau = \frac{\tau_s}{\tau_\sigma}$ (commonly known as the decoupling index) simply from a measurement (or an extrapolation) of the dc conductivity of the liquid at T_g, using the relation

$$\tau_\sigma = \frac{9 \times 10^{-13} (S\,cm^{-1}\,s)}{\sigma} \quad (\text{at } T_g) \tag{4.4}$$

including the common value of 100 (s) for the structural relaxation time at T_g, we obtain the approximation for the decoupling index at T_g (where the structure becomes fixed for all lower temperatures) as

$$R_\tau\,(at\ T_g) = 2 \times 10^{14}\ \sigma / S\,cm^{-1} \quad (\text{at } T_g) \tag{4.5}$$

with an accuracy of about a factor of 2 (Angell 1992)[77].

For superionically conducting glasses, for which conductivities at T_g can be as high as 0.1 S/cm, this index can be as high as 10^{13}. For various low-T_g protic acid glasses studied by Hodge and Angell, (Hodge & Angell 1977)[74] it proved to be no higher than 10^6, whereas for a recent case of a dihydrogen phosphate ionic liquid glassformer (Mizuno *et al.* 2006)[78], a value of 10^9 was reported. All of these latter systems become flowing liquids above T_g. Polymers, on the other hand, remain solid (rubbery solids) to much higher temperatures, because of the network or linear chain entanglement effects, so attention is usually given to the local viscosity represented by the "segmental relaxation time", which is the quantity that reaches 100 (s) at the polymer T_g. It is highly uncommon for conducting polymers to have conductivity relaxation times that are actually shorter than the segmental relaxation times. For the most common polymer electrolytes, known as "salt-in-polymer" electrolytes, the value of R_τ (at T_g) is typically 10^{-2} (Torell & Angell 1988)[79], so the possibility that this generalization might be broken by the present system is an important one to investigate.

Because we do not have the low-temperature dielectric constant and conductivity data necessary to obtain τ_σ from equation 4.3 directly, we will, for the present, assume values of ε_∞ based on the 1977 Hodge and Angell study for aqueous acids (Hodge & Angell 1977)[74] in order to obtain values of τ_σ that can then be extrapolated to the glass (Figure 4.6). Electrical conductivity relaxation times were obtained from the dc conductivity data using equation 4.3 with infinite-frequency dielectric constants estimated from earlier studies. Values extrapolated to solution glass transition temperatures indicated high levels of decoupling from 100 (s) segmental relaxation times characteristic of polymers at their standard (20 K/min scan rate) T_g. Identity of

"superionic" entities, probably protons, cannot be confirmed without separate NMR diffusivity measurements.

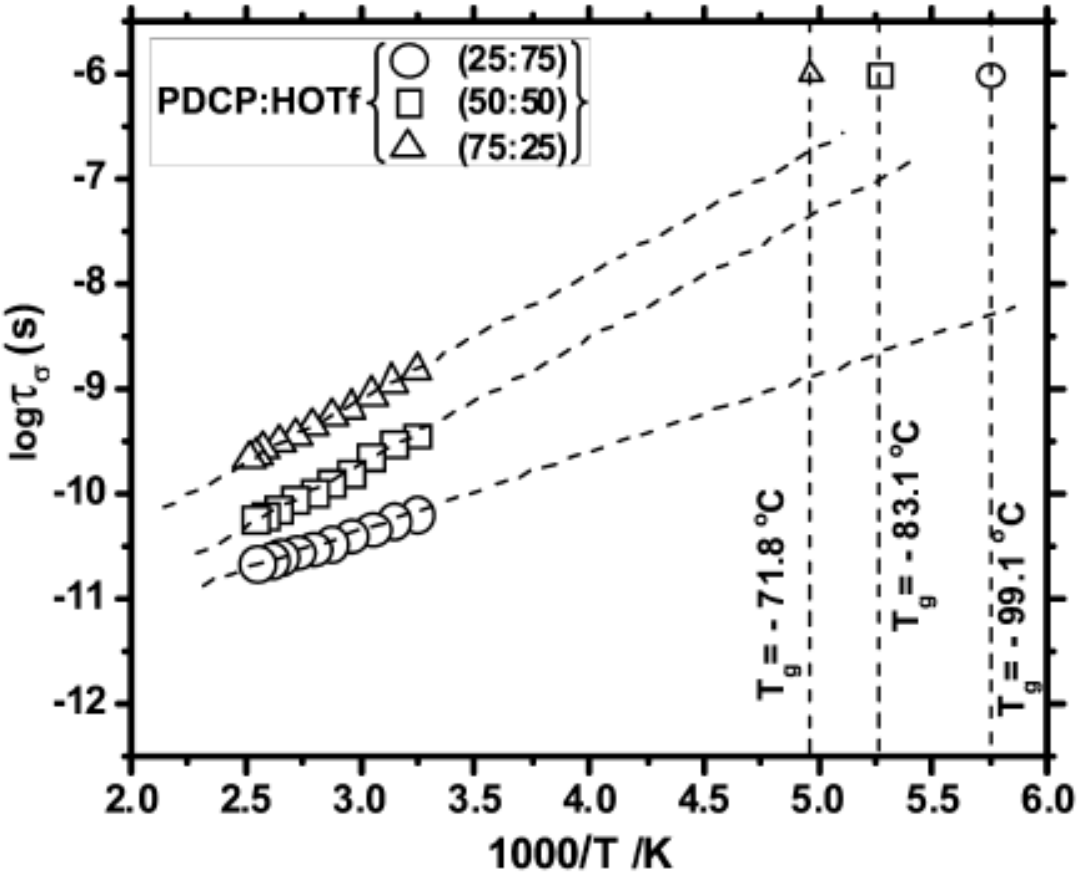

Fig 4.6. Electrical conductivity relaxation times obtained from the dc conductivity data using equation (4.3) with "infinite" frequency dielectric constants estimated from earlier studies. Values extrapolated to solutions T_g's indicate high levels of decoupling from the 100 (s) segmental relaxation times characteristic of polymers at their standard (20 K/min scan rate) T_g. Identity of "superionic" entities, probably protons, cannot be confirmed without separate NMR diffusivity measurements.

We investigated the transition temperature for different compositions to see how much they exceed the 100 (s) value of the enthalpy (and mechanical) relaxation times. This is done in Figure 4.6, where a simple Arrhenius form (probably not as appropriate as

a “super-Arrhenius” form) was used for the extrapolation. In all three cases, conductivity relaxation times at T_g that are many orders of magnitude shorter than the known structural relaxation time of 100 (s) can be identified using the intersection with the vertical dashed lines marking the T_g values. Thus, the charge-transport mechanism is indeed largely free of any mechanical restriction by the segmental motions of the polymer backbone.

Before it will be worth seeking more precise values for the proton decoupling index, it is important to first determine whether the decoupling observed is (i) purely protonic in character, as would be most interesting; (ii) due to some extraordinary anion mobility; or (iii) aided by some less extraordinary mechanism such as the coupled motion of triflate anion and proton (as undissociated HOTf molecules, although the molecules themselves cannot provide any current). Differentiating between these alternatives will require a study using pulsed-field gradient diffusivity of the protons, on one hand, and of the anion fluorine centers, on the other. The facilities for this study are available in our partner laboratories (J. L. Yarger), and the measurements will be undertaken in the immediate future.

*"**Adapted** with permission from (Younes Ansari, Kazuhide Ueno, Zuofeng Zhao, and C. Austen Angell, Anhydrous Polymer by Superacid Protonation of Cross-linked $(PNCl_2)_n$, J. Phys. Chem. C 2013, 117, 1548−1553.). Copyright (2012) American Chemical Society."*

CHAPTER 5

A novel, easily synthesized, anhydrous derivative of phosphoric acid for use in electrolyte with phosphoric acid-based fuel cells.

5.1 Introduction:

The phosphoric acid fuel cell is known as one of most researched, and commercially most advanced types of fuel cell (Srinivasan *et al.* 1999)[80] (Kreuer 2001)[56]. Initially developed as a liquid electrolyte device, prone to leaking and ionic shorts, it is now being refined, by incorporation of H_3PO_4 in polymeric materials (Yang *et al.* 2001)[81] such as polybenzimidazole, into a very promising and cost-competitive alternative (Li & Scott 2010)[59] to the Nafion fuel cell (Kwak *et al.* 2003)[82] (Asano *et al.* 2006)[83]. An advantage it holds over its Nafion rival is the higher temperature range of operation permitted by the electrolyte. It can be used up to 160ºC before water loss, to form pyrophosphoric acid, leads to reduced conductivity and poorer performance. The range may be extended by elaborate humidification and pressurization provisions, which of course also increase the expense and failure-probability of the system. The water management problem remains a barrier to the full commercialization of this type of fuel cell. Any modification of the electrolyte that could extend its operating temperature range and reduce its dependence on the presence of some water, without reducing its other favorable characteristics would be of great interest.

Here we describe an inexpensive, easily synthesized, modification of H_3PO_4 (presumed to be a binary solution with a new more complex acid) that extends the temperature range of the phosphoric acid fuel cell to, at least, 250ºC, while improving its

operating fuel efficiency considerably. To our knowledge, the current efficiency ($=i/i_{theoretical}$, i = current) obtained with the electrolyte we will describe, is higher than that of any other type of fuel cell operating at 1 atm. pressure. Its voltage efficiency is also comparable to (somewhat better than) that of the reported phosphoric acid based fuel cells. We describe only the first stage of this development, viz., the liquid electrolyte and its fuel cell performance, leaving the important second stage - development of a membrane based on proper incorporation of the liquid into a robust polymer host - to future reports.

5.2 Chemistry:

The additive is a derivative of phosphoric acid in which phosphoric acid is combined with silicon to form a silicophosphoric acid which probably has multiple molecular forms - yet to be fully resolved. Initially it was thought to be a substantial component of the electrolyte, but later work suggests that is a minor but temperature dependent component that stabilizes the phosphoric acid against loss of more than a small amount of water. Its possible molecular form will be discussed briefly below. It is the subject of continuing investigation.

The electrolyte is prepared by reacting $SiCl_4$ with anhydrous phosphoric acid obtained by fusion of the dry crystalline form (T_m = 42ºC). The schematic chart for preparation of this electrolyte is shown in Figure 5.1. The reaction is carried out under mild conditions, under gentle flow of nitrogen gas, initially 45ºC (T_b of $SiCl_4$ is 57ºC) and continuing with gradually rising temperature (reaching 100ºC) for three hours until the liquid is saturated with reaction products (becoming creamy in color due to a fine

precipitate of solid material), followed by gradually increase of temperature to 270ºC over one hour that establishes an equilibrium content of $H_4P_2O_7$. The H_3PO_4-insoluble components can be increased in quantity by extending the reaction time. The fuel cell performance has been evaluated in the presence of the stable suspension of solid silicophosphoric acid, called here SiPOH for convenience, which is believed to be essential for maintaining electrolyte properties. The solid is of highly disordered character according to X-ray diffraction patterns (Ansari *et al.* 2012)[84] to be discussed elsewhere (Huang *et al.* 2013)[85].

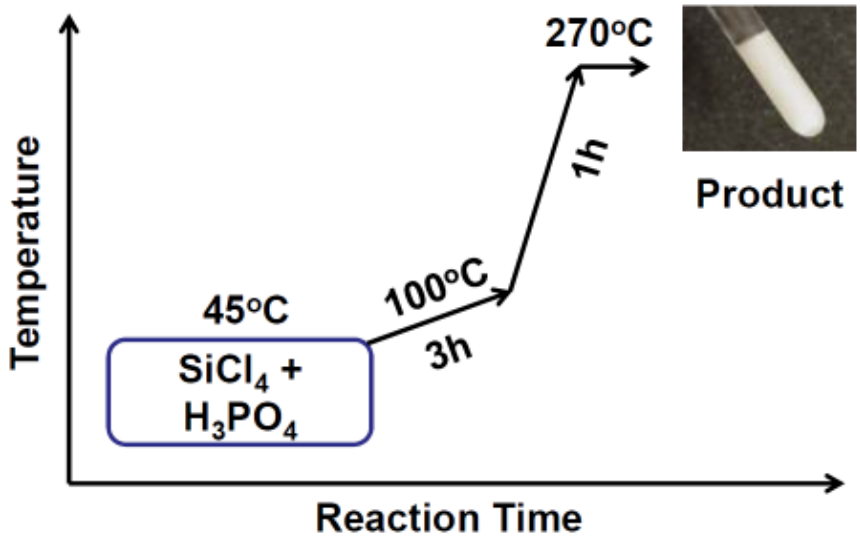

Fig 5.1. Schematic chart for preparation of the new electrolyte.

Both the liquid, and the stably suspended solid, are strongly acidic in character. The solid material contains Si in six-coordination (Huang *et al.* 2013)[85]. It has interesting properties including the ability, on solution in water and extended evaporation, to produce a clear deformable polymeric solid that has stability up to 140ºC at 1 atm, and

conductivity in excess of that of pressurized Nafion. This rubbery solid or gel-like material will be described in more detail elsewhere, but its conductivity, measured in the piston cell described in chapter 4, is included in Figure 5.2, in the results section.

5.3 Results:

5.3.1 Conductivity:

The presence of SiPOH and an equilibrium content of $H_4P_2O_7$ in the phosphoric acid, leads to an increase in electrolyte viscosity. Nevertheless, above 150ºC the electrolyte conductivity, determined using a twin electrode dip-type cell (shown in Figure 1.8 (a)) of cell constant 1.83 cm^{-1}, is superior to that of pure H_3PO_4 as shown in Figure 5.2. This is presumably due to a superior "free" proton contribution at high temperatures. The conductivity is reversible up to 285ºC. Tested at a constant 250ºC, the conductivity remained invariant within the temperature control fluctuations over a 24 hour period, and over a 48 hr at 230ºC, so loss of water has been greatly diminished, and in an operating fuel cell (producing water) would not be of consequence.

In Figure 5.2, comparison is made with anhydrous H_3PO_4, Nafion, and with the rubbery polymer obtained by hydrating the solid products of the reaction (to be described separately). Data for the diethylmethylammonium triflate [$DEMA^+$][OTf^-] (Lee *et al.* 2010 (a))[86] used in a recent protic ionic liquid fuel cell (Lee *et al.* 2010 (b))[87] (Belieres *et al.* 2006)[88], are shown as a dashed line. Even at 25ºC, the conductivity is still as good as that of the best ambient temperature protic ionic liquid fuel cell electrolyte.

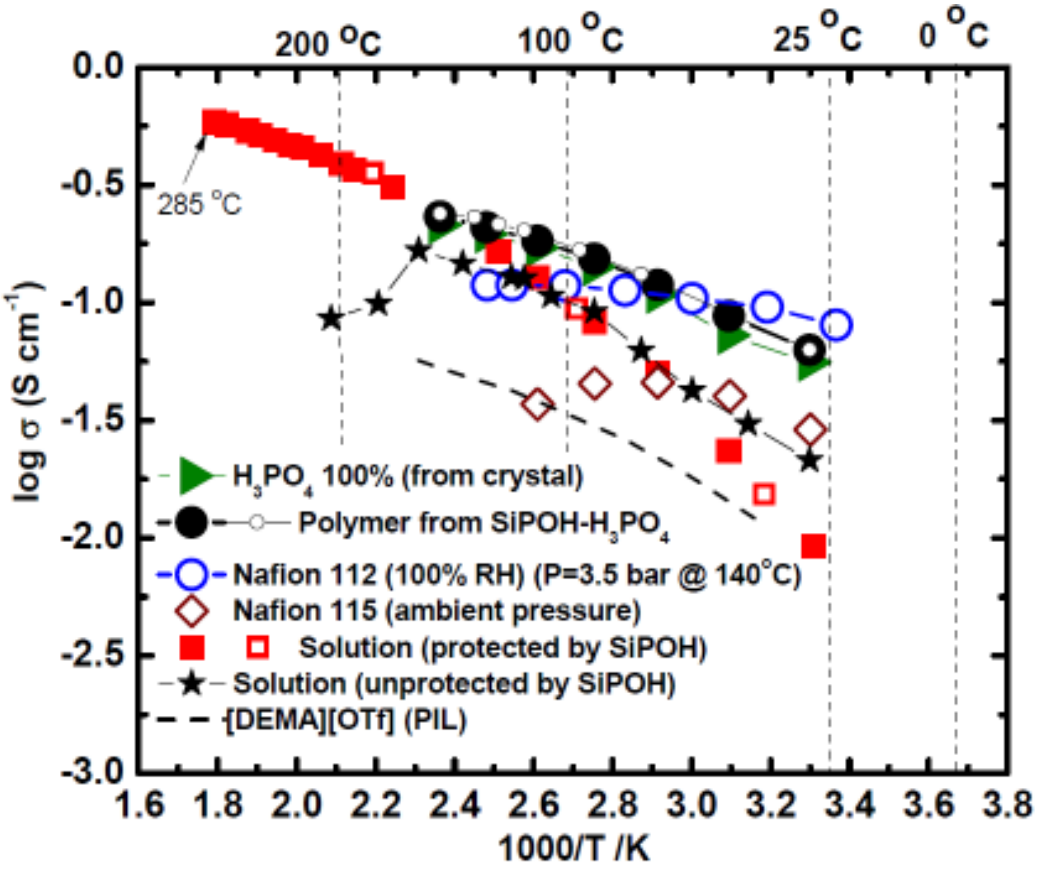

Fig 5.2. Ionic conductivities of the new SiPOH-stabilized electrolytes compared with various fuel cell electrolytes, including Nafion 112 (Asano *et al.* 2006)[83] and Nafion 115 (Kwak *et al.* 2003)[82]. Data from the present work are in solid symbols for heating runs and smaller open symbols for cooling runs, to show reproducibility. Star symbols show the conductivity of the new electrolyte after prolonged centrifuging to remove the SiPOH suspension. Only the heating data are shown. The conductivity of the protic ionic liquid DEMA triflate (Lee *et al.* 2010 (a))[86], used in a recent fuel cell membrane (Lee *et al.* 2010 (a))[86] and (Lee *et al.* 2010 (b)[87]), is shown as a dashed line for comparison.

5.3.2 Fuel Cell Performance:

The performance of our modfied H_3PO_4 liquid electrolyte, studied in the same Teflon sandwich cell with E-Tek gas diffusion electrodes, described in previous publications (Belieres *et al.* 2006)[61], is shown in Figure 5.3. Note that we are able to

operate smoothly at temperatures as high as 226ºC, and could go higher if not for the materials limits on tubular and machined components of the cell). Using unhumidified gases, we have been able to draw currents of 1 (amp cm^{-2}), with open circuit voltages (OCV) of nearly 1.0 volt. This OCV is only 0.12 V below the thermodynamic value for that temperature, and is somewhat higher than that obtained with the standard 85wt % phosphoric acid electrolyte, (also shown in the figure).

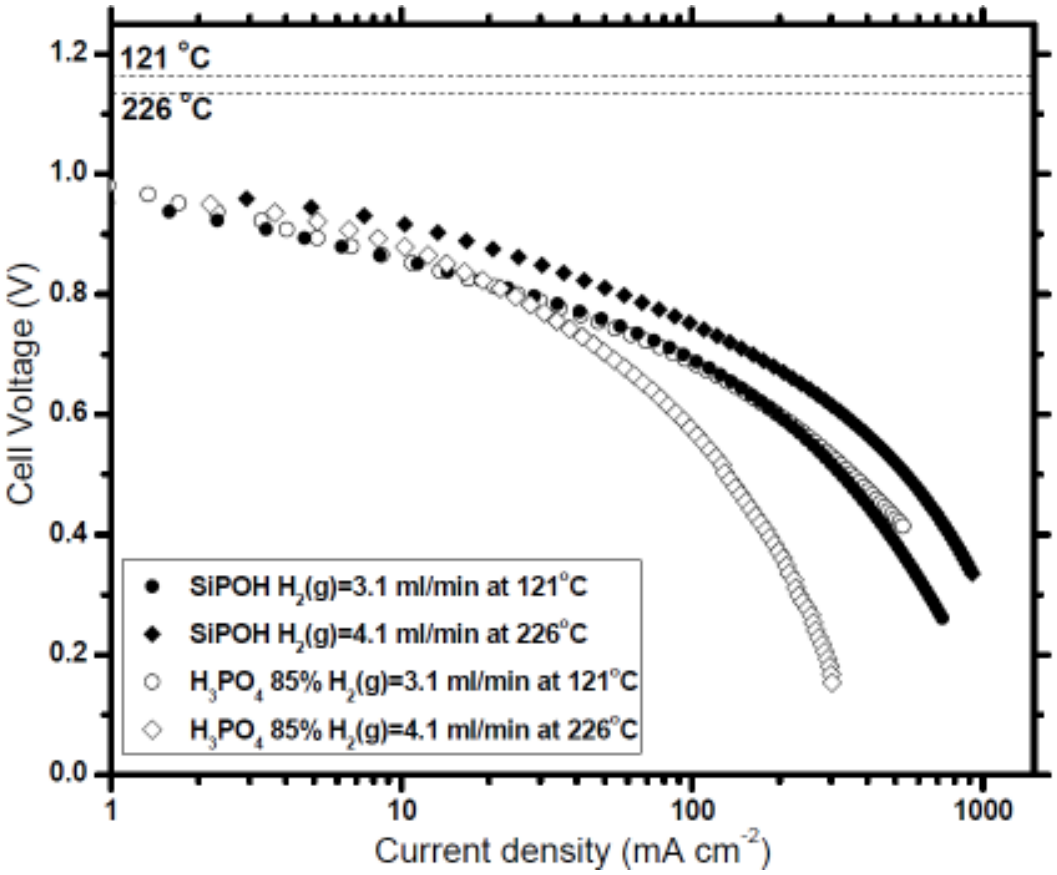

Fig 5.3. Tafel plots (IR corrected) for fuel cell performance, using the new SiPOH- stabilized phosphoric acid, compared with performance using the commercial standard, H_3PO_4 85%. The experiments used identical Teflon fuel cell blocks with identical E-Tek electrodes, and the same flow rates of H_2 and O_2 for each electrolyte at each temperature (see Table 5.1 for details). Flow rate for O_2 = 2 x flow rate for H_2. Note the high OCV, and ~1 amp cm^{-2} current, obtained at 226ºC.

The power outputs for the SiPOH-stabilized electrolyte at the two temperatures of Figure 5.3 are shown in Figure 5.4. The currents, both at (i) maximum power and (ii) where cell voltage vanishes in the uncorrected polarization curve are shown, along with open circuit voltage, voltage at maximum power, and other performance characteristics, in Table 5.1.

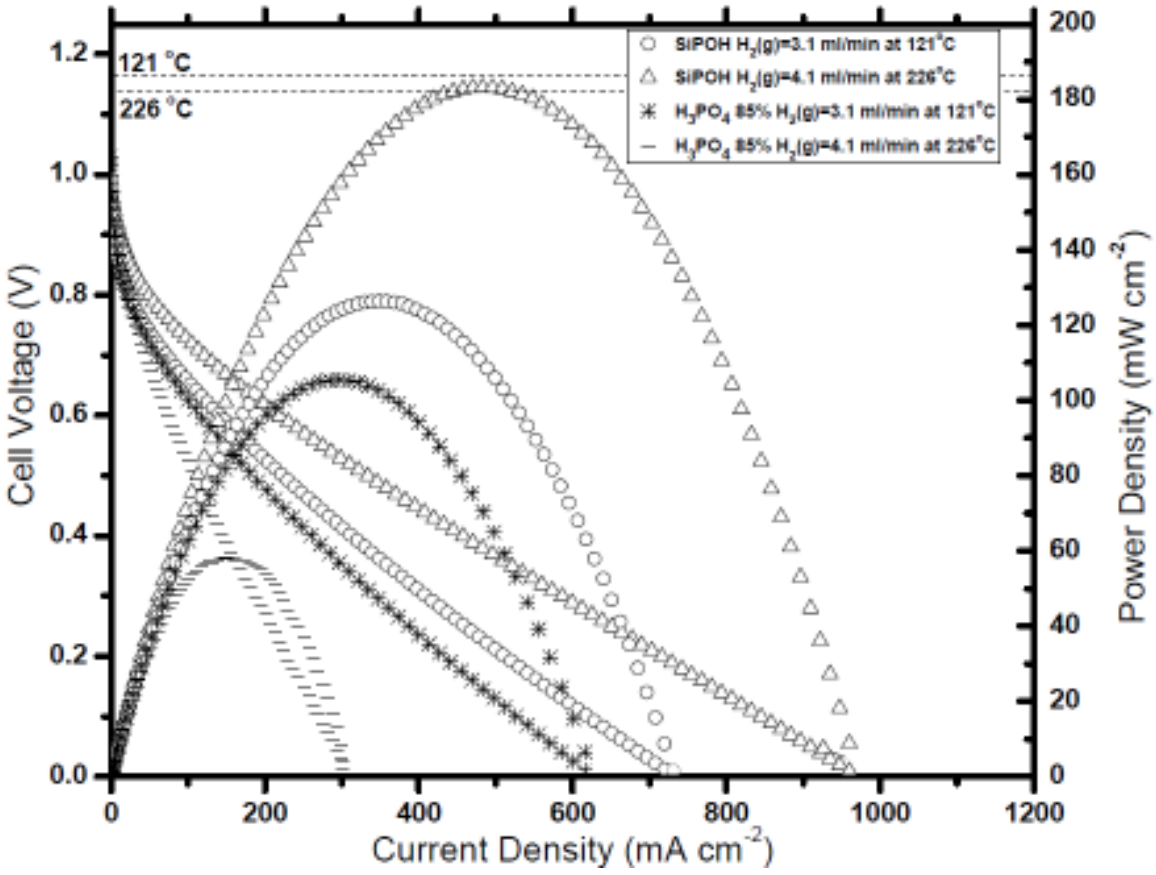

Fig 5.4. Polarization curves (linear current and no IR correction), and the corresponding power densities, for SiPOH-stabilized anhydrous H_3PO_4, and H_3PO_4 (85 wt %), electrolytes at different temperatures up to 226ºC.

An important aspect of the fuel cell performance with the present electrolyte is the fuel usage efficiency. This is a feature that is discussed in the literature less than one might expect. It is monitored by the hydrogen flow rate at maximum current. Most workers adjust the fuel flow rates to maximize the current, and then often report this flow rate, typically 10-50 ml min^{-1} without discussing the relation of fuel supplied to current obtained. This is understandable as it is usually not an encouraging number. However in the present case, the cell is burning nearly all the fuel supplied. We provide in Table 5.1, the current efficiency (defined as (1/2 the moles H_2 supplied per sec)/(Faradays of electricity flowing per sec)), both at the peak power condition. A second value based on the current flowing when the cell voltage (without IR correction) vanishes, is sometimes made, and in the case of our cells may approach 100%, but the first metric is the more relevant. In a cell of ideal design, such that the polarization curve is of rectangular form (Paula & Atkins 2002)[89], the two would be the same.

We include in Table 5.1 the current efficiencies reported by various workers for different types of fuel cells, and also calculate it in cases where both hydrogen flow rate, and current at maximum power, were reported but no current efficiency calculation was made. The current efficiency, when the standard 85% H_3PO_4 electrolyte was used in our cell, was high, consistent with experience of the favored electrolyte. Indeed, at 121ºC, it was as high as with the SiPOH-stabilized electrolyte. However a major difference arose when the higher temperature range was explored, the SiPOH-stabilized electrolyte reaching 1 amp cm^{-2} without any sacrifice in cell voltage. The power output at this temperature, shown in Figure 5.4, reached a very favorable 184 mW cm^{-2}, and this number could clearly be improved upon with more attention to cell design (to more

closely approach the ideal rectangular polarization curve (Paula & Atkins 2002)[89]). The voltage efficiency is also presented in Table 5.1, using two alternative definitions. The first is simply the [OCV/theoretical emf] x100 at the temperature of measurement, while the second (and more relevant one) is that based on the voltage at the power maximum - obviously a much smaller number. Again, the SiPOH-stabilized electrolyte is yielding favorable numbers relative to other cells for which the data are available. Again the advantage of high temperature operation is to be stressed.

We should recognize that our favorable voltage efficiencies, which would further improve with cell designs that produce a slower crossover to mass transport control, might be enhanced by the fact that our electrolyte thickness (3mm to permit exchange of liquid electrolyte without change of any other parameters) is greater than that of the common membrane. This would inhibit fuel crossover effects that diminish cell voltage. This might invalidate comparisons with some membranes. The cell was designed so that, by simple exchange of liquid electrolyte, multiple comparisons of the current flowing and the voltage (both open circuit and that at the power maximum) could be made for different protic ionic liquids (Belieres *et al.* 2006)[61], though this feature could not be utilized in the present study because of the importance of the solid SiPOH suspension to the function of the system.

	Operating Temp °C	H_2 flow rate (ml/min)	Max. Current dens (mA cm^{-2})	Current dens P_{max} (mA cm^{-2})	Current Effic %	Current Effic % at P_{max}	Voltage Effic % (OCV)	Voltage Effic % at P_{max}	Reference
Nafion 115	30.0	20.0	660.0	540.4	25.1	20.6	73.1	34.9	(a)
Nafion 117-polypropylenecomposite (70:30 weight ratio)	22.0	100.0	700.0	-	5.3	-	57.2	-	(b)
Nafion/inorganic composit membrane RH=50%	120.0	>270	580.0	433.6	1.7	1.2	81.8	35.8	(c)
Pristine Nafion membrane	60.0	300.0	1800.0	1208.5	4.6	3.1	79.4	39.8	(d)
Molten carbonate fuel cell (fluidized bed electrode)	650.0	10 (O_2)	115.6	-	8.8	-	29.1	-	(e)
[dema][TfO] in Sulfonated Polyimide	30.0	120.0	-	450.0	-	2.9	67.8	29.3	(f)
	120.0	12.0	-	190.0	-	12.1	64.6	28.2	(f)
	140.0	12.0	-	50.0	-	3.1	59.7	35.7	(f)
Phosphoric acid 85% (cell area 0.5 cm^2)	121.0	3.1	622.0	299.0	76.3	36.4	88.7	30.7	This work
	226.0	4.1	303.0	115.0	28.0	14.4	85.7	32.9	This work
SiPOH (cell area 0.5 cm^2)	121.0	3.1	731.0	345.0	89.7	38.4	85.4	33.0	This work
	226.0	4.1	966.0	477.0	89.6	44.3	85.4	33.8	This work
All results are given based on 1 bar pressure and a cell area of 1cm^2									
(a) A. Mota, P. P. Lopes, E. A. Ticianelli, E. R. Gonzalez, and H. Varela, Journal of The Electrochemical Society, 157(9) B1301-B1304									
(b) Sabit Adanur et al., NTC Project: F04-AE01, National Textile Center Annual Report: November 2006.									
(c) C. Wang, E. Chalkova, J. K. Lee, M. V. Fedkin, S. Komarneni, and S. N. Lvov, J. Electrochem. Soc., 158 (6) B690-B697 (2011).									
(d) W. Zhao, T. Haolin,n, Z. Huijie, L. Ming,nn, C. Rui, X. Pan, P. Mu, J. Membrane Sci. 421-422, 201-210 (2012).									
(e) J. Zhang, Z. Zhong, J. Xiao, Z. Fu, J. Zhao, W. Li, and M. Yang, Korean J. Chem. Eng., 28(8), 1773-1778 (2011).									
(f) S. -Y. Lee, A. Ogawa, M. Kanno, H. Nakamoto, T. Yasuda, and M. Watanabe, J. AM. CHEM. SOC. 132 (2010) 9764-9773.									

Table 5.1: Fuel cell performance conditions and metrics

The challenge now is to incorporate this electrolyte in a polymer membrane without low temperature aqueous processing which evidently produces chemical modifications (witness the hydrated polymer with extraordinary conductivity shown in Figure 5.2, the fuel cell performance of which will be described in future publications). Because it is of more acid character than hydrated H_3PO_4, the SiPOH-stabilized electrolyte should be more firmly retained in a polybenzimidazole membrane than H_3PO_4 (due to the larger proton transfer energy to the basic nitrogen (Belieres & Angell 2007)[25] (Angell *et al.* 2012)[1], so this type of membrane is an obvious first choice.

5.4 Discussion:

Phosphorus-silicon-oxygen combinations incorporating H_3PO_4 have been used previously to produce proton-conducting electrolytes for fuel cell applications. Matsuda *et al.* (Matsuda *et al.* 2002)[90] have described phosphosilicate gel powders and H_3PO_4-impregnated porous silica gel powders that have moderately high conductivity and stability at elevated temperatures, but they are made by sol-gel processes and must have chemical constitutions that are rather different from the anhydrous systems of the present work. A more closely related, but partly organic formulation, has been that of Nida *et al.* (Nida *et al.* 2002)[91], but the material of Nida *et al.*, in which dimethyldichlorosilane was reacted with phosphoric acid, was prepared as a precursor material for low-melting glass formulations. The molecular silicophosphates described to date have been very large species e.g. the 25 oxygen compound $Si_5O(PO_4)_6$ (Lejeune *et al.* 2005)[92] and related species of reference (Jänighen *et al.* 2012)[93], for which little or no solubility in H_3PO_4 would be expected.

Our active compounds are evidently of less complex character, resulting in an H_3PO_4-soluble material, probably of temperature-variable form, that strongly influences the properties of the H_3PO_4-based electrolyte.

One possible form, which high level gas phase electronic structure calculations at 298ºC (ORCA program package - using Density Functional Theory (DFT) with B3LYP/G (Becke, three-parameter, Lee-Yang-Parr) basis sets plus polarization and diffusion functions) have shown to be stable, and also of stronger acid character than H_3PO_4 itself, is $Si(PO_4H)_2$, with Si coordinated as in Figure 5.5. Calculations were done in parallel mode using a cluster of 8 nodes, and are comparable to, though somewhat

more quantitative than, those of Schaeffer and coworkers (Morris *et al.* 1997)[94] on H_3PO_4.

$Si(PO_4H)_2$ is a relatively small molecule, consistent with the high conductivity of the liquid at 280ºC. Such species are not known in the solid state, however, and are likely to be present only as a consequence of temperature-induced coordination number changes from the six-coordinated state known for most solid forms of silicophosphates (Lejeune *et al.* 2005)[92] (Jänighen *et al.* 2012)[93] (and also identified in NMR studies (Huang *et al.* 2013)[85] of the solid that forms as a component of the equilibrium described below).

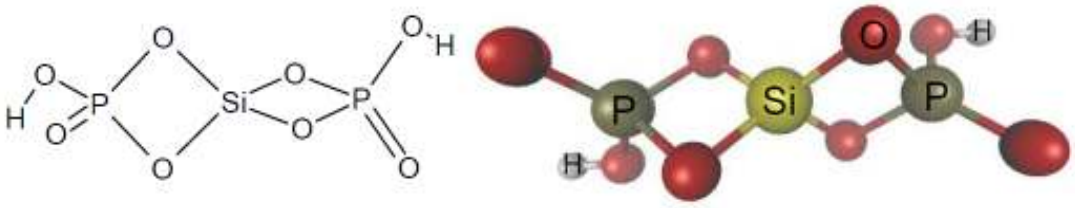

Fig 5.5. One of the possible structures of siphoric acid monomer shown in Sticks (left) and Balls and Cylinders (right) formats. Silicon (Green), Hydrogen (White), Oxygen (Red), and Phosphorous (yellow). The double edge-sharing, fourfold coordination, would constitute an unusual silicon coordination, made possible by the intense oxygen polarization by P(V). Other possibilities involving corner-linked phosphates and edge-shared phosphate octahedral, are noted below and will be considered elsewhere.

One of a variety of possible equilibria between solid and liquid forms could be that depicted in the following scheme, the right hand side being favored by higher temperatures.

$$Si(PO_4H)_2.(H_3PO_4)_2 \text{ (6-co-ord.)} = Si(PO_4H_2)_4 \text{ (4-co-ord)} = Si(PO_4H)_2 + 2H_3PO_4$$

These forms are related by the redistribution of protons, and tilting of the orthophosphate groups. Such an equilibrium would involve minimal changes in density, thus accounting for the stability of the suspension which can only be separated out by prolonged centrifugation. The molecular level characterization of the silicophosphoric acid is not needed to appreciate the fuel cell performance, so will be left for later studies (Huang *et al.* 2013)[85]. We note again , though, that the white solids that form a suspension when the reaction that produces the SiPOH electrolyte is continued, has silicon in six-fold coordination (Huang *et al.* 2013)[85] presumably with phosphate oxygen, as in the above scheme. The ambient temperature liquid state does not contain detectable ^{29}Si (Huang *et al.* 2013)[85], so the constitution of the high temperature solution, which need not be known for the present report, is uncertain at this time and is the subject of continuing study.

CHAPTER 6

A Novel Class of Anhydrous Superprotonic Ionic Liquids.

Enhancement in proton transfer in various systems such as catalysts, enzymes, proteins (Kemp 1995)[95], ionic liquids (Stoimenovski *et al.* 2010)[96] and acids with intrinsically high proton conductivity (Munson & Lazarus 1967)[97] has been investigated for years. For ionic liquids, some approaches to this issue have been suggested. The concept of ionicity, as the effective fraction of ions that are available to participate in conduction, can help to understand the ionic conduction mechanism (Yoshizawa *et al* 2003)[17] (MacFarlane *et al.* 2009)[98]. The Watanabe group recently showed that for ionic liquids produced from a super-strong base, 1,8-diazabicyclo[5,4,0]-7-ene (pK_a=13.4, known as DBU), and various Brønsted acids, a minimum ΔpK_a of 15 is required to achieve high thermal stability and high ionicity (Miran *et al.* 2012)[99]. Other ion pairs of anhydrous ionic liquid made from strong acids-weak bases and weak acids-strong bases have been studied as well (Belieres & Angell 2007)[25] (Yoshizawa *et al* 2003)[17] (MacFarlane *et al.* 2009)[15]. However, of all those, only a few show ionicities that exceeds the 0.01M KCl solution in which ion pairs are known to be fully dissociated and show ions of equal mobility.

In the absence of proton hopping mechanism (Grotthus mechanism (von Grotthuss 1806)[100]), vehicular motion is responsible for the ionic charge transfer. Therefore, higher ionic interaction between ions, causes the conductivity to decrease due to the increase in the viscosity, according to the Walden rule (Walden 1906)[19]. Amongst high conductivity materials rivaling aqueous solutions (Xu & Angell 2003)[101], (10^{-1} S

cm^{-1} at 100°C) the anhydrous protic ionic liquids reported to date have all been vehicular conductors according to the Walden plot assessments (in which equivalent conductivities are plotted against fluidities). Ionic liquids in which vehicular motion is responsible for charge transfer appear below the ideal line in the Walden plot because of the lack of free ions for conduction.

Here, we introduce a novel class of anhydrous protic ionic liquids which shows properties such as high viscosity and remarkable conductivity. In this chapter, we show two representatives of this new class which appear above the ideal line (0.01 M KCl solution discussed above) in the Walden plot due to the fact that their conductivities are largely decoupled from their viscosities (or show enhanced proton hopping mechanism). Since in this new class "protons" are moving freely between pairs of ions, where acid and base have $\Delta pK_a \leq 11$, we name our system superprotonic, instead of superionic.

Thus far, the high conductivity systems ($\sigma > 10^{-1}$ S/cm at 100ºC) in which a significant free proton contribution has been identified, have all involved water molecules in one way or another. The best known is concentrated (~4M) sulfuric acid, in which some 70% of the ionic current is carried by 'free' protons, but even the least hydrated case, phosphoric acid, widely studied for intermediate temperature fuel cells, needs at least 2 wt% water (10 mol%) to function effectively. In the present work, the absence of water is guaranteed by the presence of a strongly hydrolyzing anion, $AlCl_4^-$. In this contribution, we will describe how to decouple the protons from the possible vehicles by manipulating the properties of protic ionic liquids, PILs.

PILs, formed by transfer of protons from Brønsted acids to Brønsted bases, are a subclass of the burgeoning field of room temperature ionic liquids. The subclass has a

chemistry that is dominated by the activity of the transferred proton. Although members of this subclass have been reported in the literature since 1876, it is only recently has there been a concentrated attempt to characterize the state of the transferred proton and the driving force for its transfer. Without an adequate proton transfer driving energy (proton energy gap) highly ionic liquids cannot form.

In 2003, it was suggested (Yoshizawa *et al* 2003)[17] that, notwithstanding the anhydrous nature of the ionic liquids, the driving energy for proton transfer could be estimated approximately using the difference in pK_a values borrowed from aqueous solution data tables. This has since been supported by a number of studies (MacFarlane *et al.* 2009)[15], though with some appropriate reservations. Direct electrochemical interrogation of the ionic liquids (Bautista-Martinez *et al.* 2009)[102] , which may be supported by IR and NMR spectroscopic arguments (Stoyanov *et al.* 2006)[103] (Belieres *et al.* 2008)[104], have shown that in many cases the energy levels are, almost quantitatively, those estimated from aqueous data (as indeed would be expected if the free energies of hydration of the cation and anion are about the same). This has permitted the construction of an energy level diagram for the anhydrous systems (Belieres & Angell 2007)[25]. A new version of this diagram, updated from those in references 105 (Angell *et al.* 2007)[105] and 106 (Angell *et al.* 2011)[106], is given in Figure 6.1 below. Following Gurney (Gurney 1962)[24], the relationships between different acid-base couples are given in energy units , eV, as in redox tables, rather than in the pK_a units common to aqueous acid chemistry.

Lacking any leveling solvent, the proton potential for any given acid-base couple is located midway between those of the parent acid and base levels in the proton energy level diagram, as directly demonstrated by Kanzaki and co-worker (Kanzaki *et al.*

2007)[107]. The proton of any given proton transfer salt will relocate onto any stronger base that is introduced into the system. Accordingly, protic ionic liquids have acidities akin to those of aqueous systems, although they do not contain any hydronium ions in terms of which the pH acidity is conventionally defined. A similar situation holds for solutions of acids in non-aqueous solutions such as those in the weak base DMSO discussed by Bordwell (Bordwell 1988)[108] and many other authors. The present cases are distinguished by the absence of any solvent within which to establish a solution standard state. See figure 6.1 for more details.

	Occupied	Vacant	pK_a	E (eV)	Ref
Super-Acid	$HSbF_6$	SbF_6^-	-25	1.48	a
	$(HAlCl_4)$	$AlCl_4^-$	-23	1.36*	
	HOTf	OTf^-	-14	0.83	b
Acid Electrolytes	HSO_3F	SO_3F^-	-13	0.77	b
	HTFSI	$TFSI^-$	-12.2	0.72	b
	$PFPH^+$	PFP	-12	0.71	c
	ClF_3PyH^+	ClF_3Py	-11	0.65*	
	$HClO_4$	ClO_4^-	-10	0.59	
	H_2SO_4	HSO_4^-	-9	0.53	b
	CH_3SO_3H	$CH_3SO_3^-$ (MS)	-1.9	0.11	d
	HNO_3	NO_3^-	-1.3	0.08	
	$2\text{-}FPH^+$	2-FP	-0.43	0.03	e
	CF_3COOH	CF_3COO^- (TfAc)	-0.25	0.01	
	H_3O^+	H_2O	0	0	
Neutral Electrolytes	HPO_2F_2	$PO_2F_2^-$	0.3	-0.02	f
	H_3PO_4	$H_2PO_4^-$	2.12	-0.13	
	1,2,3-1 H-triazole H^+	1,2,3-1 H-triazole	3	-0.18	
	HF	F^-	3.2	-0.19	
	HCOOH	$HCOO^-$	3.75	-0.22	
	CH_3COOH	CH_3COOH^-	4.75	-0.28	
	$\alpha\text{-}MePyH^+$	α-MePyH	6.99	-0.41	
	hydrazine H^+	hydrazine	7.96	-0.47	
	NH_4^+	NH_3	9.23	-0.55	
	$EtNH_3^+$	$EtNH_3$	10.63	-0.63	
	Et_3NH^+	Et_3N (TEA)	11.25	-0.67	
	DBU^+	DBU	13.4	-0.79	g
	$C(NH_2)_3^+$	Guanidine	13.6	-0.8	h
	H_2O	OH^-	14	-0.83	

* Estimated Values

a) Ronan Gilson and Marcus C. Durrant, Dalton Trans., 2009, 10223–10230.
b) Keith E. Gutowski and David A. Dixon, J. Phys. Chem. A 2006, 110, 12044-12054.
c) Calculated using Advanced Chemistry Development (ACD/Labs) Software V11.02 (© 1994-2011 ACD/Labs)
d) Covington A. K.; Thompson, R. J. Solution Chem. 1974, 3, 603-617.
e) G. E. Ryschkewitsch,and K. zutshi, Inorganic Chem. 1970, 9(2) 411.
f) J. W. Larson and B. Su, J. Chem. Eng. Data 1994,39, 33-35.
g) M. S. Miran, H. Kinoshita, T. Yasuda, Md. A. B. H. Susan and M. Watanabe, Phys. Chem. Chem. Phys., 2012, 14, 5178–5186.
h) Perrin, D.D., Dissociation Constants of Organic Bases in Aqueous Solution, Butterworths, London, 1965; Supplement, 1972.

Fig 6.1. Proton free energy level diagram for acids and their conjugate bases, referenced to the H_3O^+/H_2O couple based on data measured or calculated for proton transfers in an aqueous medium. The difference between these values and those expected in the anhydrous PIL formed by transfer between pure acid and pure base, is discussed elsewhere (Gurney 1962)[24] (Kanzaki *et al.* 2010)[107], and is not expected, or found (Belieres & Angell 2007)[25] (Kanzaki *et al.* 2010)[107], to be large. The findings below will suggest that the missing numbers for $[HAlCl_4^+/AlCl_4^-]$ should be ~-23 and ~ 1.36 eV.

In the present study we seek conditions in which this proton potential is raised into the superacid range while maintaining high ionic liquid conductivity. The latter requires that the energy gap across which the proton falls in forming the ionic liquid be at least 0.7 eV (Belieres *et al.* 2008)[104] and preferably ~1.2 eV according to Miran et al. (Miran *et al.* 2012)[99]. If we choose the resonance-stabilized pentafluoropyridine (PFP), pKa = -12 (by theoretical calculation) and 5-chloro-2,4,6 trifluoropyrimidine (ClF_3Py) as bases, then Figure 5.1 shows that there are few choices available for the acid. To obtain an energy gap large enough to guarantee high ionicity, the acid must have strength comparable to that of $HSbF_6$. Remembering the manner in which Brown and Pearsall (Brown & Pearsall 1952)[109] created, in 1952, a "brilliant green" stoichiometric protic ionic liquid at -80ºC, by using a transient $HAlCl_4$ to protonate toluene, we adopt transient $HAlCl_4$ (Brown & Pearsall 1951)[110] as the protonating agent. Following Brown, dry HCl is bubbled through a stirred suspension of anhydrous $AlCl_3$ in PFP and $AlCl_3$ in ClF_3Py. Because our bases, while very weak, are stronger than toluene we are able to carry out the protonation at ambient temperature, after an initial heating to initiate the stirring (see below).

6.1 Methods of preparing novel ionic liquids:

Bubbling HCl for 3 hours at 25^{o}C dissolves all the $AlCl_3$ in PFP, producing a mobile light brown (The color can be assumed to originate in traces of organic material interacting with the $AlCl_3$.) ionic liquid ($[PFPH^+][AlCl_4^-]$) that we can study electrochemically up to at least 105ºC. The mixture was initially heated to 50^{o}C. The liquid is a good glass former and exhibits a glass transition at -63ºC with no sign of

crystallization. The mass of HCl absorbed was 10% less than that needed to form the stoichiometric $AlCl_4^-$, which we can understand, from Brown and Pearsall (Brown & Pearsall 1951)[110], in terms of rising HCl pressure as the initially formed $Al_2Cl_7^-$ is converted to $AlCl_4^-$. In some respects it resembles the α-picolinium heptachlorodialuminate studied long ago (Shuppert & Angell 1980)[111] but, by contrast, is extremely acidic in the Brønsted sense because of the weaker base (pK_a (picoline) ~ 6.0). By lowering the temperature of hydrochlorination to 0ºC using an ice-bath, the conversion to $AlCl_4^-$ can be increased to 95%, but the high temperature stability is correspondingly reduced. The $[PFPH^+][AlBr_4^-]$ was produced by the very same method using $AlBr_3$ instead of $AlCl_3$, and bubbling HBr (g).

Likewise, $[ClF_3PyH^+][AlCl_4^-]$ was produced by bubbling HCl in the mixture of ClF_3Py and $AlCl_3$ for 3 hours at 20°C until all the $AlCl_3$ was converted into $AlCl_4^-$ and $Al_2Cl_7^-$ anions. The sample was initially heated up to 50°C for 1 minute to allow stirring. The product is an ionic liquid, amber in color, which can be studied electrochemically up to 70°C. In this case the mass of HCl absorbed was 5% less than that required to form the stoichiometric $AlCl_4^-$**.** As we were expecting, the product shows higher viscosity than $[PFPH^+][AlCl_4^-]$ since ClF_3Py (pK_a ~ -11) is a slightly stronger base than PFP resulting a stronger proton transfer.

6.2 Result and Discussion:

Despite the low ΔpK_a, indicating an incomplete protonation, $[PFPH^+][AlCl_4^-]$ is indeed highly conductive. From its conductivity we may conclude that the effective energy level for $[HAlCl_4/AlCl_4^-]$ must indeed be placed at least ~0.65 eV above that of

[$PFPH^+$/PFP]), implying an energy level for [$HAlCl_4/AlCl_4^-$] near that of [$HSbF_6/SbF_6^-$] and a proton potential of the new ionic liquid indeed in the superacid range. The majority of previous references to superacids, in ionic liquids, is to their use as solvents and catalysts for chemical processes (Harmer *et al.* 2009)[112] and is quite different from the ionic liquid itself, as we identify here.

We later show that the molar conductivity of the [ClF_3PyH^+][$AlCl_4^-$] is higher than the [$PFPH^+$][$AlCl_4^-$], despite being much less fluid (see Figure 6.3), which shows an enhanced decoupling between its viscosity and its ionic conduction. This phenomenon makes it a robust superprotonic ionic liquid compared to [$PFPH^+$][$AlCl_4^-$]. In Figure 6.2 we present the ionic conductivity of [$PFPH^+$][$AlCl_4^-$], determined using a cell with variable cell constants (0.587 cm^{-1}, 0.906 cm^{-1} and 1.690 cm^{-1}). Ionic conductivities of [ClF_3PyH^+][$AlCl_4^-$] were measured using a cell with cell constants of 1.691 cm^{-1} and 1.830 cm^{-1}.

We compare these data with those of a related ionic liquid of stronger base, 2-fluoropyridinium tetrachloroaluminate, [2-FPH^+][$AlCl_4^-$] that we have prepared by the same method. In this case, where the proton energy level for the couple [2-FPH^+]/2-FP is much lower on Figure 6.1 - only 0.1 eV above the [H_3O^+]/[H_2O] reference level - we find that in the initial stage of the synthesis, in which anhydrous $AlCl_3$ is mixed with 2-FP, a liquid adduct is formed exothermically, so that the HCl is then reacting with a liquid rather than with a solid as in the previous case. During the HCl bubbling, the reaction mixture adds a mass that corresponds quantitatively (within 1 %) with the formation of the $AlCl_4^-$ anion. Figure 6.2 shows that the conductivity of this ionic liquid is as high as that of [ClF_3PyH^+][$AlCl_4^-$], but lower than that of the PFP-based salt *despite the fact that*

the viscosities of the liquid's have the following order: $[ClF_3PyH^+][AlCl_4^-]$>>$[PFPH^+][AlCl_4^-]$>$[2\text{-}FPH^+][AlCl_4^-]$ (See figure 6.3 for viscosities).

We will quantify this interesting difference below, after noting some aspects of the new type of ionic liquid's conductivity. Measurement of the viscosity of $[PFPH^+][AlBr_4^-]$ was unsuccessful with our viscometer, however the fluidity should not be higher than $[PFPH^+][AlBr_4^-]$ between 50-70^oC, as said by direct observations.

This is consistent with our recent report (Ansari *et al.* 2013)[113] of a superprotonic polymer produced a superweak base polymer (polydichlorophosphazene, PDCP) and a super acid (triflic acid, HOTf), where protons are shown to be mobilized in the polymer network comparing to the pure HOTf, either by the assisted dissociation of the acid by PDCP or by the enhancement in proton hopping. We must note that the protic ionic liquid formed by protonation of the weakest base, pentafluoropyridine, is a good conductor, with conductivity as high as the best known neutral protic ionic liquid diethylmethylammonium (DEMA) triflate which was used by Lee *et al.* (Lee *et al.* 2010)[114] in their recent testing of protic ionic liquid electrolyte based fuel cell.

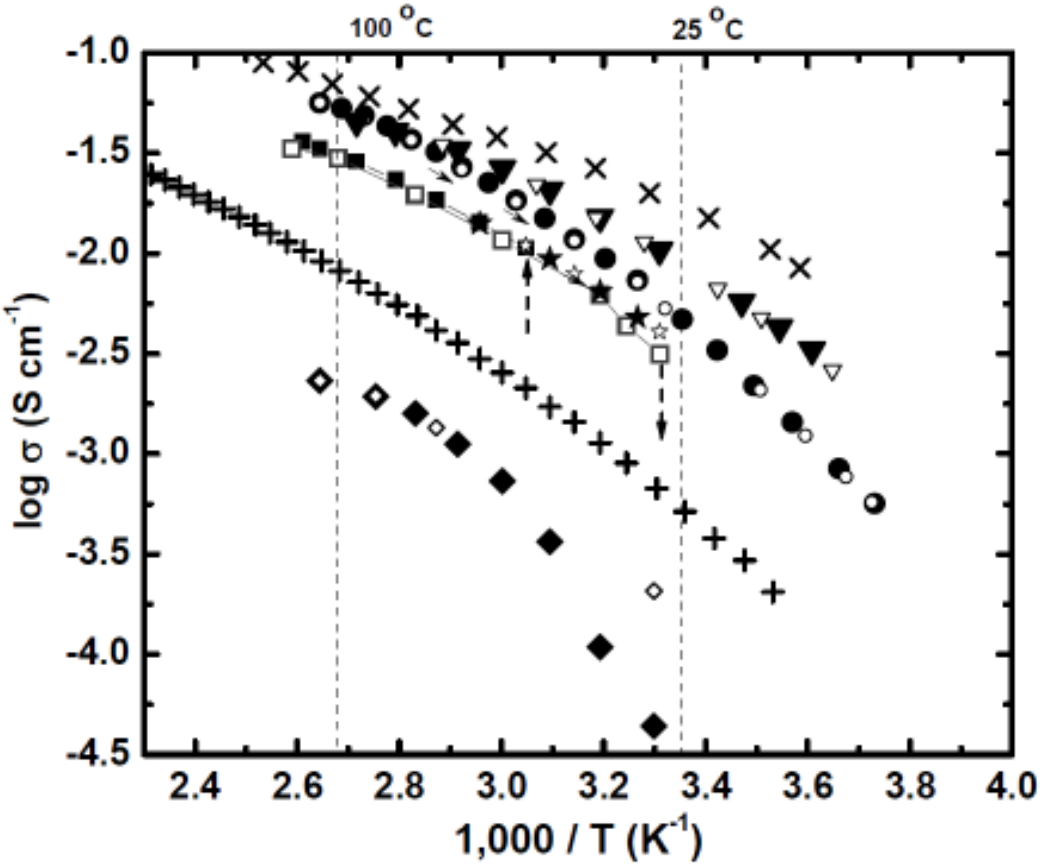

Fig 6.2. Ionic conductivity of the PILS of this work, pentafluoropyridinum tetrachloroaluminate (94.9 mol %): heating cycle (filled circles) cooling cycle (open circles), pentafluoropyridinum tetrachloroaluminate (90.0 mol %): heating cycle (filled triangles) cooling cycle (open triangles), 5-chloro-2,4,6-trifluoropyrimidinum tetrachloroaluminate (95.0 mol%): heating cycle (filled stars) cooling cycle (open stars), and 2-fluoropyridinium tetrachloroaluminate: heating cycle (filled squares) cooling cycle (open squares), pentafluoropyridinum tetrabromoaluminate (90.0 mol %): heating cycle (filled diamonds) cooling cycle (open diamonds), Comparison is made with the much studied case of the protic IL ethylammonium nitrate (cross symbols) and butylammonium hydrogensulfate (plus symbols). Note that the more nearly stoichiometric case has the higher conductivity, despite having a smaller free base content.

The compositions of three ionic liquids of this study containing (1) HCl gas that was reacted to form the ionic liquid, (2) cations ([$PFPH^+$] or [ClF_3PyH^+]), (3) anions ([$AlCl_4^-$] and [$Al_2Cl_7^-$]) and (4) unreacted pentafluoropyridine or 5-chloro-2,4,6

trifluoropyrimidine, in mole percent, are shown in Table 6.1. All of the aluminum chlorides are considered to be reacted with Cl^- to form either the tetrachloroaluminate or the heptachloroaluminate. Small percentage of the heptachloroaluminate, in all three systems, presents the tetrachloroaluminate as the principal brönsted acid which is the strongest acids (transient acid) after the well-known hexafluoroantimonate anions (SbF_6^-). The amount of the reacted-HCl(g) is consistent with the basicity of cations, $[PFPH^+] < [ClF_3PyH^+] < [2\text{-}FPH^+]$. The $AlCl_3$ reacts nearly 100% with the HCl gas, in the presence of 2-fluoropyridine, to form $AlCl_4^-$ anions. $AlBr_3$ also reacts almost 100% with HBr gas, in the presence of pentafluoropyridine; perhaps, indicating the enhanced acidity of $HAlBr_4$ compared to $HAlCl_4$.

$[PFPH^+][AlCl_4^-]$	Reacted HCl	$[PFPH^+]$	PFP	$[AlCl_4^-]$	$[Al_2Cl_7^-]$
94.9%	32.7	32.7	1.7	31.0	1.7
$[PFPH^+][AlCl_4^-]$	Reacted HCl	$[PFPH^+]$	PFP	$[AlCl_4^-]$	$[Al_2Cl_7^-]$
90.0%	32.4	32.4	3.2	28.5	3.6
$[PFPH^+][AlBr_4^-]$	Reacted HBr	$[PFPH^+]$	PFP	$[AlBr_4^-]$	$[Al_2Br_7^-]$
99.0%	33.1	33.1	0.4	33.1	0.2
$[ClF_3Py^+][AlCl_4^-]$	Reacted HCl	$[ClF_3Py^+]$	ClF_3Py	$[AlCl_4^-]$	$[Al_2Cl_7^-]$
95.0%	32.8	32.8	1.2	32.3	0.9

Table 6.1: The amounts of the HCl reacted with aluminum chloride to form tetrachloroaluminate and heptachloroaluminate anions, pentafluoropyridinum and 5-chloro-2,4,6 trifluoropyrimidinum cations along with the amount of unreacted pentafluoropyridine and 5-chloro-2,4,6 trifluoropyrimidine in three novel ionic liquids, all in mole percent. The values for $[PFPH^+][AlBr_4^-]$ are included as well.

Viscosities reported in this study were measured by series of Cannon-Manning Semi-Micro Extra Low Charge Viscometers. Viscosity of the two novel ionic liquids introduced here are compared to the $[2\text{-}FPH^+][AlCl_4^-]$, having stronger base, and ethyl

ammonium nitrate (EAN) ,as the well-known good ionic liquid, in Figure 6.3. We should note that the effects of additional nitrogen sites in the ClF_3Py are reflected in this plot. $[ClF_3PyH^+][AlCl_4^-]$ is more viscous than the $[2\text{-}FPH^+][AlCl_4^-]$, although they almost have the same conductivity (please see figure 6.2) . The high viscosity of $[ClF_3PyH^+][AlCl_4^-]$ is perhaps due to the enhanced hydrogen bonding in this sample because of the excess nitrogen-site present in the system compared to PFP and 2-FP. From the conductivity plot, if protons in the $[ClF_3PyH^+][AlCl_4^-]$ were carried through the sample via vehicular motion, one would expect that its conductivity would be much lower than $[2\text{-}FPH^+][AlCl_4^-]$. Thus their conductivity suggests that vehicular motion is not the dominant mechanism for the charge transfer in the liquid. This can also be attested to evaluating the mobility of protons in the system.

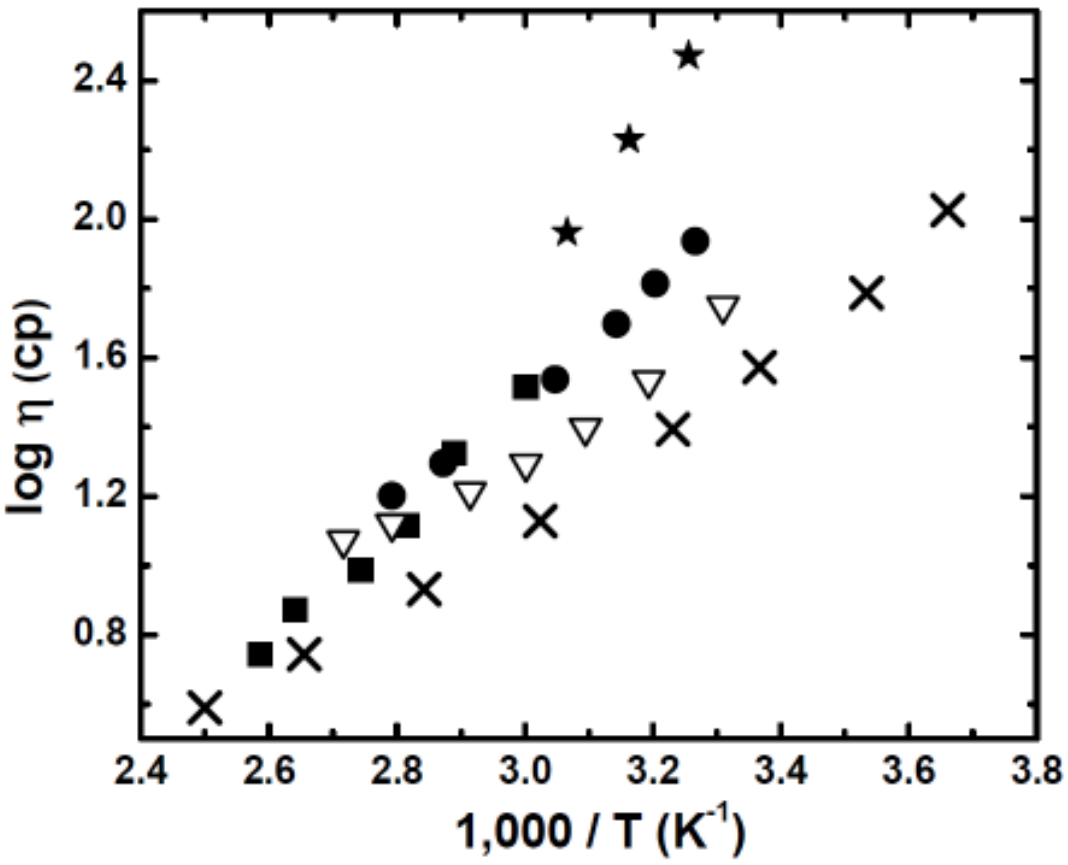

Fig 6.3. Arrhenius plots of viscosity data for three different levels of hydrochlorination of $AlCl_3$, pentafluoropyridinum tetrachloroaluminate 94.9 mol% (triangles), pentafluoropyridinum tetrachloroaluminate 90.0 mol% (circles), 5-chloro-2,4,6-trifluoropyrimidinum tetrachloroaluminate 95.0 mol% (stars). Comparison is made with the 100% [$AlCl_4^-$] salt of the stronger base 2-fluoropyridinium tetrachloroaluminate (squares) and with the classical protic ionic liquid, ethyl ammonium nitrate (crosses) from previous studies. Note that 5-chloro-2,4,6-trifluoropyrimidinum tetrachloroaluminate has the highest viscosity but not the lowest conductivity (see figure 6.1 for conductivities).

We can assess the ionic mobilities relative to the fluidities using the Walden plot. According to the Walden rule (established originally for aqueous solutions (Walden 1914)[19]), the flow of ions under an electric field is controlled by the friction with the

viscous medium. The ideal Walden line is shown as a dashed line, based on data for aqueous KCl solution in which the two ions are known to have equal mobilities.

In the superacid region of the proton free energy level diagram, one would expect the bond length between the proton and the nearest nitrogen to increase when the ΔpK_a between the pair of ions decreases. This can cause proton to interact loosely with its environment; hence, marks a higher mobility. To show this phenomenon, we performed a set of *ab initio* calculations. Figure 6.4 shows the result of geometry optimizations performed by Gaussian software package 03, using HF method and 6-31G(d,p) basis set. The geometry optimization of various cations ($PFPH^+$, ClF_3PyH^+, $2\text{-}FP^+$, and $PyridineH^+$) with the $AlCl_4^-$ anion suggests that the bondlength between the nitrogen site and the proton increases when the proton affinity of the cation decreases, indicating a lower interaction between the proton and its corresponding nitrogen. The gap between the neighboring chlorine and the proton (shown as dotted line) also noticeably increases by an increase in the basicity of the cation. The pyridine, the strongest base (pK_a=5.17 (Hosmane & Liebman 2009) [115]) among the bases of this study, shows the lowest $[N\text{---}H]^+$ bondlength indicating an enhanced N-H interaction. The Geometry optimizations were followed by frequency optimizations to confirm absence of any imaginary frequencies which validates the result of the geometry optimization using the applied basis set.

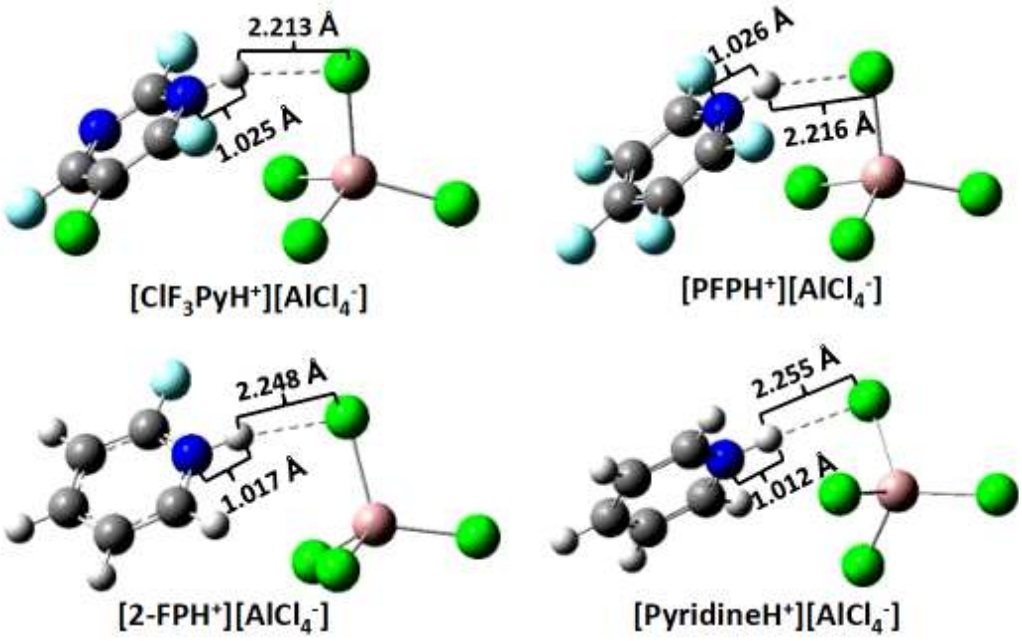

Fig. 6.4. Shows the result of *geometry optimizations* when pentafluoropyridine, 5-chloro-2,4,6-trifluoropyrimidine, 2-fluoropyridiniu and Pyridine acts as the base and the transient $HAlCl_4$ acts as the super acid. It is shown that the distance between the nitrogen site and proton decreases by cation's proton affinity disallowing the proton mobility to increase. Carbon (Gray), chlorine (green), nitrogen (Blue), aluminum (Salmon), fluorine (Cyan) and Hydrogen (white).

When an ionic liquid is formed by adding a super strong acid to a super weak base, the proton does not surely belong to any of the available sites. Such loose proton is capable of hopping freely between vacant sites without sensing any significant interactions. This causes the conductivity of the ionic liquid to be somewhat independent of its viscosity. Figure 6.5 shows protons hopping independently between vacant sites where a combination between a super weak base and a super strong acid is available. This leads the system to behave differently from all the other protic liquids that have been studied, in which protons are mostly localized by the base (or the acid).

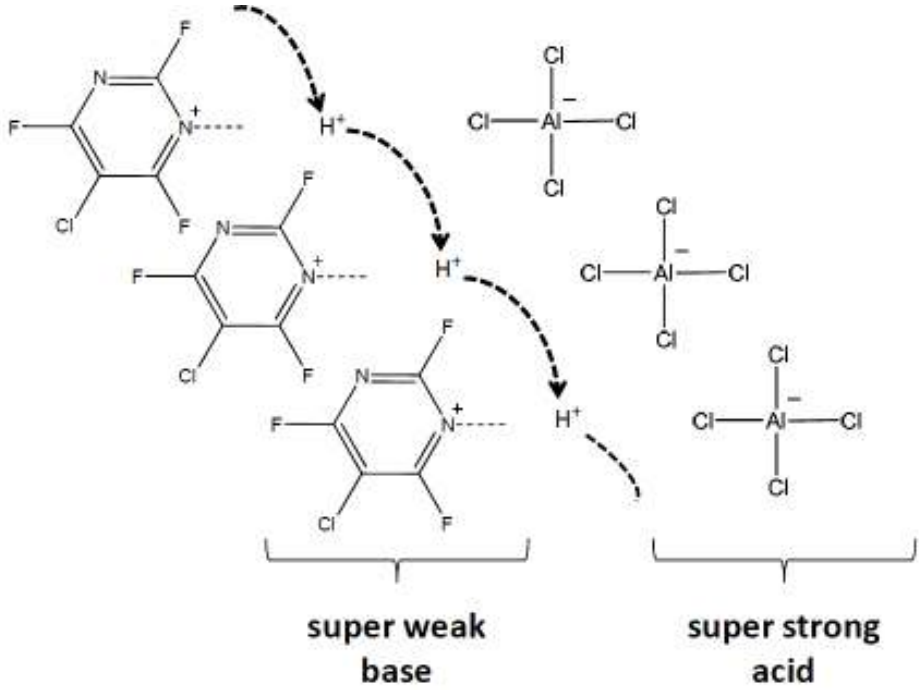

Fig. 6.5. Shows the behavior of proton in a sample containing a super weak base (i.e. 5-chloro-2,4,6 trifluoropyrimidine) and a super strong acid (i.e. tetrachloroaluminate). The proton moves freely between 5-chloro-2,4,6 trifluoropyrimidinium cations and tetrachloroaluminate anions without being obstructed.

The equivalent conductivities of the ionic liquids of this study are compared with their fluidities in Figure 6.6, also contains data for some other known systems that will be discussed later. The measured densities are used to convert the specific conductivities of Figure 6.2 to equivalent conductivities.

Figure 6.6 shows what we had hoped to find, namely, that in the superacid region of the proton free energy level diagram, as the binding of the proton to its environment becomes looser, its mobility starts to become less dependent on the motions of the entities to which it is normally bound, (either the acid from which it derived, or the base to which it transferred). Under these circumstances, the behavior normally associated

only with very small ions like Li^+, or small highly polarizable ions like Ag^+ in solvent-free media (Angell 1990)[116], appears, and the liquids become "superionic" (or in the present case "superprotonic").

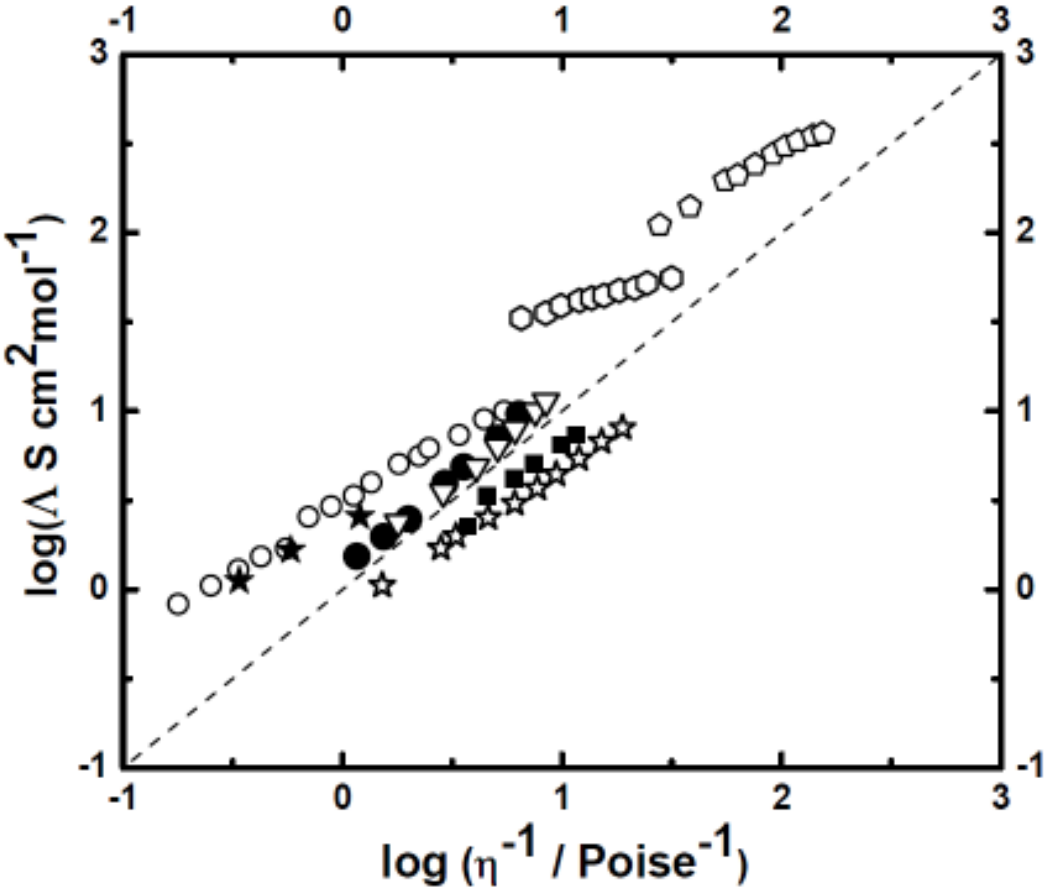

Fig. 6.6 Walden plot for assessment of excess (superionic or super-protonic) contributions to the conductivity of ionic liquids of this study, pentafluoropyridinum tetrachloroaluminate 94.9 mol% (triangles), pentafluoropyridinum tetrachloroaluminate 90.0 mol% (filled circles), 5-chloro-2,4,6-trifluoropyrimidinum tetrachloroaluminate 95.0 mol% (filled stars) and 2-fluoropyridinium tetrachloroaluminate (squares). Comparison of data for systems of the present study is made with superprotonic systems 4M sulfuric (pentagons) and phosphoric acid 98% (open circles), a superionic silver halide-alkali halide glassformer (hexagons), and with ethylammonium nitrate (open stars). Note the intermediate position of the PIL made from the monofluorinated pyridine.

For protonic motion, this is usually referred to as a Grotthus (Grotthus 1806)[20] mobility mechanism, though no such term is used for the free motion of lithium ions in ionic liquids and glasses where the "decoupling ratio" (Moynihan *et al.* 1971) [117] can amount to ten or more orders of magnitude (Moynihan *et al.* 1971)[117]. By contrast, the decoupling in $[PFPH^+][AlCl_4^-]$ seems to be increasing with increasing temperature, as the protons become increasingly plasma-like. Unfortunately, higher temperature studies would require high pressure equipment to repress the loss of HCl, a measurement that goes beyond the scope of this study. The enhanced superionicity in $[ClF_3Py^+][AlCl_4^-]$ is perhaps due to the presence of additional nitrogen sites and the enhancement in the hydrogen bonding of the system which allows the proton hopping more effectively. For the same reason, phosphoric acid is known to be superprotonic by itself even under anhydrous condition.

For the purpose of assessing the "superprotonicity" of the present liquids, we include, in the Figure 6.6, of some data for liquids already known to be proton conductors. The case of aqueous acid solutions, studied originally by Grotthus (Grotthus 1806)[20], is the best known. The dominance by proton motion reaches its maximum in supercooled dilute acid solutions as the tetrahedral network of hydrogen bonded water molecules builds up. Rather than showing this limiting case, we make comparison, in Figure 6.6, with the important practical cases of 4M sulfuric acid ("battery acid") and the lightly hydrated phosphoric acid that is used in current phosphoric acid fuel cell technology. The new type of ionic liquid introduced here is clearly superprotonic. The increasing decoupling with increasing temperature in $[PFPH^+][AlCl_4^-]$, perhaps due to the absence of any binding to the conjugate bases, $AlCl_4^-$ or $Al_2Cl_7^-$, suggests the

conductivity could reach or exceed that of 4M sulfuric acid if the temperature could be further raised. This should be possible if a less volatile halide system such as HBr + $AlBr_3$, the solid acid $HAl(Tf)_4$, or $HSbF_6$ itself, were used to protonate bases weaker than PFP, such as toluene. According to figure 6.1 and the observed fluidity of the $[PFPH^+][AlBr_4^-]$, this ionic liquid should not show a superprotonic behavior perhaps due to an increase in the ΔpK_a of the system, exceeding the optimum value for the proton gap (~0.65-0.72 eV) in the superacid region of the generalized proton free energy level diagram. Figure 6.7 shows the result of the Differential Scanning Calorimetry (DSC) for four samples of this study. The glass transition temperatures (T_g) were determined using a differential scanning calorimeter model DSC-7, Perkin−Elmer. The instrument was calibrated by the two-point method with cyclohexane (solid-solid transition, $T_{S1\rightarrow S2}$ = −86.6°C) and indium (T_m = 156.6°C) as the two standards for high temperature and low temperature regions, respectively. Since our ionic liquids were corrosive to aluminum pans, a PIRANI 10 Sputter Coater Model S150B was used to make gold coated aluminum pans in order to avoid any corrosion. All samples were scanned at a rate of 20 $Kmin^{-1}$ under helium atmosphere.

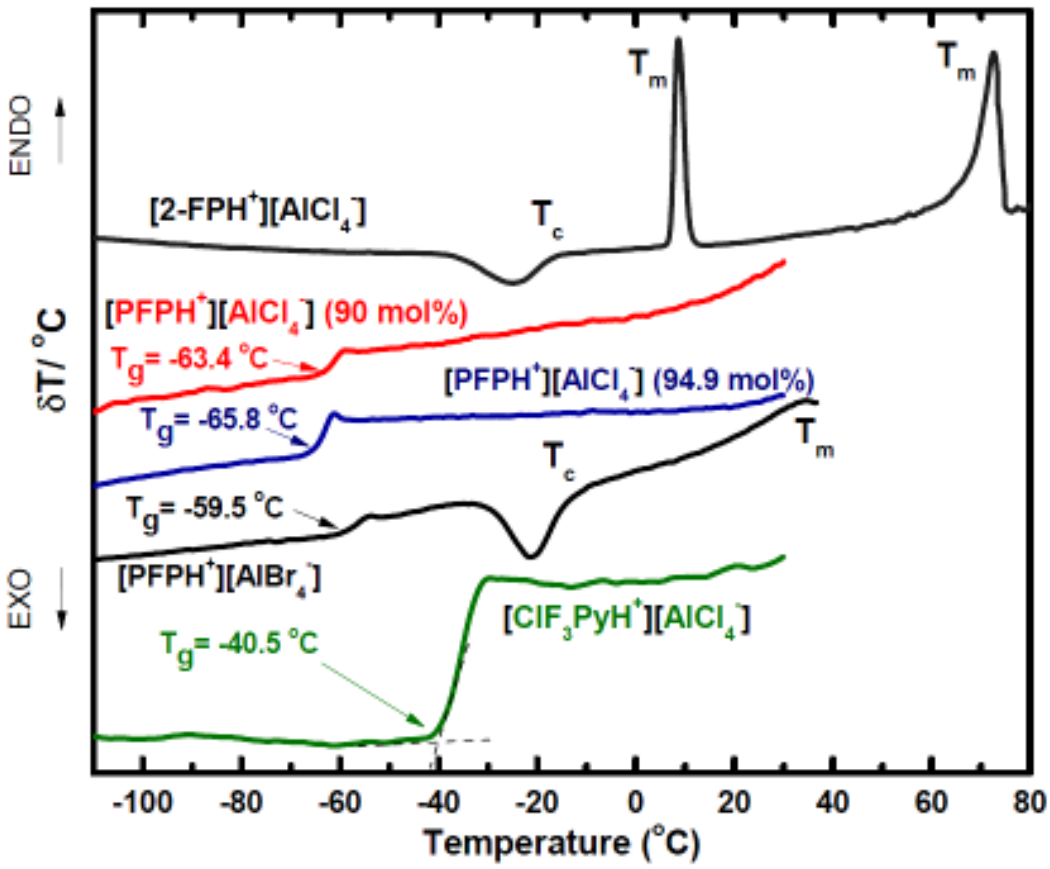

Fig. 6.7. Differential Scanning Calorimetry (DSC) of the $[ClF_3PyH^+][AlCl_4^-]$, $[PFPH^+][AlBr_4^-]$, two compositions of $[PFPH^+][AlCl_4^-]$, and $[2\text{-}FPH^+][AlCl_4^-]$ are shown. All of the novel superprotonic ILs show good glass-forming behavior. The $[2\text{-}FPH^+][AlCl_4^-]$ does not show any glass transition temperature. $[2\text{-}FPH^+][AlCl_4^-]$ perhaps behaves like a plastic crystal by having some degrees of rotational disorder (MacFarlane *et al.* 1999)[118]. The DSC on the $[PFPH^+][AlBr_4^-]$ was abandoned at high temperatures for the safety of the instrument.

Higher T_g value for $[ClF_3PyH^+][AlCl_4^-]$ can be related to its hydrogen bonding network or high viscosity. The behavior of the $[2\text{-}FPH^+][AlCl_4^-]$ is similar to the plastic crystalline lithium conductor reported by Macfarlane *et al.* (MacFarlane *et al.* (1999)[118] showing a first order solid-solid transition prior to melting.

In future, it will be possible to provide the same low binding conditions as we have established in this chapter, using involatile multi-site bases and other solid acids (Angell *et al.* 2007)[18], in order that the ultimately desirable "proton sea" condition can be more closely approached.

CHAPTER 7

Concluding Remarks

In the PDCP:HOTf system, assuming that the pulsed field gradient studies to be performed confirm the extreme (~10 orders of magnitude) decoupling of the proton motion from the segmental relaxation time, then the challenge will become one of anchoring the anion to the P−N backbone so that the proton-donating moiety cannot be leached out of the rubbery matrix. This will be necessary if this type of proton-conducting polymer is to find useful application as a fuel cell membrane. One can expect that, as in the case of other proton-transfer salts, there will be a proton binding energy that optimizes the cathodic reduction of oxygen but, for a PDCP-based system, it will necessarily require proton donation from a superacidic moiety.

A molecular electrolyte system consist of a modified phosphoric acid, Siphoric acid (SiPOH), was successfully made to protect phosphoric acid against decomposition up to at least 250^{o}C. Assuming that the good performance of this fuel cell electrolyte, is partly a consequence of the higher temperatures that can be reached, but partly also a consequence of some favorable modification of the surface tension that improves the complex kinetics at the three-phase boundary (gas/catalyst/electrolyte). This is an interesting topic for future investigations.

A new type of anhydrous protic ionic liquids can be made from a combination of a super strong acid and super weak base. The two representatives of this type of protic ionic liquid, studied in this thesis, show superprotonic behavior. This is due to the fact that proton is loosely bound to the conjugate-acid which makes it capable of hopping

freely in the system. Theoretical studies are performed to confirm the less interacting proton in this system. Such behavior particularly causes due to the decoupling of the conductivity from the liquid's viscosity. Unlike other superprotonic systems studied previously, this new type of protic ionic liquid is completely anhydrous which makes it a great candidate to be used as fuel cell electrolytes.

REFERENCES

[1] Angell, C. A. Ansari, Y. Zhao, Z. Ionic liquids: past, present and future. *Faraday Discuss.* **154** (2012) 9-27.

[2] Barrer, R. M. The viscosity of pure liquids. II. Polymerized ionic melts, *Trans. Faraday Soc.* **39** (1943) 59-67.

[3] Krossing I., Slattery J. M., Daguente C., Dyson P. J., Oleinikova, A. and Weingartner, H., Why Are Ionic Liquids Liquid? A Simple Explanation Based on Lattice and Solvation Energies, *J. Am. Chem. Soc.* **128** (41) (2006) 13427-13434.

[4] Angell, C. A. Xu. W. Yashizawa-Fujita, M. Hayashi, A. Beleires, J.-P. Lucas, P. Videa, M. Zhao, Z.-F. Ueno, K. Ansari, Y. Thomson, J. and Gervasio, D. *Electrochemical aspects of ionic liquids.* by Ohno, H. 2nd ed. John Wiley & Sons, Inc. (2011) 5-30.

[5] Tamura T., Hachida T., Yoshida K., Tachikawa N., Dokko K., Watanabe M. New glyme–cyclic imide lithium salt complexes as thermally stable electrolytes for lithium batteries. *J. Power Sources* **195** (2010) 6095-6100.

[6] Hurley, F. H. and WIer, T. P. Jr. Electrodeposition of Metals from Fused Quaternary Ammonium Salts*J. Electrochem. Soc.* **98** (1951) 203.

[7] Hussey, C. L. Room Temperature Molten Salt Systems. *Advances in Molten Salt Chemistry* **5** (1983) 185-230.

[8] Fuller, J. Carlin, R. T. De Long, H. C. and Haworth, D. Structure of 1-ethyl-3-methylimidazolium hexafluorophosphate: model for room temperature molten salts. J. Chem. Soc., Chem. Commun. 0 (1994) 299-300.

[9] Bonhôte, P. Dias, A.-P. Papageorgiou, N. Kalyanasundaram, K. and Grätzel, M. Hydrophobic, highly conductive ambient-temperature molten salts. *Inorg. Chem.* **35** (1996) 1168-1178.

[10] Angell, C. A. Xu, W. Yoshizawa, M. Belieres, J.-P. Hayashi, A. Lucas, P. Videa, M. Zhao, Z.-F. Gervasio, D. *Electrochemical aspects of ionic liquids*, by Ohno, H. Wiley Pub. Chapter 2 (2011) 5-23.

[11] Fericola, A. Navarra, M. A. and Panero, S. Aprotic ionic liquids as electrolyte components in protonic membranes. *J. Appl. Electrochem.* **38** (2008) 993-996.

[12] Noritomi, H. Minamisawa, K. Kamiya, R. Kato, S. Thermal stability of proteins in the presence of aprotic ionic liquids. *J. Biomed. Sci. Eng.* **4** (2011) 94-99.

[13] Fujita K., MacFarlane D. R., Forsyth M., *Chem. Commun.* (2005) 4804.

[14] Hangarge, R. V. Jarikote, D. V. and Shingare, M. S. Knoevenagel condensation reactions in an ionic liquid. *Green Chem.* **4** (2002) 266-268.

[15] Macfarlane, D. R. Forsyth, M. Izgotodina, E. I. Abbott, A. P. Annat, G. and Fraser, K. On the concept of ionicity in ionic liquids. *Phys. Chem. Chem. Phys.* 11 (2009) 4962-4267.

[16] Xu, W. Cooper, E. I. and Angell, C. A. Ionic liquids: ion mobilities, glass temperatures, and fragilities. *J. Phys. Chem.* B **107** (2003) 6170-6178.

[17] Yoshizawa M., Xu W., and Angell C. A. Ionic liquids by proton pransfer: vapor pressure, conductivity, and the relevance of ΔpK_a from aqueous solutions. *J. Am. Chem. Soc.* **125** (2003) 15411-15419.

[18] Angell, C. A. Byrne, N. and Belieres, J.-P. Parallel developments in aprotic and protic ionic liquids: physical chemistry and applications. *Acc. Chem. Res.* **40** (2007) 1228.

[19] Walden, P. Über organische lösungs und ionisierungsmittel. III. Teil: innere Reibung und deren zusammenhang mit dem leitvermögen. *Z. Phys. Chem.* **55** (1906) 207-246.

[20] Grotthus, C. J. T., Sur la décomposition de l'eau et des corps qu'elle tient en dissolution à l'aide de l'électricité galvanique. *Ann. Chim.* **58**, (1806) 54.

[21] Kawaguchi et al. *Fuel cells and polymers.* Pub.Page 68 (Japan) (2005).

[22] Ohno, H. Yoshizawa-Fujita, M. and Mizumo, T. *Electrochemical aspects of ionic liquids*, 2nd edition, by Ohno, H. Chapter 6, 87-93, Published by John Wiley & Sons, Inc (2011).

[23] Monk, P. M. S. *Fundamentals of electro-analytical chemistry*, John Wiley & Sons Ltd. 253-262 (2001).

[24] Gurney, R. W. *Ionic processes in solution;* Dover Publications, New York, page 275 (1962).

[25] Belieres, J.-P. and Angell, C. A. Protic ionic liquids: preparation, characterization, and proton free energy level representation. *J. Phys. Chem.* B **111** (2007) 4926-4937.

[26] Bautista-Martinez, J. A. Tang, L. Belieres, J.-P Angell, C. A. and Friesen, C. Hydrogen redox in protic ionic liquids and a direct measurement of proton thermodynamics. *J. Phys. Chem. C* **113** (2009) 12586-12593.

[27] Kanzaki, R. Uchida, K. Song, X. Umebayashi, Y. and Ishiguro, S. Acidity and basicity of aqueous mixtures of a protic ionic liquid, ethylammonium nitrate. *Anal. Sci.* **24** (2008) 1347-1349.

[28] Belieres, J.-P. *Protic ionic liquids, high temperature electrolytes for fuel cell applications*, Ph.D. thesis. Arizona State University, page 95 (2005).

[29] Srinivasan, S. *Fuel cells: from fundamentals to applications, springer science and business media*, LLC., page 197 (2006).

[30] Larminie, J. and Dicks, A. *Fuel Cell Systems Explained*, second edition, West Sussex: John Wiley & Sons Ltd (2003).

[31] Larminie J., and Dicks A., *Fuel Cell Systems Explained*, second edition, pages 1-6, Wiley (2003).

[32] Wang, C. Waje, M. Wang, X. Tang, J. M. Haddon, R. C. and Yan, Y. Proton exchange membrane fuel cells with carbon nanotube based electrodes. *Nano Lett.* **4** (2004) 345-348.

[33] Brett, A. Holmberg, b. Xinwang, a. Yan, Y. Nanocomposite fuel cell membranes based on Nafion and acid functionalized zeolite beta nanocrystals. *J. Membrane Sci.* **320** (2008) 86-92.

[34] Reid, J.H. Process of generating electricity. U.S. Patent 736,016, 11 August 1903.

[35] Gülzow, E. Alkaline fuel cells: a critical view. *J. Power Sources* **61** (1996) 99-104.

[36] Kordesch, K. V. and Simader, G. R. Environmental impact of fuel cell technology. *Chem. Rev.* **95** (1995) 191-207.

[37] Bischoff, M. Molten carbonate fuel cells: A high temperature fuel cell on the edge to commercialization. *J. Power Sources* **160** (2006) 842-845.

[38] Minh, N. Q. Solid oxide fuel cell technology-features and applications. *Solid State Ionics* **174** (2004) 271-277.

[39] Vincent, C. A. and Scrosati, B. *Modern Batteries*, 2nd edition, Page 16-27 Arnold, London (1997).

[40] Shibata, A. and Sato, K. Development of vanadium redox flow battery for electricity storage. *Power Engineering Journal* **13** (1999) 130-135.

[41] Lex, P. and Jonshagen, B. The zinc/bromine battery system for utility and remote area applications. *Power Engineering Journal* **13** (1999) 142-148.

[42] Zito, R. *Process for energy storage and/or power delivery with means for restoring electrolyte balance*, US patent 5612148.

[43] Price, A. Bartley, S. Male, S. and Cooley, G. A novel approach to utility scale energy storage [regenerative fuel cells]. *Power Engineering Journal* **13** (1999) 122-129.

[44] Hoogers G., *Fuel Cell Technology Handbook*, CRC Press (2003).

[45] Haile, S. M. Fuel Cell Materials and Components. *Acta Materialia* **51** (2003) 5981-6000.

[46] Mench, M. M. *Fuel cell engines*, page 121, John Wiley and Sons (2008).

[47] Mench, M. M. *Fuel cell engines*, page 126, John Wiley and Sons (2008).

[48] Kolb G, *Fuel Processing: for fuel cells*, page 355, John Wiley and Sons, Wiley-VCH. (2008).

[49] Teagan, W. P. Bentley, J. and Barnett, B. Cost reductions of fuel cells for transport applications: fuel processing options. *J. Power Sources* **71** (1998) 80-85.

[50] Garche, J. and Jorissen, L. *PEMFC fuel cell systems, in the Handbook of Fuel Cells* (eds W. Vielstich and A.A.G.H. Lamm), Wiley, Chichester. **4**, page (2003) 1244.

[51] Bard, J. A. and Faulkner, L. R. *electrochemical Methods: fundamentals and applications*, 2nd edition John Wiley & Sons, Inc. (2001).

[52] Barsoukov, E. Macdonald, J. R. *Impedance spectroscopy theory, experiment, and applications*, 2nd edition, John Wiley & Sons, Inc. (2005).

[53] Gamry Instruments, Inc.m Application Note, Basics of Electrochemical Impedance Spectroscopy, Rev. 1.0 9/3/2010 (2010).

[54] Viswanath, D. S. Ghosh, T. S. Prasad, D. H. L. Dutt, N. V. K. Rani, K. Y. *Viscosity of liquids: Theory, Estimation, Experiment, and Data*, Springer (2007).

[55] Daniels, T. *Thermal Analysis*, chapter 4, John Wiley & Sons, New York (1973).

[56] Kreuer, K. D. On the development of proton conducting polymer membranes for hydrogen and methanol fuel cells. *J. Membr. Sci.* **185** (2001) 29-39.

[57] Yang, C. Srinivasan, S. Bocarsly, A. B. Tulyani, S. Benziger, J. B. A comparison of physical properties and fuel cell performance of Nafion and zirconium phosphate/Nafion composite membranes. *J. Membr. Sci.* **237** (2004) 145-161.

[58] Hasiotis, C. Qingfeng, L. Deimede, V. Kallitsis, J. K. Kontoyannis, C. G. Bjerrum, N. J. Development and Characterization of Acid-Doped Polybenzimidazole/Sulfonated Polysulfone Blend Polymer Electrolytes for Fuel Cells. *J. Electrochem. Soc.* **148** (2001) A513-A519.

[59] Li, M.-Q. and Scott, K. A polymer electrolyte membrane for high temperature fuel cells to fit vehicle applications. *Electrochim. Acta* **55** (2010) 2123-2128.

[60] Narayan, S. R. Yen, S.-P. Liu, L. and Greenbaum, S. G. Anhydrous proton-conducting polymeric electrolytes for fuel cells. *J. Phys. Chem.* B **110** (2006) 3942-3948.

[61] Belieres, J.-P, Gervasio, D. and Angell, C. A. Binary inorganic salt mixtures as high conductivity liquid electrolytes for >100 °C fuel cells. *Chem. Commun.* (2006) 4799.

[62] Thomson, J. Dunn, P. Holmes, L. Belieres, J.-P. Angell, C. A. Gervasio, D. A Flourinated ionic liquid as a high-performance fuel cell electrolyte. *ECS Trans.* **13** (2008) 21-29.

[63] Nakamoto, H. and Watanabe, M. Brønsted acid–base ionic liquids for fuel cell electrolytes. *Chem. Commun.* (2007) 2539-2541.

[64] Ansari, Y. Ueno, K. and Angell, C. A. to be published 2013.

[65] Allcock, H. R. *Chemistry and Applications of Polyphosphazenes*; Wiley-Interscience: New York (2003).

[66] Tura, D. R. Pergushov, D. V. Babin, I. A. Papkov, V. S. Zezin, A. B. Simulation of the development of the mosaic surface structures in polyethylene. *Polym. Sci. Ser.* B **51** (2009) 360-376.

[67] Wycisk, R.; Pintauro, P. N. Polyphosphazene Membranes for Fuel Cells. *Adv. Polym. Sci.* **216** (2008) 157-183.

[68] Heston, A. J. Panzner, M. Youngs, W. J. and Tessier C. A. Acid-base chemistry of $[PCl_2N]_3$. *Phosphorus, Sulfur, Silicon Rel. Elem.* **179** (2004) 831-837.

[69] Xu, B.-Q. Sood, D. S. Gelbaum, L. T. and White, M. G. Toluene carbonylation catalyzed by mixtures of water and trifluoromethanesulfonic acid. *J. Catal.* **186** (1999) 345-352.

[70] Russell, D. G. and Senior, J. B. Studies on trifluoromethanesulfonic acid. Part 2. Conductivities of solutions of metal trifluoromethanesulfonates and other bases in trifluoromethanesulfonic acid. *Can. J. Chem.* **58** (1980) 22-29.

[71] Asensio, J. A. Borrós, and S. Gómez-Romero,You have full text access to this content Proton-conducting polymers based on benzimidazoles and sulfonated benzimidazoles. P. *J. Polym. Sci. A: Polym. Chem.* **40** (2002) 3703-3710.

[72] Coleman, M. M. Zarian, J. Painter, P. C. Vibrational Spectra and Normal Coordinate Calculations of Chlorophosphazene Compounds. III. Polydichlorophosphazene. Appl. Spectrosc. **36** (1982) 277-281.

[73] Macedo, P. B. Moynihan, C. T. Bose, R. Role of ionic diffusion in polarization in vitreous ionic conductors. *Phys. Chem. Glasses* **13** (1972) 171-179.

[74] Hodge, I. M. and Angell, C. A. Electrical relaxation in amorphous protonic conductors. *J. Chem. Phys.* **67** (1977) 1647-1658.

[75] Ambrus, J. H. Moynihan, C. T. and Macedo, P. B. Conductivity relaxation in a concentrated aqueous electrolyte solution. *J. Phys. Chem.* **76** (1971) 3287.

[76] Angell, C. A. Dynamic processes in ionic glasses. *Chem. Rev.* **90** (1990) 523-542.

[77] Angell, C. A. Mobile ions in amorphous solids, *Annu. Rev. Phys. Chem.* **43** (1992) 693-717.

[78] Mizuno, F. Belieres, J.-P. Kuwata, N. Pradel, A. Ribes, M. and Angell, C. A. Highly decoupled ionic and protonic solid electrolyte systems, in relation to other relaxing systems and their energy landscapes. *J. Non-Cryst. Solids* **352** (2006) 5147-5155.

[79] Torell, L. M. and Angell, C. A. Ion-matrix coupling in polymer electrolytes from relaxation time studies. *Br. Polym. J.* **20** (1988) 173-179.

[80] Srinivasan, S. Mosdale, R. Stevens, P. and Yang, C., Fuel Cells: Reaching the era of clean and efficient power generation in the twenty-first century. *Annual Review of Energy and the Environment* **24** (1999) 281-328.

[81] Yang, C. Costamagna, P. Srinivasan, S. Benziger, J. and Bocarsly, A. B. Approaches and technical challenges to high temperature operation of proton exchange membrane fuel cells. *J. Power Sources* **103** (2001) 1-9.

[82] Kwak, S.-H. Yang, T.-H. Kim, C.-S. and Yoon, K. H. Nafion/mordenite hybrid membrane for high-temperature operation of polymer electrolyte membrane fuel cell. *Solid State Ionics* **160** (2003) 309-315.

[83] Asano, N. Aoki, M. Suzuki, S. Miyatake, K. Uchida, H. and Watanabe, M. Aliphatic/Aromatic polyimide ionomers as a proton conductive membrane for fuel cell applications. *J. Amer. Chem. Soc.* **128** (2006) 1762-1769.

[84] Ansari, Y. Tucker, T. and Angell, C. A. *Provisional Patent application* 2012 (2012).

[85] Huang, W. Ansari, Y. Yarger, J. L. and Angell, C. A. (to be published) (2013).

[86] Lee, S.-Y. Yasuda, T. and Watanabe, M. Fabrication of protic ionic liquid/sulfonated polyimide composite membranes for non-humidified fuel cells. *J. Power Sources* **195** (2010) 5909-5914.

[87] S.-Y. Lee, A. Ogawa, M. Kanno, H. Nakamoto, T. Yasuda, and M. Watanabe, Nonhumidified intermediate temperature fuel cells using protic ionic liquids. *J. Am. Chem. Soc.* **132** (2010) 9764-9773.

[88] J.-P. Belieres, D. Gervasio, and C. A. Angell, Binary inorganic salt mixtures as high conductivity liquid electrolytes for >100 °C fuel cells. *Chem. Commun.* (Cambridge) (2006) 4799-4801.

[89] J. De Paula and P. W. Atkins, *Physical Chemistry 7th. Edition*, W. H. Freeman and Co. New York. (2002) (see Ch. 29.7, Fig. 29.23).

[90] Matsuda, A. Kanzaki, T. Tadanaga, K. Tatsumisago, M. and Minami, T. Proton conductivities of sol–gel derived phosphosilicate gels in medium temperature range with low humidity. *Solid State Ionics* **154-155** (2002) 687-692.

[91] Nida, H. Takahashi, M. Uchino, T. and Yoko, T. Preparation and structure of organic–inorganic hybrid precursors for new type low-melting glasses. *J. Non-Cryst. Solids*. **306** (2002) 292-299.

[92] Lejeune, C. Coelho, C. Bonjomme-Coury, L. Azais, T. Maquet, J. and Bonhomme, C. Studies of silicophosphate derivatives by 31P→29Si CP MAS NMR. *Solid State Nucl. Magn. Reson.* **27** (2005) 242-246.

[93] Jänighen, S. Brendler, E. Böhme, U. and Kroke, E. Synthesis of silicophosphates containing SiO_6-octahedra under ambient conditions – reactions of anhydrous H_3PO_4 with alkoxysilanes. *Chem. Commun.* **48** (2012) 7675-7677.

[94] Morris, R. A. Knighton, W. B. Viggiano, A. A. Hoffman, B. C. and Schaefer III, H. F. The gas-phase acidity of H_3PO_4. *J. Chem. Phys.* **106** (1997) 3545-3547.

[95] Kemp, D. S. How to promote proton transfer? *Nature* **373** (1995) 196-197.

[96] Stoimenovski, J. Izgorodina, and E. I. MacFarlane, D. R. Ionicity and proton transfer in protic ionic liquids. *Phys. Chem. Chem. Phys.* **12** (2010) 10341-10347.

[97] Munson R. A. and Lazarus, M. E. The Influence of ionic solutes upon the conductivity of molten phosphoric acid. *J. Phys. Chem.* **71** (1967) 3245-3248.

[98] MacFarlane, D. R. Forsyth, M. Izgorodina, E. I. Abbott, A. P. Annata G. and Frasera, K. On the concept of ionicity in ionic liquids. *Phys. Chem. Chem. Phys.* **11** (2009) 4962-4967.

[99] Miran, M. S. Kinoshita, H. Yasuda, T. Susan Md. A. B. H. and Watanabe, M. Physicochemical properties determined by ΔpK_a for protic ionic liquids based on an organic super-strong base with various Brønsted acids. *Phys. Chem. Chem. Phys.* **14** (2012) 5178–5186.

[100] von Grotthuss, C. J. D. Sur la décomposition de l'eau et des corps qu'elle tient en dissolution á l'aide de l'électricité galvanique. Ann. Chim. LVIII (1806) 54. Agmon, N. The Grutthuss mechanism. *Chem. Phys. Lett.* **244** (1995) 456-462.

[101] Xu, W. and Angell, C. A. Solvent-free electrolytes with aqueous solution - like conductivities. *Science* **302** (2003) 422-425.

[102] Bautista-Martinez, J. A. Tang, L. Belieres, J.-P. Angell, C. A. and Friesen, C. Hydrogen Redox in Protic Ionic Liquids and a Direct Measurement of Proton Thermodynamics. *J. Phys. Chem.* **113** (2009) 12586-12593.

[103] Stoyanov, E. S. Kim, K.-C. Reed, and C. A. An NH infrared vibration frequency scale for weakly basic anions. Implications for single-molecule acidity and superacidity. *J. Amer. Chem. Soc.* **128** (2006) 8500-8508.

[104] Belieres, J.-P. Byrne, N. and Angell, C. A. Characterization of strong and super acids, using protic ionic liquids made with tertiary amine bases: The N-H chemical shift. Abstracts of papers of the ACS (I&EC) **236** Meeting Abstract: (2008) 82.

[105] Angell, C. A. Byrne, N. and Belieres, J.-P. Parallel developments in inorganic, aprotic, and protic ionic liquids: physical chemistry and applications. *Acc. Chem. Res.* **40** (2007) 1228-1236.

[106] Angell, C. A. Xu, W. Yoshizawa, M. Hayashi, A. Belieres J.-P. Electrochemical Aspects of Ionic Liquids, Chapter 2, Ed. By Ohno, H. Wiley Pub. Hoboken, New Jersey (2011).

[107] Kanzaki, R. Uchida, K. Hara, S. Umebayashi, Y. Ishiguro, S. et al., Acid-base property of ethylammonium nitrate ionic liquid directly obtained using ion-selective field effect transistor electrode. *Chem. Lett.* **36** (2007) 684-685.

[108] Bordwell, F. G. Equilibrium acidities in dimethyl sulfoxide solution. *Acc. Chem.l Res.* **21** (1988) 456-463.

[109] Brown, H. C. and Pearsall, H. W. The action of the catalyst couple aluminum chloride-hydrogen chloride on toluene at low temperatures; the nature of friedel-crafts complexes. *J. Amer. Chem. Soc.* **74** (1952) 191-195.

[110] Brown, H. C. Pearsall, H. W. The catalytic halides. I. A study of the catalyst couple, aluminum chloride-hydrogen chloride, and the question of the existence of $HAlCl_4$. *J. Am. Chem. Soc.* **73** (1951) 4681-4683.

[111] Shuppert, J. W. and Angell, C. A. Proton NMR studies of the Lewis acid-base reactions between pyridinium chlorides and the acids zinc chloride and aluminum chloride. *J. Phys. Chem.* **84** (1980) 538-542.

[112] Harmer, M. A. Junk, C. P. Rostovtsev, V. V. Marshall, W. J. Grieco, L. M. et al., Catalytic reactions using superacids in new types of ionic liquids. *Green Chem.* **11** (2009) 517-525.

[113] Ansari, Y. Ueno, K. Zhao, Z. Angell, C. A. Anhydrous superprotonic polymer by superacid protonation of cross-linked $(PNCl_2)_n$, *J. Phys. Chem.* C **117** (2013) 1548-1553.

[114] Lee, S. -Y Ogawa, A. Kanno, M. Nakamoto, H. Yasuda, T. *et al.*, Nonhumidified intermediate temperature fuel cells using protic ionic liquids. *J. Am. Chem. Soc.* **132** (2010) 9764-9773.

[115] Hosmane, R. S. and Liebman, J. F. Paradoxes and paradigms: why is quinoline less basic than pyridine or isoquinoline? A classical organic chemical prospective, *Struct. Chem.* **20** (2009) 693-697.

[116] Angell, C. A. Dynamic processes in ionic glasses. *Chem. Rev.* **90** (1990) 523-542.

[117] Moynihan, C. T. Balitactac, N. Boone, L. Litovitz, T. A. Comparison of Shear and Conductivity Relaxation Times for Concentrated Lithium Chloride Solutions. *J. Chem. Phys.* **55** (1971) 3013-3020.

[118] MacFarlane, D. R. Huang, J. H. Forsyth, M. Lithium-doped plastic crystal electrolytes exhibiting fast ion conduction for secondary batteries. *Nature* **402** (1999) 792-794.